# THE ROLE OF INTERNAL STRESS IN STRENGTHENING HEAVILY CODEFORMED TWO-PHASE MATERIALS

by

**MATTHEW J. KILLICK**
B.A.Sc., The University of Alberta, 2003

A THESIS SUBMITTED IN PARTIAL FULFILLMENT OF
THE REQUIRMENTS FOR THE DEGREE OF

MASTER OF APPLIED SCIENCE

in

**THE FACULTY OF GRADUATE STUDIES**

(MATERIALS ENGINEERING)

THE UNIVERSITY OF BRITISH COLUMBIA

AUGUST 2006

# ABSTRACT

Heavily codeformed two-phase materials can show anomalous increases in strength as a function of the level of deformation. The strength of these materials can vary considerably from what is predicted by the rule of mixtures. Understanding the mechanisms responsible for the strengthening of these materials can lead to the better understanding of the strengthening of the individual phases and aid in the development of other materials that exhibit similar properties.

This thesis examines the role of internal stresses on the strengthening of heavily codeformed two-phase materials. The magnitude of these stresses and the effects of annealing on them are studied in various types of copper-niobium composites: bundle drawn and *in-situ* drawn wire produced at the National High Field Magnet Laboratory in Los Alamos, USA; and a layered composite produced at the University of British Columbia as part of this work. Tensile testing was done to determine the mechanical properties of the copper-niobium composites and load-unload or tension-compression tests were done to quantify the levels of internal stresses in the material.

The wire drawn composites were found to possess flow stresses much higher than predicted by the rule of mixtures and to contain considerable levels of internal stress. Internal stresses, measured by investigating the Bauschinger effect, and the flow stresses of all the drawn materials were found to decreases as the annealing temperature increased; however, the *in-situ* composite was found to be more resistant to annealing than the bundle drawn wire. The strength of the laminate composite, produced via multiple roll bonding, was found to be adequately described by the rule of mixtures. Although the rolling strain was not sufficient to produce anomalous strengthening, the internals stresses in the laminate where found to be more than twice that predicted by the rule of mixtures.

# TABLE OF CONTENTS

# LIST OF TABLES

# TABLE OF FIGURES

# ACKNOWLEDGMENTS

First and foremost, I would like to thank Dr. Chad Sinclair for all of the support he has given me during my time at the University of British Columbia. For his patience during the writing of this thesis, I am especially grateful.

Special thanks are also due to: Dr. Ke Han at the National High Field Magnet Laboratory in Florida, USA, for providing the wire drawn material studied in this work; Mary Mager for her guidance throughout many hours on the SEM and TEM; and finally, Ross Mcleod and the rest of the machine shop for keeping the rolling mill in tip-top shape.

I would also like to thank Babak Raeisinia and Reza Roumina, both brilliant scientists and equally amazing officemates. The remainder of my fellow graduate students, especially Jacky Cheng, Evan Lu and Sujay Sarkar, also deserve recognition for many hours of discussion, helpful advice and keeping it real out on the field and on the ice.

And Finally, I would like to express my sincere gratitude to my parents and sister for the continuous support they have given me through all of my adventures.

# CHAPTER 1

# INTRODUCTION

The fundamental objectives of material science are to be able to control, predict and understand the mechanical, physical and chemical properties of materials. In order to accomplish this, one must understand the interactions of chemical composition, processing methods and conditions, and initial microstructures. It is the objective of the present work to explore the mechanical properties of fine scale codeformed materials as a function of microstructural evolution, and to identify both the relative magnitude of internal stresses present and the role internal stresses play in strengthening these materials.

Over the past 20 years considerable interest has developed in the areas of metal matrix composites and nanocrystalline materials. Where these two areas overlap exciting materials can be produced. Particular interest has been shown toward the binary system of copper and niobium. In this system the desirable mechanical and physical properties of each element combine to produce a material with high strength while maintaining a significant fraction of the electrical conductivity of copper. Early studies of copper-niobium wire drawn composites have shown materials containing only 0.20 volume fraction niobium can have strengths exceeding 2 GPa [1] while maintaining a electrical conductivity of approximately 70 %IACS [2]. Applications for such materials include coils for high field magnets and space tethers.

The copper-niobium system has been selected for investigation in this work for a number of reasons. The system is among the less complex currently of interest. Copper and niobium have very low mutual solubility. The implication of this is that there are no intermetallic phases formed by the two metals. Producing these composites via wire drawing or accumulated roll bonding allows for freedom in designing materials with controlled volume fraction of components as well as in the microstructural scale of the material. Wire drawing and roll bonding also allow for the production of relatively large amounts of material through 'bulk' fabrication. The copper-niobium system is also of interest here as it shows a large strengthening effect through the addition of moderately low volume fractions of niobium. Finally this system has been extensively studied over the last two decades in terms of its fabrication and basic mechanical response, but only recently has the issue of internal stresses been raised as an important issue for the strength and stability of these materials.

Previous studies on fine-scale two-phase composite materials, fabricated by means of co-deformation, have been shown to exhibit remarkable levels of strengthening when the scale of the microstructure is sufficiently reduced, however there are underlying mechanisms at work that are still not well understood. The source of this strength is a fundamental question of interest both to the copper-niobium system as well as to other fine scale materials. Recently, there has been an increased awareness that the original mechanistic explanations based on modified Hall-Petch laws (e.g. [3, 4]) together with the concept of geometrically necessary dislocations (e.g. [5, 6]) may not be able to completely account for the strengthening mechanisms in these materials. It is the goal of this work to examine the role internal stresses may play in the strengthening of fine scaled codeformed composite materials.

Following this introduction, Chapter Two will present a review of processing methods, mechanical properties and generally accepted models uses to predict the

strength of copper-niobium fine-scaled composites. The experimental procedures employed during this work will be discussed in Chapter Three, and the results of these experiments are given in Chapter Four. Experimental results and their implications with respect to current strengthening models are discussed in Chapter Five. Finally, the conclusions of this work and suggestions for future work are presented in Chapter Six.

# CHAPTER 2

# BACKGROUND AND LITERATURE REVIEW

This chapter is intended to serve as a review of the current state of understanding and knowledge pertaining to copper-niobium codeformed composite materials. The information found in this chapter will provide the necessary background required to understand the discussions found in later chapters. Other systems, such as copper-silver or pearlite (iron-cementite), may be used for comparison or in place of copper-niobium where no relevant data exists. Methods used to fabricate these materials are discussed first, followed by an overview of the mechanical properties they exhibit. Next, proposed mechanisms for the strengthening of two-phase fine-scaled materials will be discussed. The final section of this chapter will deal with the internal stresses in these heavily codeformed materials.

## 2.1. Fabrication Methods of Metallic Multilayered Composites

In this section an overview of the methods currently used to produce fine-scale metallic composites is provided. Each of the different methods discussed in this section result in different microstructures, which in turn results in variations in mechanical and physical properties.

### 2.1.1 Physical Vapor Deposition

Physical vapour deposition (PVD) techniques used to produce multilayers include: electron beam evaporation, thermal evaporation, ion beam sputtering, molecular beam epitaxy and magnetron sputtering [7]. There are several advantages to using magnetron sputtering for multilayer production including the ability to produce layers with highly uniform thicknesses [8,9] down to 1 to 2 atomic monolayers.

When using the magnetron sputtering technique the thicknesses of the deposited layers are controlled by varying experimental parameters such as target-to-substrate separation, gas pressure, applied voltage bias and substrate temperature. When the magnetron sputtering process parameters are controlled optimally, the process has the ability to produce multilayered material with a high degree of homogeneity in the layer thickness.

Although PVD allows precise control of material fabrication, the amount of material produced is limited by the size of the substrate as well as the deposition rate. For example Misra *et al.* [10] used a deposition rate of approximately 0.35 nm/s to produce alternating layers of 0.75 μm thick copper and niobium. The resulting sample required approximately 6 hours to deposit with an overall thickness of 7.5 μm.

### 2.1.2 Wire Drawing

Fine-scale copper-niobium composites are most commonly produced via wire drawing. Wire drawing allows for the imposition of large macroscopically uniform strains (e.g. $\varepsilon = 12$). As a result the microstructure of these materials can become very fine resulting in large increases in yield and ultimate tensile strength.

Wire drawn copper-niobium composites can be produced via several routes. The different types of drawn composites are defined by the initial structure of the system. The most commonly employed method involves the casting of a billet containing the desired

volume fraction of both copper and niobium produced via casting. The billet is then machined to remove impurities and drawn [11,12]. The drawn wire can be bundled with other wires to allow for more deformation without the diameter of the resulting wire becoming too fine [13]. This method has been termed *in-situ* drawing since the microstructure is refined during deformation [14]. A second method involves first producing a single drawn wire from a sample produced from a niobium rod wrapped in copper, then bundling the wire and redrawing [15]. This method is called bundle drawing. A third method is termed jelly-roll processing [15,16,17]. This method involves winding copper and niobium foil around a copper core to create a jelly-roll type structure. The jelly-roll can be extruded 'as-is' or first inserted into a cylindrical copper billet that has been machined to hold several rolls, which is then extruded. Typical flow charts for each production method are shown in Figure 2.1.

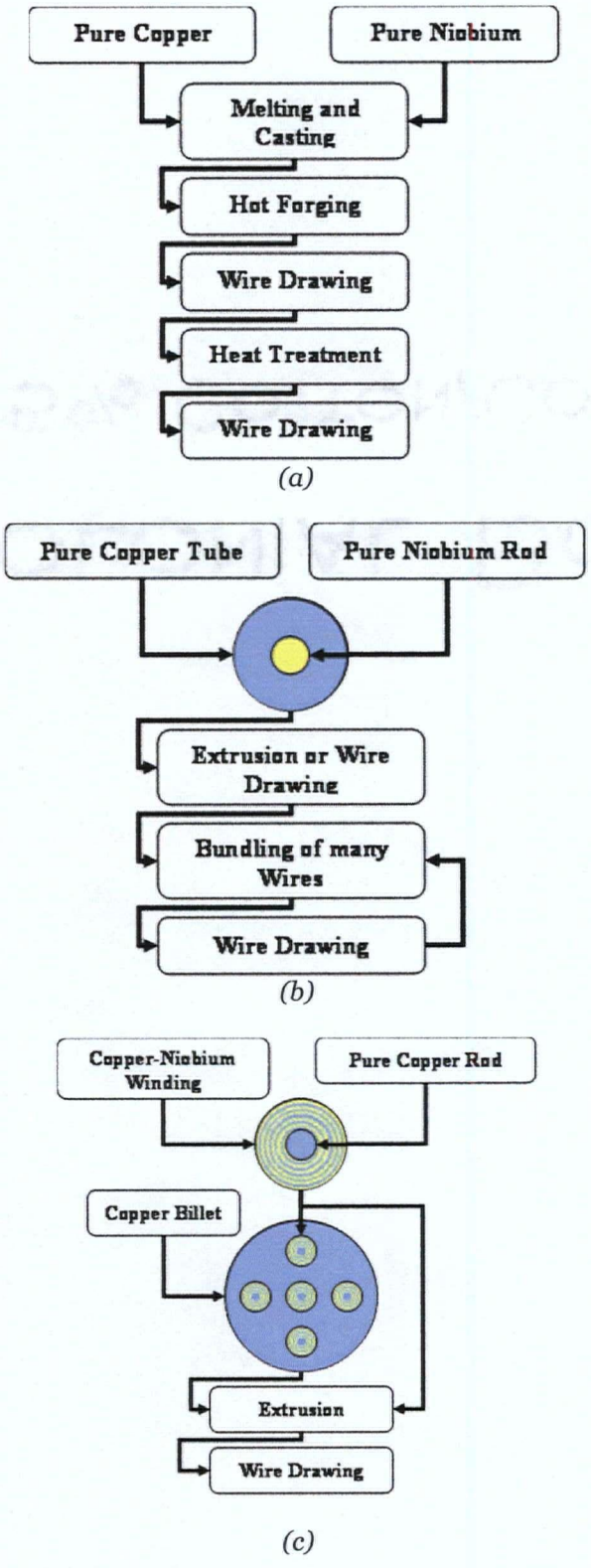


**Figure 2.1** *Process flow charts for: (a) production of in-situ Cu-Nb wires; (b) for the production of bundle drawn Cu-Nb wires; (c) jelly-roll processed wire.*

The microstructures formed by the *in-situ* and bundle drawing routes are different in two important ways. The first difference is the homogeneity in the fiber distribution through the axial cross section. Bundle drawing produces an ordered distribution of niobium filaments while *in-situ* production produces a random distribution of niobium in the copper matrix. Second, at low strains the *in-situ* method produces a large number of thin but discontinuous niobium filaments while bundle drawing produces long continuous fibers. At large strains, however, the *in-situ* composite will consist of fibers that are virtually continuous (i.e. aspect ratios much greater than 10).

### 2.1.3 Rolling

Copper-niobium composites can also be formed as multilayers by rolling. There are two methods used to produce copper-niobium alloys that employ rolling techniques: *in-situ* rolling and the more complicated press-roll bonding. *In-situ* rolling involves a process similar to *in-situ* wire drawing, except the drawing portion is replaced with rolling. Once rolled, the ribbon can be cut up into smaller pieces then rolled again to introduce more strain.

Multilayers can also be produced via the press-rolling method similar to the *in-situ* method. Figure 2.2 shows a typical process flow sheet for the press-rolling of copper-niobium multilayers [18].

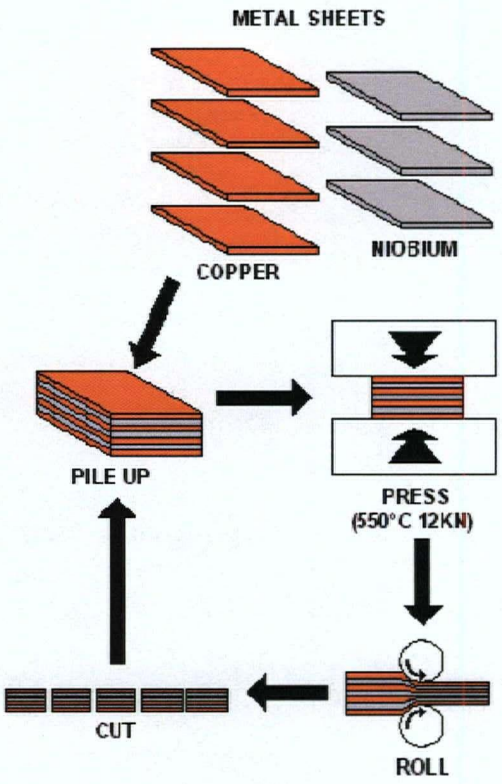


**Figure 2.2** *Process flow sheet for the production of Cu-Nb multilayered composites via repeated press rolling as described in [18].*

The microstructures produced via these methods, while similar, have differences. *In-situ* rolling produces a structure which contains plates of niobium in a copper matrix while repeated press-rolling produces a regular layered structure where the layers are essentially continuous in two dimensions.

### 2.1.4 Summary

Table 2.1 summarizes the different methods described above. Although there are several methods currently used to produce copper-niobium alloys only wire drawing has been used successfully to produce large bulk quantities of material. Each method produces a unique microstructure which also leads to variations in mechanical properties; this will be discussed further in a subsequent section.

**Table 2.1.** *Summary of methods used to produce Cu-Nb composites.*

| ***Fabrication Method*** | ***Resulting Structure*** | ***Minimum Microstructure Scale*** | ***Possibility of 'Bulk' Production*** |
|---|---|---|---|
| *In-situ* wire drawing | Nb ribbons in Cu matrix | <50nm | YES |
| Bundling and drawing | Nb ribbons in Cu matrix | <50nm | YES |
| *In-situ* rolling | Nb plates in Cu matrix | <50nm | YES |
| Stacking and rolling | Nb and Cu alternating layers | <50nm | NO |
| Magnetron sputtering | Nb and Cu alternating layers | ~1 monolayer | NO |

## 2.2. Mechanical Properties of Deformation Processed Cu-Nb

Fine-scale two phase composite materials fabricated by co-deformation can exhibit remarkable mechanical properties when the scale of the microstructure is sufficiently reduced. For example it has been shown that the strength of highly deformed copper-niobium wires can have flow stresses that significantly exceed what a rule of mixtures between the flow stress of the bulk components would predict [19]. The rule of mixtures for predicting the flow stress ($\sigma_C$) and elastic modulus of a composite ($E_C$) are found as Equation 2.1 and Equation 2.2 respectively [20].

$$\sigma_C = V_1\sigma_1 + V_2\sigma_2 \qquad \textit{Equation 2.1}$$

$$E_C = V_1E_1 + V_2E_2 \qquad \textit{Equation 2.2}$$

In the previous equations, $V$, $\sigma$ and $E$ represent the volume fraction, yield stress and elastic modulus respectively for either phase 1 or 2. It is the intent of this chapter to be a basic review effect of processing methods on the mechanical properties exhibited by the copper-niobium system.

### 2.2.1 Copper and Niobium in the Pure State

The two-phase system of copper-niobium has been thoroughly studied over the past 30 years. There are several reasons for selecting the copper-niobium system as the material for this study. First, copper and niobium have limited mutual solubility; i.e. maximum 0.8 wt%Nb in copper and 0.15 wt%Cu in niobium [21]. Moreover, there are no intermediate copper-niobium phases. Thus, a purely two-phase system is formed with sharp interfaces between the copper and niobium phases. Since the copper-niobium composite system contains essentially pure phases, their properties are not affected by alloying.

The difference in crystal structure of the two phases, niobium is body centered cubic (BCC) while copper is face centered cubic (FCC), has been promoted as one of the reasons for the high strengths obtained in this material. The mechanical properties of the two phases are similar with regards to their elastic properties (at room temperature $E_{Nb}$ = 103 GPa and $E_{Cu}$ = 128 GPa [22]) but quite different in terms of the yield and flow stress; at room temperature the annealed yield strengths are 275 MPa for niobium and 33 MPa for copper while the tensile strengths are 585 MPa and 209 MPa [22].

### 2.2.2 Copper and Niobium Composites

Interest in the copper-niobium system revolves around the ability to produce a composite material that maintains the thermal and electrical properties of copper while exhibiting strengths in excess of that possible from typical copper alloys (e.g. precipitation hardening systems). The addition of a reinforcing phase is shown to always reduce the conductivity of the materials yet the strength of the material always improves as compared to pure copper. With the copper-niobium system it has been possible to achieve strengths in excess of 1400 MPa with electrical conductivities of better than 60% of the international annealed copper standard [16].

The majority of the work done on the copper-niobium system has been done on materials with volume fractions of niobium between 18-20 percent. The addition of larger fractions of niobium results in a material that posses higher strength, however this leads to the degradation of ductility and electrical conductivity [23].

Spitzig *et al.* published the results of experiments comparing the strength of heavily drawn copper, niobium and *in-situ* drawn composite (Figure 2.3). The strength of copper was shown to rise slowly above 500 MPa (draw ratio of 7*) reaching an approximately constant flow stress. Niobium was also shown to approach a nearly constant strength of close to 1400 MPa after a draw ratio of approximately 11 [19].

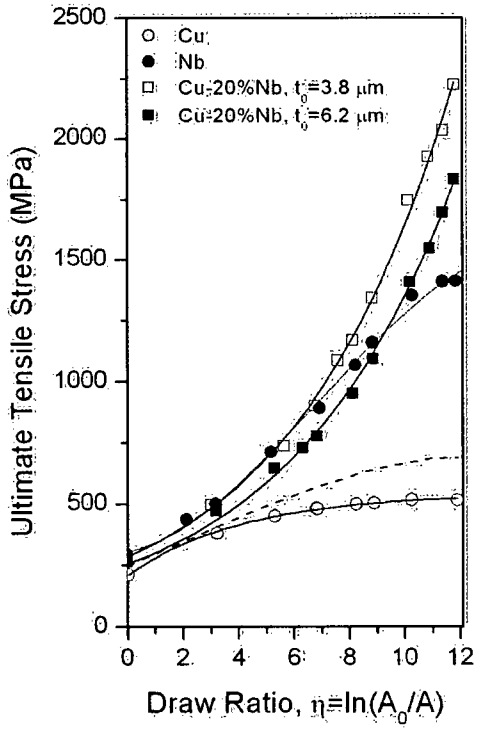


**Figure 2.3** *Ultimate tensile strength as a function of draw ratio for the copper-niobium system replotted from [19]. The initial scale of the Nb phase is indicated as $t_o$. The dotted line represents the rule of mixtures prediction of the strength based on the properties of the bulk copper and bulk niobium.*

* The draw ratio is defined as, $\eta = \ln(A_0/A)$ where $A_o/A$ is the ratio of the initial (before drawing) wire cross-sectional area and the cross-sectional area after drawing.

In contrast, the *in-situ* material, when drawn to strains of 12, shows no indication that the strength will reach a maximum and plateau. The 20% niobium composite was shown to have a maximum strength of 2200 MPa. Considering the rule of mixtures between the flow stress (at a given draw ratio), the strength of the composite is observed to be significantly larger. The strength of the copper-niobium is also significantly higher than the strength of either the copper or niobium, suggesting differing strengthening mechanisms for the single and two-phase materials. Several models for strengthening of the composite material will be presented in the following sections.

The two curves representing Cu-20% Nb composite wire show the effect of the scale of the initial dendritic structure, and thus the scale of the final microstructure, has on the strengthening of these materials. For a given amount of deformation, the material with the finer initial microstructure always has a higher strength.

## 2.3. Review of Current Strengthening Models

It was seen in the previous section that copper-niobium composites can exhibit very high (greater that 2000 MPa) tensile strengths. Understanding why these gains in strength occur as a function of deformation has been challenging and several models have been proposed to explain the observed strength [23]. The barrier model by Spitzig *et al.* [19, 24-25] suggests that the increase in strength is due to the difficulty of propagating plastic flow between the FCC copper and the BCC niobium. The barrier model correlates strength to the spacing of the niobium phase in accordance with a Hall-Petch [26-27] relationship. An opposing view has been put forward by Funkenbusch and Courtney [28-29] who argue that an increase in dislocation density, attributed to strain incompatibility between the copper and niobium, is responsible for the strength of these materials. Since the dislocations formed by this strain accommodation are geometrical in origin this model is referred to as the geometrically necessary dislocation model.

Both the Barrier model and the geometrically necessary dislocation model predict the bulk mechanical response of copper-niobium composites with a good degree of accuracy. However care must be exercised when applying these models to certain types of materials. These limitations will be discussed in more depth as this chapter progresses. This chapter will also examine the relevance of the idea of dislocation starvation and the role it could play in the strengthening in heavily deformed materials.

### 2.3.1. Hall-Petch – Dislocation Pile-Up

Embury and Fisher [30] were the first to suggest a modified Hall-Petch equation for the prediction of strength of drawn pearlite wire. The heavily deformed wire consists of long ribbons of cementite ($Fe_3C$) in a ferrite matrix. The ferrite-cementite interface spacing as a function of drawing strain is given by

$$\frac{1}{\bar{r}} = \frac{1}{\bar{r}_0}\exp\left(\frac{\eta}{2}\right) \qquad \textit{Equation 2.3}$$

where $\bar{r}_0$ is the mean initial interface spacing and $\bar{r}$ is the mean interface spacing after a true drawing strain of $\eta$.

In this model the cementite-ferrite interfaces are considered as barriers to dislocation motion. In analogy to the Hall-Petch relation for single phase, polycrystalline metals the yield stress ($\sigma_y$) of the pearlite wire would be expected to be a function of the mean interface (barrier) spacing according to

$$\sigma_y = \sigma_i + k\left(c\bar{r}_\varepsilon\right)^{-1/2} \qquad \textit{Equation 2.4}$$

where $\sigma_i$ is the apparent friction stress of the ferrite matrix, $k$ is the Petch slope, $c$ is a geometrical factor relating the mean slip distance to the barrier spacing and has been proposed to have a value of 2 (see Embury and Fisher [30] for more details).

Equations 2.3 and 2.4 combine to give,

$$\sigma_f = \sigma_i + \frac{k}{\sqrt{2\bar{r}_0}} \exp\left(\frac{\eta}{4}\right) \qquad \textit{Equation 2.5}$$

where the yield stress is defined as a function of initial barrier spacing and applied true strain. It is assumed in Equation 2.5 that the plastic strain is distributed homogeneously through the wire, the barrier spacing decreases proportionally to the wire diameter and that no boundaries are generated or destroyed during deformation.

Spitzig and Krotz [24] extended this model to the copper-niobium system examining a cast hypoeutectic copper-niobium alloy. Upon drawing the niobium dendrites break up and form long ribbons in a copper matrix. The effect of drawing strain, $\varepsilon$ , on the filament spacing, $\bar{\lambda}$ , and filament thickness, $\bar{t}$ ,was found to be

$$\frac{\bar{\lambda}}{\bar{\lambda}_0} = \frac{\bar{t}}{\bar{t}_0} \exp(-0.37\eta) \qquad \textit{Equation 2.6}$$

where $\bar{\lambda}_0$ and $\bar{t}_0$ are the mean initial filament spacing and thickness. The factor of 0.37 in Equation 2.6 comes from an empirical fit to data.

The form of the relationship given by Equation 2.3 or 2.6 has been shown to be adequate to describe a variety of codeformed two-phase systems. Data from press-rolled iron-silver [31], for instance, shows that at low compression ratios the reduction in layer spacing is linear and can be described by an equation similar to Equation 2.3 or Equation 2.6. At larger strains there appears to be a small deviation from linearity, however the linear curve reasonably predicts the layer thickness considering the error in thickness measurement is large for small thicknesses.

The model proposed by Spitzig *et al.* for the flow stress of drawn material was based on the initial dendrite thickness $\bar{t}_0$ and the true drawing strain given by

$$\sigma = 82 + 459(\bar{t}_0)^{-\frac{1}{2}} \exp\left(\frac{\eta}{5.4}\right) \qquad \textit{Equation 2.7}$$

where $\sigma$ is the ultimate tensile strength and the constants have been determined from experimental results for a niobium volume fraction of 0.20. Equation 2.7 was shown to provide an adequate fit the ultimate tensile strength in tension based on the applied drawing strain and the initial niobium dendrite size.

Funkenbussch and Courtney produced a model similar to that of Spitzig *et al.* that combines the rule of mixtures and a Hall-Petch relationship [32]. The rule of mixtures was used to describe the work hardening and solution strengthening of the two phases, while a Hall-Petch relation was utilized to predict the increase in strength associated with a reduction in the microstructural scale. The model predicted the ultimate tensile strength of the composite, $\sigma_C$, as

$$\sigma_C = \sigma_{ROM} + \Delta\sigma_D \qquad \textit{Equation 2.8}$$

where $\sigma_{ROM}$ is the strength predicted by the rule of mixtures (equation 2.1) and $\Delta\sigma_D$ is the strengthening predicted by the Hall-Petch effect.

Although the barrier model has been shown to fit the strengthening of highly deformed two-phase materials, it does not completely describe the mechanisms responsible for the strength. For instance, equation 2.7 predicts that the strength of the material should only depend on the scale of the microstructure. In this case, the strength should be the same for the materials processed by different methods to the same microstructural scale. To test this hypothesis, Everett [33] compiled ultimate tensile strength data for several systems (silver-copper, copper-chromium and copper-iron) as a function of the scale of the phases. The scale of the phases was described as the sum of the average lamina thickness for each phase. Everett compared data for materials produced by means of deformation processes to that from material produced via vapor deposition with equivalent microstructural scale and equivalent volume fraction of phases. It was observed that in all the systems examined the material produced by

deformation had strengths greater that the material produced via a non-deformation based process with the same scale and volume fraction of phases. These results suggest the barrier model does not fully describe the strengthening mechanism at work, since the model would predict the same strength for materials of a given layer spacing independent of how it was produced. The difference in strength of the deformation processed material and the layered material for FCC-BCC systems was also found to be larger than that of the FCC-FCC silver-copper system. The FCC-BCC systems also were found to have larger Hall-Petch slopes than the FCC-FCC pair.

In summary, the barrier model is a semi-empirical model that can be used in some cases to predict the anomalous gains in strength that are observed, however it does not explain the mechanisms responsible for the strengthening. The model assumes the phase interfaces act as barriers to dislocation motion, but the true nature of these interfaces is unknown. A model that better describes the strengthening of these materials may consist of a combination of the barrier model and a more theoretical approach.

### 2.3.2 Geometrically Necessary Dislocations

Ashby [34] proposed that two-phase materials work harden much faster than single-phase materials because the two phases are not equally easy to deform. Since the two phases may have differing elastic moduli and flow stresses it is reasonable to say that as the overall composite is deformed, one phase will deform plastically more than the other. If the material must deform in a compatible fashion (i.e. without debonding of interfaces or voids opening within the material) these gradients in plastic strain, with a wavelength equal to the spacing of the phases, must be accommodated in two ways. One way the phases can accommodate the deformation gradient is by elastic straining of the material that undergoes less plastic strain. This results in internal stresses, a subject that will be dealt with in the next section. The second way the deformation can be

accommodated is by extra local plastic deformation. The requirement for the local plastic deformation is the creation of more stored dislocations called geometrically necessary dislocations. The accumulation of extra elastic strain and stored dislocations are not mutually exclusive, both can act in parallel to accommodate the deformation gradient.

Funkenbusch and Courtney [28, 29] proposed a model that relates the anomalous strengthening of fine-scale two-phase composites to geometrically necessary dislocations. In copper-niobium composites these dislocations are hypothesized to form due to the incompatibility of plastic deformation of the FCC copper and the BCC niobium [23].

The geometrically necessary dislocation argument builds on Ashby's 'thought experiment' [35] regarding the deformation of a single phase polycrystalline material. If individual grains are strained independently they will adopt a final shape characteristic of their crystallographic orientation. If a polycrystal is assembled from these grains, there will be some areas with gaps and others with overlap between grains. In order to fill gaps between grains, material must shift from the regions of overlap to the regions where there are voids. This is done through the addition of geometrically necessary dislocations.

The average dislocation density, $\overline{\rho}_G$ , produced by this accommodation process is

$$\overline{\rho}_G \approx K\left(\frac{\varepsilon}{D}\right) \qquad \textit{Equation 2.9}$$

where $\varepsilon$ is the imposed plastic strain (assuming a proportional, monotonic strain path), $D$ the grain size, and $K$ is a constant that accounts for the geometry of the grains/phases and the fraction of the imposed strain that must be accommodated. This model has been used to describe the effect of grain size on the strengthening of single

phase materials [36] as well as the strengthening of composites containing ceramic or intermetallic particles [34].

Two-phase composites are positioned between the situations for polycrystalline materials, where the difference in plastic behaviour between neighbouring regions is expected to be relatively small, and dispersion hardened materials containing ceramic or intermetallic particles, where the difference in mechanical response of the matrix and particles is large. Some modifications to Equation 2.9 are therefore necessary for highly deformed two-phase materials. First, $D$ is taken to be the average interphase spacing rather than the grain size. Second, $D$ is a function of the true deformation strain, $\varepsilon_T$, following a dependence similar to that in Equation 2.3 e.g.,

$$D = D_0 \exp(-\varepsilon_T / n) \qquad \textit{Equation 2.10}$$

where $D_0$ is the initial interphase and $n$ is a constant depending on the mode of deformation. As discussed in section 2.3.1, this assumes that the interphase spacing changes according to the macroscopically imposed strain.

Considering Equation 2.10, the average geometrically necessary dislocation density now becomes

$$\bar{\rho}_G = K \int_0^{\varepsilon_T} \frac{1}{D_0 \exp(-\varepsilon_T/2)} \mathrm{d}\varepsilon_T \qquad \textit{Equation 2.11}$$

After integration, Equation 2.11 gives

$$\bar{\rho}_G = 2K\left[1 - \exp(\varepsilon_T/2)\right]/D_0 \qquad \textit{Equation 2.12}$$

Equation 2.12 has two important implications. First is that the density of geometrically necessary dislocations is directly proportional to $K$ and hence the plastic strain mismatch between phases. Furthermore, if the strength of material is assumed to be controlled by forest hardening arising from dislocation-dislocation interactions

Equation 2.12 predicts the strength to be a function of the inverse square root of the interphase spacing, (i.e. the Hall-Petch relation) as will be shown below.

Funkenbusch and Courtney expanded on this idea [28] by accounting for the fact that the two phases may accommodate the plastic strain mismatch differently resulting in different geometrically necessary dislocation densities in each of the phases. They suggest the partitioning of dislocation density could arise from differences in strength, local effects such as the extent of overlap on any particular grain, phase size and phase volume fraction. The geometrically necessary dislocation densities in phases A and B were taken to be

$$\rho_{G_A} = P_A \frac{\bar{\rho}_G}{V_A} \qquad \textit{Equation 2.13}$$

and

$$\rho_{G_B} = P_B \frac{\bar{\rho}_G}{V_B} \qquad \textit{Equation 2.14}$$

where $\rho_{G_{A,B}}$ are the geometrically necessary dislocation densities in the respective phase, $V_{A,B}$ are the phase volume fractions, and $P_{A,B}$ are empirical dislocation partitioning coefficients which define the degree to which each of the phases accommodates the plastic strain misfit by geometrically necessary dislocations. The partitioning coefficients must have values between 0 and 1, such that

$$P_B + P_A = 1 \qquad \textit{Equation 2.15}$$

In the limiting case of a polycrystalline material the partitioning coefficients would be assumed nearly equal for each of the grains while at the other extreme, the partitioning coefficient for the matrix in a dispersion hardened material would equal 1 since the embedded particles cannot deform plastically.

Assuming that the flow strength of a polycrystal, $\sigma$, is a function of the total dislocation density, $\rho_T$, shear modulus, $\mu$, and the Burgers vector, $b$, as

$$\sigma = \sigma_0 + \alpha\mu b\sqrt{\rho_T} \qquad \textit{Equation 2.16}$$

where $\sigma_0$ is a constant derived from the intrinsic lattice resistance to dislocation motion, $M$ is a orientation factor, and $\alpha$ is a constant on the order of unity. The total dislocation density is the sum of geometrically necessary dislocations and statistical dislocations. This represents a major assumption that is often criticized in the literature since it would be expected that the geometrically necessary dislocations should be concentrated near the phase interface and not averaged over the volume of the phases [37].

To predict the density of statistical dislocations Funkenbusch and Courtney use a Kocks-Mecking model [38],

$$\mathrm{d}\rho_S \approx \left[C_1\sqrt{\rho_T} - C_2\rho_T\right]\mathrm{d}\varepsilon_T \qquad \textit{Equation 2.17}$$

where $C_1$ and $C_2$ are constants that are determined by fitting the equation to experimental data for the individual phases. The term $C_1\sqrt{\rho_T}$ accounts for dislocation multiplication as a function of dislocation spacing, while $C_2\rho_T$ account for dynamic recovery.

The total dislocation density is the sum of the geometrically necessary dislocation and statistical dislocation densities. If the derivative of Equation 2.12 is taken and then added to Equation 2.17 an equation for the total dislocation density in phase A is given by

$$\mathrm{d}\rho_{T_A} = \left[C_{1_A}\sqrt{\rho_{T_A}} - C_{2_A}\rho_{T_A} + P_A K \exp\left(\varepsilon_T/2/\left(V_A D_0\right)\right)\right]\mathrm{d}\varepsilon_T \qquad \textit{Equation 2.18}$$

where an equivalent expression can be written for phase B.

At large strains the third term will dominate Equation 2.18. In this case, substituting Equation 2.18 into Equation 2.16 a Hall-Petch like dependence of the flow stress on the interphase spacing, assuming a rule of mixtures for the overall strength of the composite, is found. This argument was also proposed in a similar manner by Rollet [39].

Figure 2.4 shows the fit of Funkenbusch and Courtney's geometrically necessary dislocation model to experimental data as a function of strain and volume fraction of Nb for wire drawn copper-niobium [29]. Beyond the assumptions listed above in deriving this model, one must also use the partitioning coefficients and K as fitting parameters.

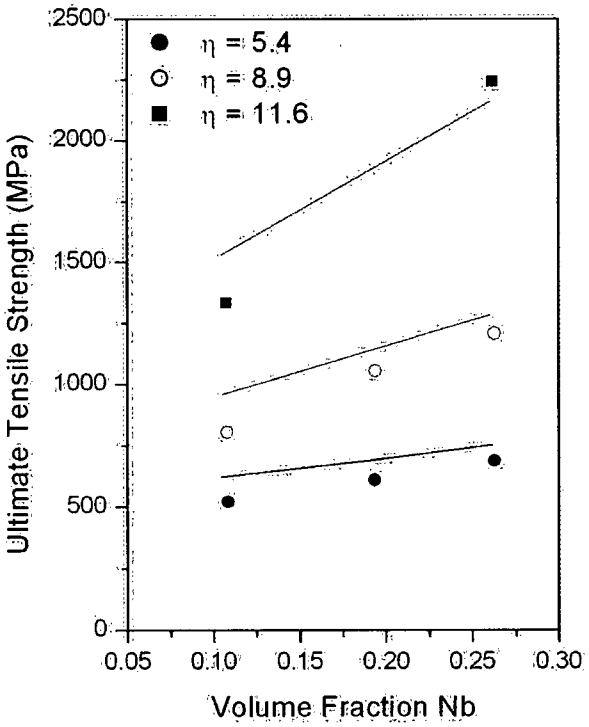


**Figure 2.4** *Prediction of the strength of Cu-Nb wire using the geometrically necessary dislocation model of Funkenbusch and Courtney [32] (lines) versus experimental data (symbols). Re-plotted from [32].*

On the basis of this model the geometrically necessary dislocation densities begin to dominate at strains as low as 4, and rapidly increase as the microstructure continues to be refined.

Bevk *et al.* [40] reported high dislocation densities, on the order of $10^{13}$ $cm^{-2}$, based on resistivity measurements. However, these measurements have been called into question owing to the possibility for other sources contributing to the resistivity. More recent TEM analysis shows that the dislocation densities predicted by this model are only similar to experimental values at low levels of deformation (strain<4), where at high levels of strain the observed dislocation densities are much lower than the model predicts [41].

Although this model reproduces the behavior of these materials well it is not without it weaknesses. Some of the main arguments against the geometrically necessary dislocation model were outlined in a series of articles by Spitzig *et al.* and Funkenbush and Courtney [42,43,44,45,46]. These arguments were summarized in a review of heavily deformed *in-situ* composites by Sevillano [47]. First the misfit parameters, $C_1$ and $C_2$, for the phases cannot be predicted. This model also assumes that the accumulation and annihilation, through dynamic recovery, of the dislocations is independent of scale. Furthermore, statistically stored dislocations are treated equally to the geometrically produced dislocations in terms of dynamic recovery and the role they play in strengthening. Finally it assumes both phases undergo an enhancement in work hardening (both $C_1$ and $C_2$ are assumed positive), rather than the harder phase deforming less than the softer one.

### 2.3.3 'Whisker-like' Behaviour and Dislocation Starvation

TEM analysis has shown that above a critical level of strain the dislocation density may begin to decrease in fine-scale two phase materials (e.g. [19,48,49]. For instance observations of silver-copper material revealed that for interphase spacings of less than 50 nm the fibres appear almost dislocation free [48]. The strength of the material continues to increase as the microstructure is refined however, suggesting

mechanisms other than dislocation storage are important in determining the strength [44].

The concept of these codeformed composites containing extremely fine, almost dislocation free, second phases is similar to observations on the mechanical behaviour of dislocation free single crystal microcrystals and whiskers. It is observed that high purity single crystals of copper that, in bulk form would yield at stresses of a few MPa, exhibit strengths of several GPa [50,51]. It has been argued that this stress must be associated with the stress necessary to nucleate dislocations from within the crystal [50].

This idea has been discussed more recently by Greer *et al.* [52,53] in their study of the compression response of free standing, single crystal gold pillars. The strength of the pillars is observed to be highly dependent on the size of the pillar with smaller diameter pillars being stronger than larger diameter pillars. Their results mimic the bending strength - whisker diameter relationship obtained for various metallic whiskers as tabulated by Webb and Forgeng [54].

The explanation put forth by Greer *et al.* for the behavior is the concept of dislocation starvation. Dislocation starvation proposes that once the crystal becomes smaller than a critical size most dislocations annihilate at the free surfaces before they encounter another dislocation. There is, therefore, a reduced probability of dislocation interaction that would lead to dislocation multiplication combined with a loss of dislocations from the sample. In order to maintain the imposed rate of deformation new dislocations must be nucleated, a process that requires very large stresses [43-46]

The above described properties of fine-scale single-phase materials has been also considered in relation to the strengthening of heavily codeformed composite materials [19,47,49,55]. In this situation, as the scale of one or both phases decreases it is envisioned that dislocations reach phase boundaries where they are either transmitted or annihilated before they can be trapped. The supply of dislocations is thus controlled

either by the process of slip transmission from one phase to the other, or by the nucleation of new dislocations from the phase interface [55].

## 2.4 Internal Stress in Two-Phase Codeformed Materials

In materials containing two phases, internal stresses may be present due to differences in the mechanical and thermo-elastic properties of the reinforcing phase and the matrix. The magnitude of the internal stresses can be used as a tool to help understand the differences in the *in-situ* mechanical properties of the component phases. This section will focus on the generation and interpretation of internal stress in codeformed fibre and laminate composites.

### 2.4.1 Development of Internal Stresses

Internal stresses in codeformed composites are typically attributed to either inhomogeneous plastic flow during low temperature deformation processing, but can also be introduced by thermal treatments [2,56]. During the production of *in-situ* copper-niobium composites internal stresses are generated during rapid cooling from casting and hot forging due to the difference in thermal expansion coefficient of the two metals. These internal stresses are further modified as the material is wire drawn or rolled.

Internal stresses are divided into three categories [57]. Type I internal stresses have the largest wavelength and are common to both single and two phase materials. Any thermal or mechanical treatment which occurs non-uniformly over a part will result in these macroscopic internal stresses [58].

Type II internal stresses occur on a smaller scale than those of type I. These internal stresses are a result of variations in elastic straining between different grains. Similar to Ashby's thought experiment [35] described in Section 2.3.2 plastic and elastic

anisotropy at the level of each grain or phase would tend to create overlap and gaps inside the material if mechanisms of maintaining compatibility didn't exist. Rather than using geometrically necessary dislocations to ensure compatibility, the addition of elastic strains can be used to avoid overlaps/gaps within the material.

Wood [59] and Sinclair *et al.* [55] postulated that internal stresses are generated during deformation due to imperfect plastic strain matching as dislocations move through one phase to the other. Sinclair *et al.* [55] suggest a dislocation passing through an interphase boundary will result in a residual interface dislocation. As a result the copper will be in a state of compression and the niobium in a state of tension. Elastic strain will increase with continuing deformation until the stress exceeds the strength of one of the two phases or some other mechanism of relaxation becomes active.

The third type of internal stress (Type III) arises due to intragranular variations in plastic strain. The interaction of dislocation and the inherent strain fields associated with these dislocations results in strain gradients within individual grains. The effects of these internal stresses will be discussed in the next subsection.

### 2.4.2 Modelling Internal Stress

Several models have been used to estimate the amount of internal stress in a material. Some are simple continuum based models and some are more complex micro-mechanical descriptions of what is thought to be occurring in codeformed materials.

#### *Elastic-Plastic Masing Model*

A simple model describing the mechanical behavior of two-phase materials was first proposed by Masing (as cited by [29,60]). In this model, stresses and strains are considered in only one direction, with the imposed strains being assumed equal to the

strains in the individual phases. The classical Masing model considers two elastic, perfectly plastic, phases whose yield stresses are the same in tension and compression. The two phases can have different elastic moduli, however here equal moduli are assumed for simplicity. In order for internal stress to be generated it is required that the two-phases have different yield stresses. A graphical description of the Masing model is shown in Figure 2.5.

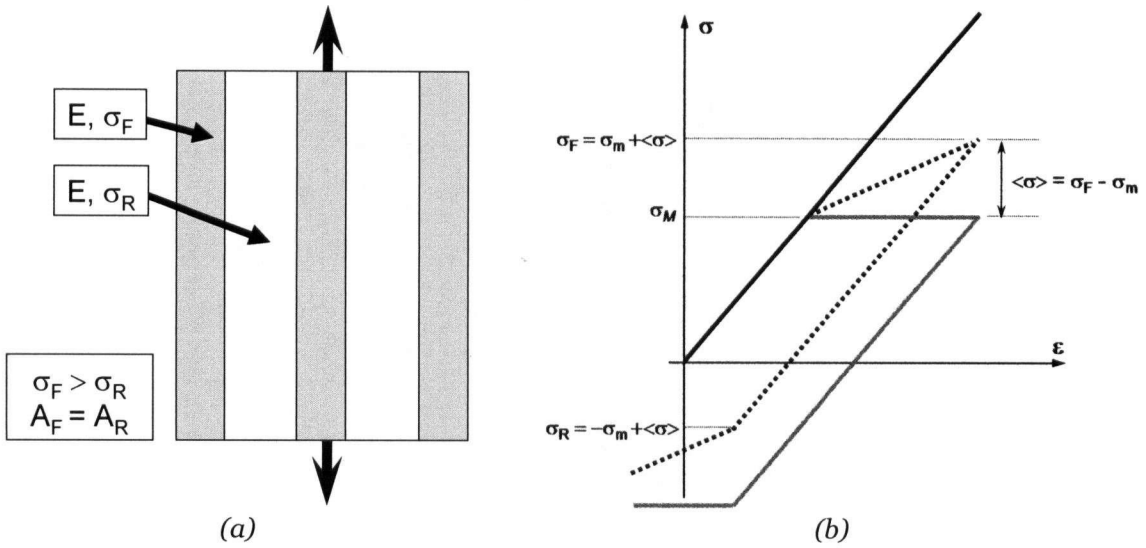


**Figure 2.5** *Masing model description: (a) elastic perfectly plastic elements with two different yield strengths; (b) the forward and reverse stress-strain behavior of the individual elements and the two-phase composite. Phase 1 is shown in grey, phase 2 in black and the composite response as the dashed line.*

As the composite undergoes uniaxial tensile loading, phase one will yield at a stress of $\sigma_m$ at $\varepsilon_1$. As loading continues, phase 1 continues to plastically deform while phase 2 continues to deform elastically. After a plastic strain of $\varepsilon_2$, the second element will begin to yield and, assuming equal volume fractions of the two phases, the stress on the composite will be $\sigma_F = \sigma_m + 0.5E\varepsilon_2$.

If the composite was to undergo reverse loading, after the initial forward loading, the composite behaves elastically to a strain where phase 1 begins to yield in compression (denoted as $\sigma_R$ in Figure 2.5). It is important to understand that the magnitude of the

yield stress of the composite in the forward direction is not equivalent to that observed in the reverse direction. This results from the fact that, at the point of unloading from tension, the composite stress is higher than that in the plastically deforming phase. Thus, as the composite is unloaded elastically, the stress in the softer phase will reach its yield stress before the composite stress reaches $-\sigma_m$. The difference between the composite stress and the stress in phase 1 can be thought of as a compressive internal stress that is acting on phase 1. Similarly, there will be a balancing tensile internal stress in phase 2 (i.e. the stress in phase 2 is higher than the composite stress). This compressive stress, the difference between the composite stress and the stress in phase 1, is often referred to as the mean internal stress and is defined by

$$\langle\sigma\rangle = \frac{1}{2}(\sigma_F + \sigma_R) = (\sigma_F - \sigma_m) \qquad \textit{Equation 2.19}$$

where $\sigma_F$ is the composite flow stress in the tensile (forward) direction, $\sigma_R$ is the composite reverse yield stress and $\sigma_m$ is the current flow stress of phase 1 (matrix). It is conventional to re-plot the reverse portion of the flow curve in the positive quadrant of the stress-strain diagram as illustrated in Figure 2.6. Plotted in this way, one can graphically observe the origin of Equation 2.19.

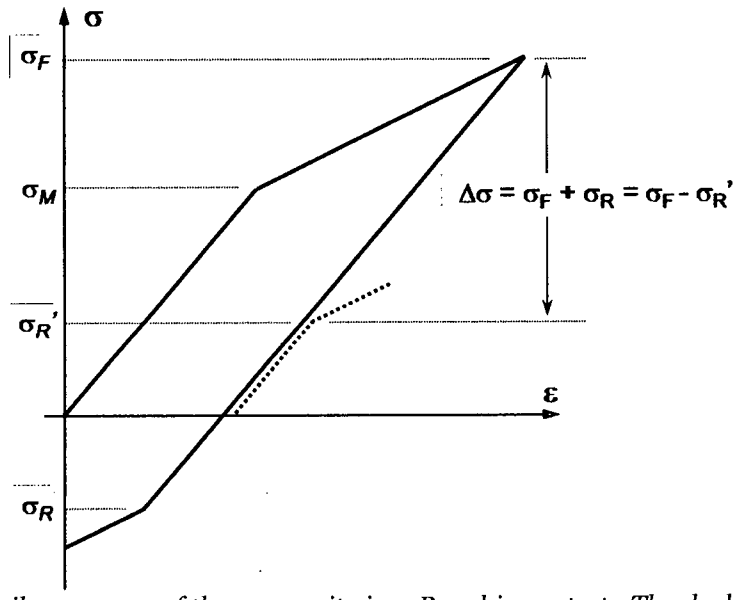


**Figure 2.6** *Tensile response of the composite in a Bauchinger test., The dashed line represents the compressive component of the curve re-plotted in the positive quadrant, i.e. it is mirrored about the elastic loading curve. The dotted line represents the extension of the forward curve.*

Considering the case where the soft phase has yielded and the hard phase is still elastic, the forward flow stress may be written as,

$$\sigma_f = \sigma_m + Ef\varepsilon_p \qquad \textit{Equation 2.20}$$

where $E$ is the elastic modulus, $f$ is the volume fraction of the second phase and $\varepsilon_p$ is the total plastic strain imposed on the composite. Similarly the reverse flow stress obtained on unloading from this position is given by,

$$\sigma_r = \sigma_m - Ef\varepsilon_p \qquad \textit{Equation 2.21}$$

Substituting equations 2.20 and 2.21 into Equation 2.19 gives

$$\langle\sigma\rangle = Ef\varepsilon_p \qquad \textit{Equation 2.22}$$

as the mean internal stress in the soft phase. It is important to notice the Masing model shows the internal stress to scale with both the volume fraction of the second phase as well as the total imposed plastic strain.

In the Masing model, it is assumed that the difference in plastic deformation between the two phases is accommodated solely by *elastic* internal stresses. As discussed

above (cf. section 2.5.1), some of this difference could also be accommodated if the plastically deforming phase was to undergo extra 'redundant' *plastic* deformation thereby generating geometrically necessary dislocations. In this case, the value of the plastic strain difference that would need to be accommodated by elastic internal stresses would be reduced. Moreover, once plasticity spreads to both phases, the rate of generation of internal stresses will drop to close to zero, though the internal stresses developed during the elastic-plastic regime remain.

### *Eshelby Model*

A more general model for calculating the internal stresses in two phase materials was originally put forth by Eshelby in 1957 [61]. In the Eshelby model, the full three dimensional stress state within an ellipsoidal phase embedded within a matrix can be calculated based on a 'stress free transformation' which results in a size change in the ellipsoid. When the ellipsoid is placed back in hole where it originated it will no longer fit without inducing a stress field. This internal stress is what the Eshelby model describes.

For the case of a single inclusion embedded in an infinitely large matrix where both phases are deforming plastically, the stress free transformation strain ($\varepsilon^T$) is the difference in plastic strain between the two phases. The stress within the inclusion resulting from this transformation strain is,

$$\sigma_I = C_M \left(S - I\right)\varepsilon^T \qquad \textit{Equation 2.23}$$

where $I$ is the identity matrix, S is the so-called Eshelby tensor (a function of the inclusion shape and elastic properties) and $C_M$ is the stiffness of the phases (assuming in this case that the elastic properties are the same for the two phases).

Since Eshelby's model applies to only a single inclusion in an infinite matrix, the mean stress in the matrix is zero (where the mean stress is defined as the difference between the average stress carried by the phase and the applied stress). In non-dilute

systems the mean elastic stress in the matrix is calculated from stress balance of the mean stress in the inclusions, $\langle\sigma\rangle_I$, and the mean stress in the matrix. The balance is given as

$$(1-f)\langle\sigma\rangle_M + f\langle\sigma\rangle_I = 0 \qquad \textit{Equation 2.24}$$

where $f$ is the volume fraction of inclusions. Thus the mean stress in the matrix is

$$\langle\sigma\rangle_M = -fC_M(S-I)\varepsilon^T \qquad \textit{Equation 2.25}$$

Equation 2.25 is important because again it shows that in the case of a plastically deforming material the mean stress in the matrix scales with the volume fraction of inclusions and the plastic strain. Simplifying to one dimension for embedded fibres or plates aligned parallel to the axis of loading, equation 2.29 reduces to [62,63],

$$\langle\sigma\rangle_M = fE_M\varepsilon^T \qquad \textit{Equation 2.26}$$

which is the same result as the Masing model described in the previous section.

### 2.4.3 Experimentally Quantifying Internal Stress

Several methods can be used to quantify internal stresses in a material. Two common experiments used to determine the magnitude of internal stress will be discussed in this section: The Bauschinger test and diffraction (x-ray and neutron).

#### *Bauschinger Tests*

As seen in the previous discussion of the Masing model (section 2.5.2) the presence of internal stresses results in different forward and reverse loading curves. Real materials containing internal stresses do exhibit a reduction in the compressive yield stress but also exhibit a rounding of the initial plastic region of the reverse curve as compared to the forward curve. This 'transient softening' effect was first published by Bauschinger in 1881 (as cited by Sowerby and Uko [64]). This difference in the

magnitude of the yield stress and the 'roundness' of the tensile and compressive loading curves is generally referred to as the Bauschinger effect (see e.g. Abel [65] and Sowerby and Uko [64] for detailed reviews).

The Bauschinger effect has been observed in many materials ranging from porous sintered steel [66] to directionally solidified aluminium-nickel alloys. However, it is most prominent in materials which contain strong elastic second phase particles that are in the form of rods or plates oriented parallel to the direction of loading [67].

Based on the models presented in the previous section, the results of a Bauschinger test can be used to identify the internal stress in the matrix, $\langle\sigma\rangle_M$, via the Bauschinger stress, $\Delta\sigma$

$$\Delta\sigma = 2\langle\sigma\rangle = \sigma_F + \sigma_R \qquad \textit{Equation 2.27}$$

Where the terms in equation 2.27 have been defined above (cf. figures 2.5 and 2.6). Although in the ideal case the Bauschinger test is a relatively simple way to measure the magnitude of the internal stresses in a material, it does have its limitations. Stobbs and Paetke [68] studied the Bauschinger effect in patented steel wire and discussed some of these difficulties. First, the transient softening or the rounding of the initial plastic portion of the reverse curve makes it difficult to pinpoint the reverse yield stress to be used in Equation 2.27. It has been argued [63] that the reverse yield stress should be taken at the point where the forward and reverse curves become parallel. In most materials in order for the curves to become parallel a large amount of compressive strain must be achieved, but due to the geometry of typical Bauschinger test samples the required strains are difficult to achieve without barreling or buckling of the sample. In materials containing fibres or plates parallel to the axis of loading, the magnitude of reverse loading may be limited by the onset of micro-buckling at the microstructural scale (e.g. Tao and Embury [69]). Moreover, it has been argued from a theoretical point

of view that the forward and reverse curves may never become exactly parallel in real materials [70].

To avoid large reverse strains several studies have attempted to semi quantitatively assess internal stresses by using only small reverse strains. Moan and Embury [71] and Corbin *et al.* [72] showed that this method could capture the evolution of the internal stresses in aluminium-copper and aluminium-SiC composite materials. Sinclair *et al.* [55] used simple load-unload tests where samples where loaded first in tension then unloaded but not into compression. This can be implemented if the internal stresses are large enough to cause reverse yielding on unloading from tension. From these tests and Equation 2.19 the magnitude of internal stresses were semi-quantitatively evaluated.

### *Diffraction Experiments*

The use of diffraction techniques has proven to be a valuable tool in the investigation of internal stresses because it allows for the direct measurement of the internal strain in both phases of the composite [73]. In this method the change in the lattice parameter of the crystal lattice is used to determine the elastic strains in each of the component phases. If the measurements are made when the material is in the unloaded state then the measured elastic strains correspond to the mean internal stresses defined above (refer to the discussion of the Eshelby Model in Section 2.5.2.). Early experiments by Wilson [67] and Wilson and Konnan [74] used x-ray diffraction to measure internal stresses of iron alloys containing carbide particles during tensile, torsion and bending. These experiments showed that during the uniaxial loading of high carbon steel the internal strain in the ferrite saturated after small strains of less than 1% while the strain in the cementite increased to macroscopic strain of 6%. Upon unloading residual strain in the cementite was found to be much larger than in the ferrite, leading

to the conclusion that the internal stress in the matrix is balanced by larger stress of the opposite sign in the hard cementite particles. By comparing low carbon and high carbon steels they were also able to show that 60% of the additional work hardening of the high carbon steel could be accounted for by the internal stress in the ferrite matrix [74]. By comparing data from Bauschinger tests and x-ray diffraction on similar samples, Wilson was able to show that Equation 2.27 adequately described the behaviour of these materials.

More recently neutron diffraction has allowed for more accurate studies of internal stresses. While x-rays generated from laboratory x-ray sources penetrate only a short distance into the surface of a material, neutron's can penetrate through several centimeters of a metal. This eliminates uncertainties created by surface relaxation and deformation induced during surface preparation [70]. Neutron diffraction has, for instance, been used extensively to study residual stresses in drawn pearlite wire [70,75,76].

A neutron diffraction study of copper-12.5 wt% niobium wire was made by Han *et al.* [56] to examine the internal stresses developed in the radial direction as a function of drawing strain. It was found that the residual tensile elastic strains carried by the niobium were exceedingly high (up to 1.4% after a drawing strain of 1.7). Klassen *et al.* [73] examined the internal strain of copper-25 wt% niobium parallel to the drawing direction as a function of annealing time at various temperatures. The effect of thermal treatment on the lattice strain is show in Figure 2.7. Again, after drawing the copper is left in residual compression and the niobium in residual tension. It was also found that annealing temperatures greater that 300°C were required to initiate relaxation in the niobium phase at heat treatment times of 15 hours.

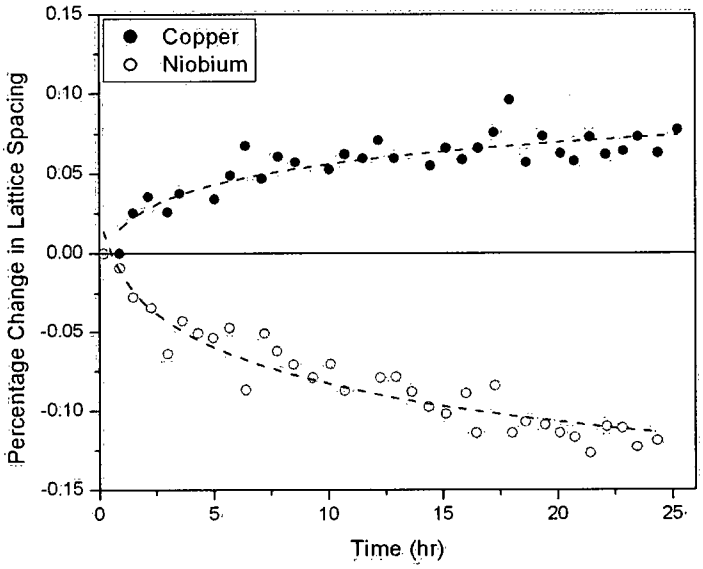


**Figure 2.7** *Percentage change in lattice spacing versus time at 375°C for copper, measured by (222) peak, and niobium, measuared by (220) peak re-plotted from [73].*

# CHAPTER 3

# SCOPE AND OBJECTIVES

The objective of this investigation is to examine the mechanical response of several codeformed copper-niobium composites in order to determine:

- the roll internals stresses play in strengthening two-phase codeformed materials,
- the dependence of internal stress on the deformation method and resulting microstructure,
- the thermal stability of internal stresses and the consequences that may come with the relaxation of such stresses.

The presence of internal stresses and their magnitude will be studied using monotonic tensile, load-unload and tension compression tests. This study will examine three types of codeformed copper-niobium composites. Two wire drawn materials, *in-situ* and bundle drawn wire, and a layered copper-niobium sheet will be investigated to determine the effect that various processing methods may have on internal stresses. Annealing various samples at temperatures ranging from 400°C to 600°C will allow for the assessment of the effects of temperature on the strength and levels of internal stress in the copper-niobium composites.

# CHAPTER 4

# EXPERIMENTAL METHOD

The experimental work completed during this thesis will be discussed in this chapter. The experimental methods will be discussed in three parts. First, the materials used will be discussed, followed by the processing methods. Finally, the methods used to characterize the processed material will be reviewed.

## 4.1 Materials

Two forms of fine-scale codeformed copper-niobium material were studied. As drawn wires of copper-niobium were obtained from the National High Field Magnet Laboratory (NHFML), Florida, USA. Also, copper-niobium sheet fabricated by roll bonding at the University of British Columbia (UBC) has been studied. The conditions used to produce these materials will be discussed.

### 4.1.1 Cu-18vol%Nb Wire

This study investigated the properties of both copper-niobium *in-situ* drawn wire and bundle drawn composite wire produced at NHFML for use as high strength electrical conductors. A detailed description of the processing routes used to fabricate these materials can be found elsewhere [2]. Here the salient details regarding the material fabrication will be given.

The *in-situ* composite wire contained 18 volume percent niobium. The material was initially cast with the proper chemistry to form a rod containing dendrites of Nb in a Cu matrix. To allow for drawing, the rod was forged to reduce its diameter. Forging was followed by wire drawing to a total processing strain of approximately 9.

The bundle drawn wire was also produced to contain approximately 18 volume percent niobium. Niobium was initially hot extruded to form a rod, and then placed in a copper tube ('can') and again extruded to reduce the diameter. The copper-niobium rod was then drawn to form a wire with a hexagonal cross section. Approximately 400 wires were bundled and then redrawn to further reduce the microstructure. The bundling and drawing steps were repeated until the wire had undergone a total processing strain of 7. Both types of wire received from NHFML had been given a small amount of rolling reduction following drawing to create flat surfaces to facilitate the winding of the wire into electrical coils.

### 4.1.2 Temperature Treatments

Annealing of the *in-situ* and bundle drawn wire was done in a stirred salt bath. Samples were placed directly in the molten salt once the bath had reached the desired temperature. Annealing treatments occurred for a time of 3 hours, following which the samples were removed from the molten salt and quickly quenched in still water.

### 4.1.3 Starting Materials for the Layered Composite

Pure copper and niobium sheet was used to produce the rolled-bonded material. The pure copper was cut from an ingot of 99.99% Cu, cold rolled to a thickness of approximately 0.180 mm, and then annealed in a salt bath at a temperature of 500°C for 10 minutes to obtain a fully recrystallized sheet. Table 4.1 shows the composition of the copper used to produce the layered composites.

**Table 4.1** *Copper composition in ppm*

| Na | Si | P | K | Ca | Ti |
|---|---|---|---|---|---|
| < 10 | <10 | <100 | <50 | <10 | 0.5 |

| Fe | Ni | Ag | Sn | Sb |
|---|---|---|---|---|
| <10 | <0.5 | 11.7 | 2.05 | 3.05 |

Niobium was purchased from Alfa Aesar as 99.8% niobium foil with a thickness of 0.127 mm. The niobium was received in an annealed state. Table 4.2 shows the composition of the niobium.

**Table 4.2** *Niobium Composition in ppm*

| Al | C | Cr | H | Mo | Ni | Si | W |
|---|---|---|---|---|---|---|---|
| <20 | 40 | <20 | <3 | <30 | <20 | <50 | <30 |

| Be | Co | Fe | Hf | N | O | Ta | Zr |
|---|---|---|---|---|---|---|---|
| <5 | <10 | <40 | <50 | <20 | <50 | 300 | <50 |

## 4.2 Processing of Layered Composites

Details of the processing methods used in producing the copper-niobium laminate examined in this study are covered in this section. The compression procedure and apparatus used will be discussed first, followed by the rolling procedure.

### 4.2.1 Compression

Samples were made by cutting the rolled and annealed copper and niobium foil into 12.5 mm by 25.0 mm rectangles. Both the copper and niobium sheets where rinsed with acetone followed by a 2 minute ultrasonic washing in denatured ethanol. To produce a fresh copper surface, the copper foils where then etched in a solution of 50% nitric acid ($H_2NO_3$) and water for several seconds. Samples were then rinsed in flowing water followed by denatured ethanol. The copper and niobium foils were dried in a stream of warm air.

The copper and niobium foils were stacked, alternating copper and niobium. The stacks always started and ended with copper layers, thus the number of copper layers in the stack is equal to $N_{Nb}+1$, where $N_{Nb}$ is the number of niobium layers.

This study examined copper-niobium laminate composites containing three different volume fractions of niobium. This was done by varying the number of copper foils in a layer of copper. At the largest volume fraction niobium 1 copper layer was used for every niobium layer while at the lowest volume fraction niobium 3 copper foils were used for each niobium layer. Table 4.3 describes the initial layer structure of the samples.

**Table 4.3** *Description of method of achieving three volume fractions of niobium*

| Number of Copper Foils | Copper Foils per Niobium Layer | Number of Niobium Layers | Niobium Volume Fraction |
|---|---|---|---|
| 15 | 1 | 14 | .40 |
| 20 | 2 | 9 | .24 |
| 21 | 3 | 6 | .17 |

Hot compression was used to provide an initial diffusion bond between the copper-niobium layers. This was accomplished using a MTS servo-hydraulic load frame controlled with an INSTRON 8500R controller. Two 500 Watt heating cartridges were used to heat each platen to a temperature of 550°C. Compression was performed under a load of 20 kN. On a sample with dimensions of 12.5 mm by 25 mm a load of 20 kN results in a stress of approximately 64 MPa on the stack. The setup is shown schematically in Figure 4.1. Bonding was done for a period of 4 hours. The time and temperature for bonding were determined through initial trial and error. To prevent the stacks from bonding to the compression platens the stacks where wrapped in stainless steel foil.

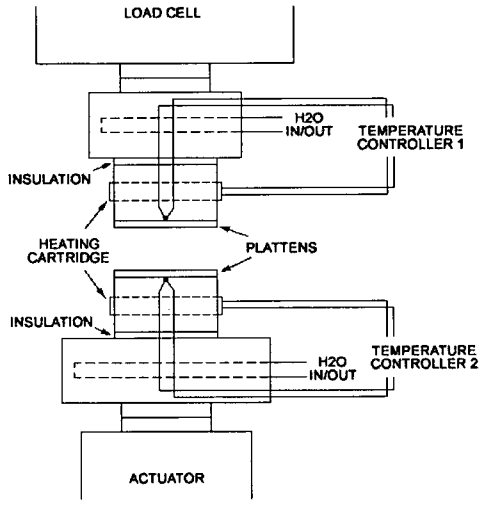


**Figure 4.1** *Compression setup used to initially bond copper-niobium foils.*

### 4.2.2 Accumulated Roll Bonding

A laboratory scale rolling mill was used to perform co-deformation on the bonded copper-niobium material. The roll diameter was 152 mm and turned at a rate of 14 rpm. Before rolling, the rolls were cleaned using 180 grit sand paper and oil to remove contamination, followed by washing with degreaser and finally washing with acetone. No lubrication was used.

Accumulated roll bonding started with removing any niobium oxide from the sides of the as bonded copper-niobium stack sample using 400 grit sand paper, and removing any copper oxide from the top and bottom of the stack with 600 grit sand paper. The initial thickness was measured using a digital micrometer and noted. The sample was then cold rolled to a thickness of approximately 0.25 mm. The strip was then cut to lengths of 100 mm. In order to facilitate folding without layer de-cohesion and to aid in the accuracy of folding small slits were cut at one-quarter, one-half and three-quarters of the samples length (Figure 4.2).

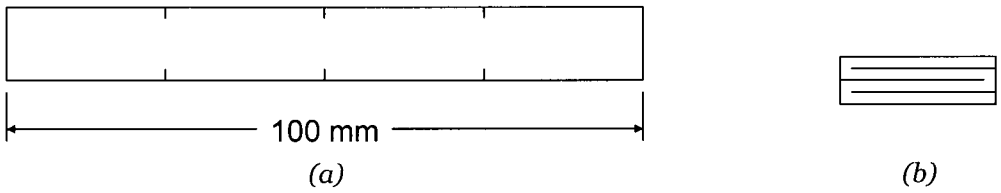


**Figure 4.2** *Illustration of the folding process for accumulated roll bonding: (a) the cut strip; (b) the folded stack*

Before the sample was folded it was washed with acetone to remove any grease transferred during rolling and handling. Then the 100 mm strip was folded at the slits, the ends were pinched using a hammer and anvil to tightly fold the new stack. The stack was then placed in a tube furnace for a period of 300 seconds at a temperature of 200°C.

The sample was removed from the furnace and immediately rolled. The sample illustrated in Figure 4.2b would have been rolled from right to left. A minimum reduction of approximately 40 percent was required to produce bonding sufficiently strong to tolerate the next rolling step. The sample was then cold rolled to a minimum thickness of approximately 0.25 mm. Again the thickness of the strip was measured with a digital micrometer and recorded. This folding and rolling procedure was repeated until the desired strain was imposed on the sample.

## 4.3 Material Characterization

This section describes the techniques used to characterize the properties of the copper-niobium composites examined in this work. The various types of tensile tests carried out will be described first followed by the procedure used for taking micro hardness measurements.

### 4.3.1 Tensile Testing

All of the tensile related tests carried out during this study where done using an MTS servo-hydraulic load frame and an INSTRON 8500R digital controller (the same as

in the case of the hot compression described above). Hydraulic grips were used to hold the samples during testing.

The dimensions of the samples used for tensile and load-unload tests on the roll-bonded copper-niobium are shown in Figure 4.3.

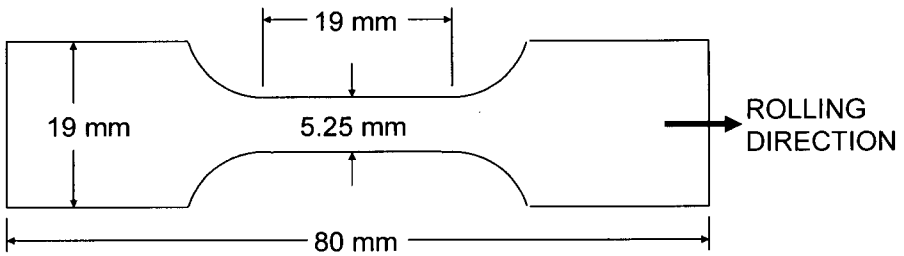


**Figure 4.3** *Sample geometry used for tensile and load-unload test on laminate composite.*

### *Monotonic Tensile*

Monotonic tensile tests were used to determine the mechanical response of the various composites studied. Samples for tensile testing were punched from the rolled strip to be pulled in a direction parallel to the rolling direction. All tests were done under displacement control at a crosshead speed of 0.0125 mm/s resulting in a strain rate on the order of $10^{-3}$ /s. An extensometer with a gauge length of 12.5 mm was used to measure strain. All tests were done under ambient conditions (temperature approximately 25°C).

### *Load-Unload Tests*

Simple load-unload tests were conducted on the layered and *in-situ* composite. For the layered material the sample size is the same as described in Figure 4.3. For the *in-situ* wire a gauge length of 20 mm was etched into the sample using 50 % nitric acid in water by first cutting a short section of wire then applying protective lacquer to the grip ends in order to allow etching to occur only in the gauge section. As a result the cross

section of the wire in the gauge section was reduced to approximately 2.8 mm by 1.8 mm (rectangular).

Once the sample had been secured in the hydraulic grips of the tensile machine, the extensometer with a gauge length of 12.5 mm was placed in the center of the gauge section. Samples were loaded under displacement control, at a strain rate of approximately $10^{-3}$ /s, until a predetermined value of engineering strain was reached. At that point the sample was unloaded under load control to a value of 0 kN. The rate at which the sample was unloaded was matched to the time required to reach the desired strain during the initial loading. After each load-unload cycle the permanent plastic strain was taken as the new zero point and the load-unload cycles continued until the sample failed.

### *Bauschinger Tests*

Bauschinger tests were limited to the bundle drawn copper-niobium wire owing to the necessity of avoiding buckling and/or barreling during the compressive portion of the test. Previous investigators have identified a ratio of 3:1 – 4:1 between the gauge length and cross-sectional diameter of samples to be ideal for avoiding inhomogeneous deformation on compression [70, 72]. To achieve these sample dimensions, a gauge section of approximately 10 mm, was etched into the wire by first applying lacquer to the grip end and submerging the sample in an acid solution. To allow for the removal of both copper and niobium a solution of $2H_2NO_3$:2HCL:$2H_2O$:1HF was used. An artificial fillet was added to the gauge section by removing the sample from the acid and removing a small amount of lacquer from the areas near the gauge section, then placing the wire back in the acid to complete the etching. The sample was removed from the acid solution and rinsed when the cross section in the gauge section reached a dimension of approximately 2.2 by 3.1 mm.

The dimensions of the sample were measured using a digital micrometer and recorded. Next the sample was placed in the tensile rig and two directionally opposing extensometers placed on the sample. One extensometer was placed in the gauge length while the other was placed slightly outside on the grip sections in order to check for alignment of the sample during the test and to observe the onset of inhomogeneous deformation in compression. Alignment within the grips was checked with a traveling microscope and alignment of the load train was checked by bringing the grips, containing a tensile sample cut in half, close together. The load train was then adjusted to make the surfaces of the cut sample parallel. The sample was loaded elastically to a load of 0.25 kN under displacement control at a rate 0.0125 mm/s then unloaded to a load of 0 kN to ensure proper attachment of the extensometers. Bauschinger tests were done by straining the samples to either to 1 or 2 % plastic strain in tension followed by loading in compression. Compression was continued until the extensometers showed buckling and the test was stopped.

### 4.3.2 X-Ray Diffraction Techniques

X-ray diffraction was done on a Bruker AXS D8 Discover with a GADDS (2D area detector). The unit used a copper anode using Cu-Kα radiation. Pole figure data was manipulated with POPLA texture software which allowed for reconstruction, rotation and plotting of the pole figures.

### 4.3.3 Micro Hardness Measurements

Micro hardness measurements were made on a Micromet 3 micro hardness tester. Before testing, samples were polished to a 1 μm diamond finish. A minimum number of 5 hardness values where taken, and the average was used as the data point.

## 4.4 Microscopy

### 4.4.1 Metallography

SEM samples prepared for metallography were first mounted in epoxy, then ground and polished by hand to a 1 μm finish. The samples were then placed in an automatic vibratory polisher with only the sample holder as a weight. They were polished at 80 % speed for 3 hours then the speed was reduced to 40% for a period of 1 hour. Samples were viewed in a Hitaichi S-3000N variable-pressure ESEM, thus it was not required that they be broken from their epoxy mounts.

Fracture surfaces where examined in either a Hitaichi S-3000N variable-pressure ESEM or a Hitatchi S-2300 SEM.

### 4.4.2 Extracted Niobium Filaments

Niobium filaments for SEM analysis were taken from both the in-situ and bundle drawn copper-niobium composite. First the copper matrix was dissolved from a small piece of wire in concentrated nitric acid. When the solution no longer reacted with the sample the filaments were allowed to settle at the bottom of the test tube and the acid was removed using a pipette. The filaments were then washed with distilled water 3 times until there was no trace of acid. Once the acid was completely removed, the water was replaced with ethyl alcohol. Using a pipette, the alcohol suspension of niobium filaments was placed on a copper TEM grid. After evaporation of the alcohol the samples were observed in a Hitachi S-570 SEM using secondary electrons and a 20 kV beam.

### 4.4.3 Transmission Electron Microscopy

The process for creating TEM specimens first involved cutting 25 mm strips from the as rolled composite. A 2 mm thick layer of copper was then electroplated onto the strips using a solution of 200 g $CuSO_4$, 100 g $H_2SO_4$, 1 g Dextrin and enough $H_2O$ to make 1L at a current density of 100-150mA/cm$^2$. Using a small abrasive saw 1 mm slices from the

sample were cut from the plated strip and thinned using 600 grit grinding paper such that 3 mm disks could be cut from the center of the slices using a small mechanical punch. The disks were then thinned to a thickness of 70-100 μm using a disk grinder on 600 grit grinding paper lubricated with water. To further thin the samples they were placed in a VRC Group Dimpler, which thinned only the center of the 3 mm disk using a small grinding wheel and 6 μm polishing media. The dimple was polished using a polishing wheel wrapped in polishing cloth and 0.5 μm Syton. The dimpler reduced the thickness in the middle of the sample to approximately 10 μm. In order to produce a wedge with electron transparent edge the sample was then ion milled using an VCR Group unfocused argon ion miller. The sample was milled at an angle of 30° for several hours, and then milled at 15° until a hole formed in the center of the sample. TEM observation was carried out on a Hitachi H-800 TEM at 200 kV.

# CHAPTER 5

# EXPERIMENTAL RESULTS

The purpose of this chapter is to present the results of the experimental work described in the previous chapter. Chapter 4 will be divided into 3 sections. First, the results pertaining to the production, characterization and mechanical testing of the multiple roll bonded copper-niobium laminate will be given. Next, the results of the characterization and mechanical testing of the *in-situ* wire followed by the bundle drawn wire will be put forth.

## 5.1 Copper-Niobium Laminate

### 5.1.1 Laminate Production

Roll bonding was done according to the technique discussed in chapter 3. The initial bonding parameters were chosen after a series of initial experiments that varied the bonding temperature, time and load. A bonding temperature of 550 °C for 4 hours at a load of 20 kN resulted in a bond sufficient to withstand the first roll pass yet minimized the time required for the production of a single stack.

Rolling the stack to a thickness of 250 μm resulted in a strip with a length on the order of 45 cm. As a consequence of the rolling process the rolled strip had significant edge cracking, which needed to be removed after the sample was folded. Figure 5.1 shows the sample at different stages of the roll bonding process. It was found to be very important to completely remove the edge cracks produced by the previous rolling as their

severity increased with each pass. It was also found that a folded sample with a length of 25 mm resulted in the smallest amount of 'layer sliding' during rolling. The direction the sample was fed into the rolls also helped to minimize the layer sliding during the rolling process.

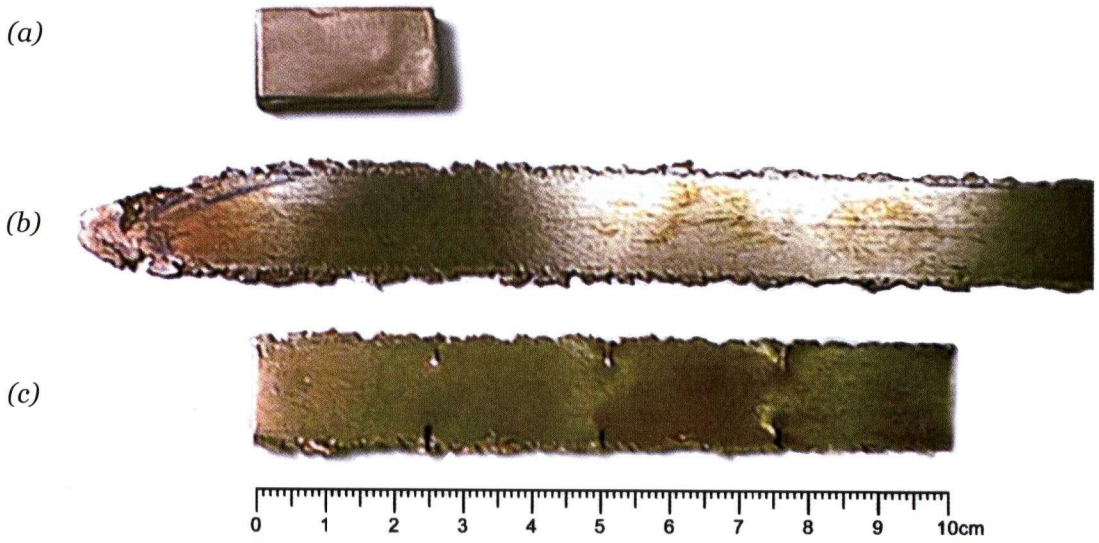


**Figure 5.1** *Images of rolled copper-niobium sheet:(a) as-bonded stack; (b) rolled strip; and (c) 10 cm strip ready for folding followed by further rolling.*

As the imposed strain increased it became more difficult to successfully bond the folded stack. This was attributed to the hardness of the sample after each rolling pass. For samples at process strains less than 5 it was found that during 300 seconds of heating at 200°C the material had sufficiently softened to allow for the sample to bond on the next rolling step. However, at process strains greater than 5 the hardness of the sample was no longer affected by the heat treatment as shown in Figure 5.2.

During a process of trial and error it was found that in order to produce bonding sufficient to withstand further rolling an initial reduction of approximately 40 percent was required. Reductions of less than 40 percent resulted in poor bonds, while greater reductions tended to result in the layers of the stack sliding against one another.

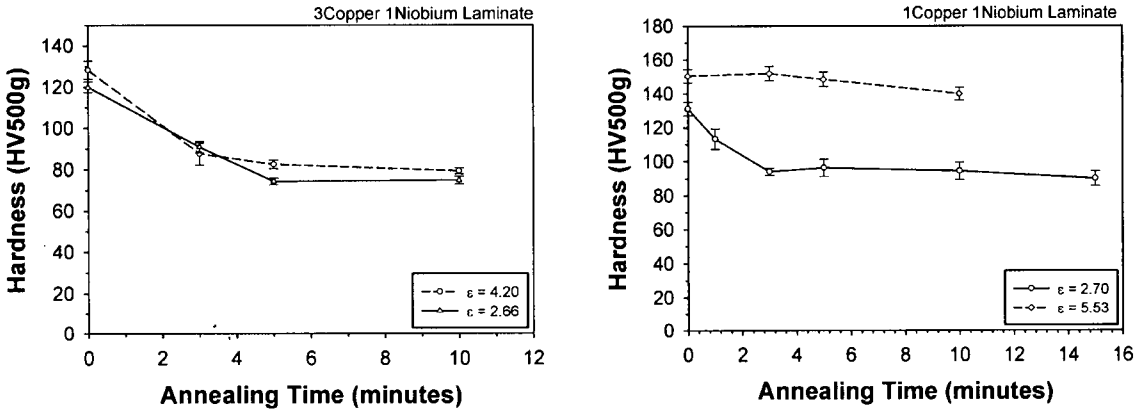


*(a)* *(b)*

**Figure 5.2** *Variation of hardness with annealing at 200°C for two different levels of rolling strain : (a) 17 vol.% Nb and (b) 40 vol.% niobium. Hardness values are in kg/mm².*

## 5.1.2 Microstructural Characterization

Materials containing three volume fractions of niobium, 40, 25 and 17 percent, have been studied. For each volume fraction samples were processed to total imposed rolling strains of approximately 2.5, 5 and 7. Figure 5.3 and Figure 5.4 show the evolution of the microstructure as a function of total imposed strain and niobium volume fraction as viewed parallel to the rolling direction (Figure 5.3) and transverse direction (Figure 5.4). The niobium layers were observed to remain largely continuous up to the largest strain levels, though strong variations in layer thickness were observed. This was found to be particularly true for samples viewed perpendicular to the rolling direction (Figure 5.4).

Figure 5.5 shows three TEM micrographs of the 17 volume percent niobium composite processed to a strain of 7 viewed with the rolling direction out of the page. Preparation of TEM foils was found to be difficult due to the resistance of the Nb layers to the ion milling. In many cases, the viewable areas were found to be formed within the electroplated copper and not in the sample itself. For this reason, only this one condition was focused on for TEM observation.

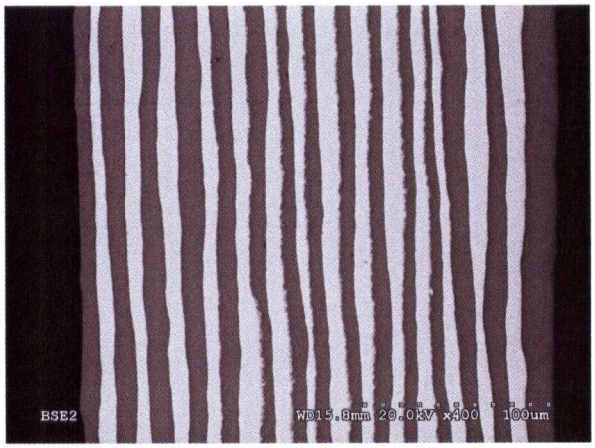


*(a)*

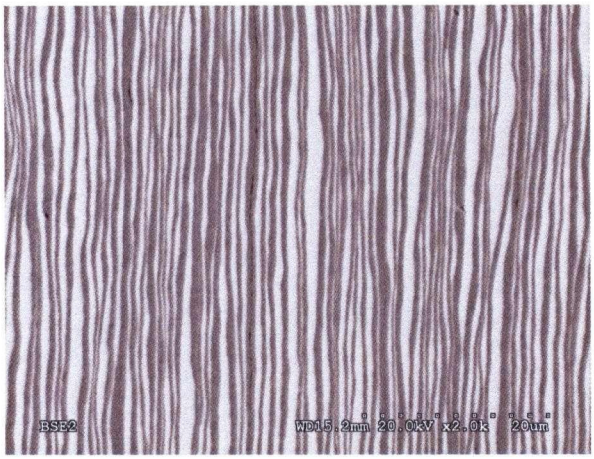


*(b)*


*(c)*

**Figure 5.3** *Secondary electron SEM micrographs of laminate showing the evolution of the microstructure for: (a) 40% Nb ε=2.76; (b) 40% Nb ε=5.70; (c) 40% Nb ε=6.99; (d) 25% Nb ε=2.76; (e) 25% Nb ε=5.87; (f) 40% Nb ε=7.22; (g) 17% Nb ε=2.66; (h) 17% Nb ε=5.53; (i) 17% Nb ε=7.00. Rolling direction is vertical and the normal to the sheet is horizontal in these images.*

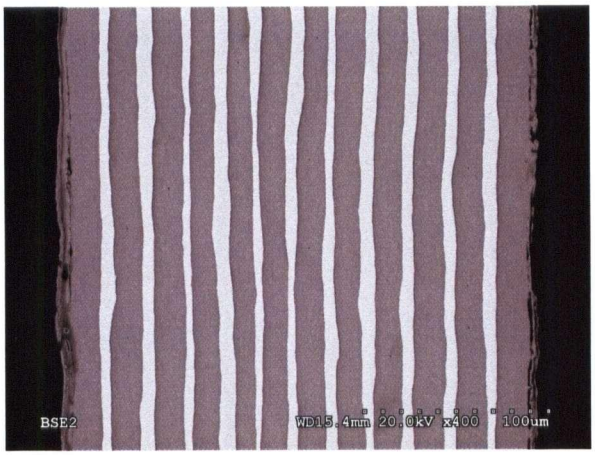


*(d)*

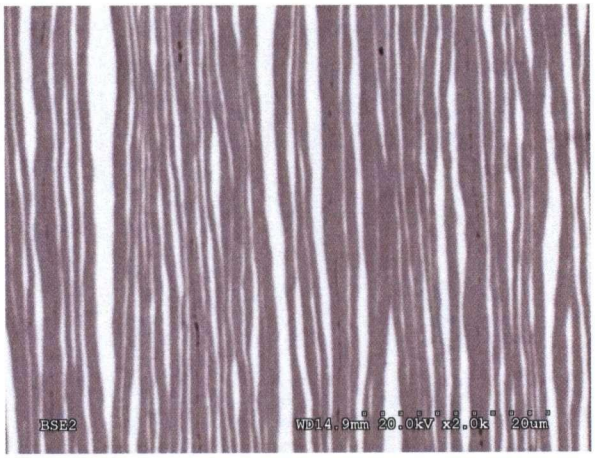


*(e)*

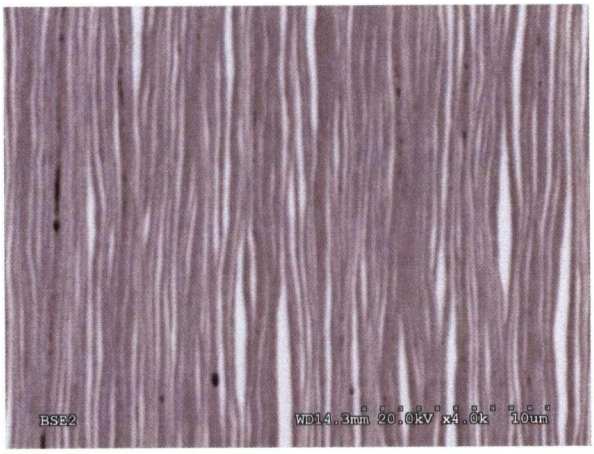


*(f)*

**Figure 5.3** *(continued) Secondary electron SEM micrographs of laminate showing the evolution of the microstructure for: (a) 40% Nb ε=2.76; (b) 40% Nb ε=5.70; (c) 40% Nb ε=6.99; (d) 25% Nb ε=2.76; (e) 25% Nb ε=5.87; (f) 40% Nb ε=7.22; (g) 17% Nb ε=2.66; (h) 17% Nb ε=5.53; (i) 17% Nb ε=7.00. Rolling direction is vertical and the normal to the sheet is horizontal in these images.*

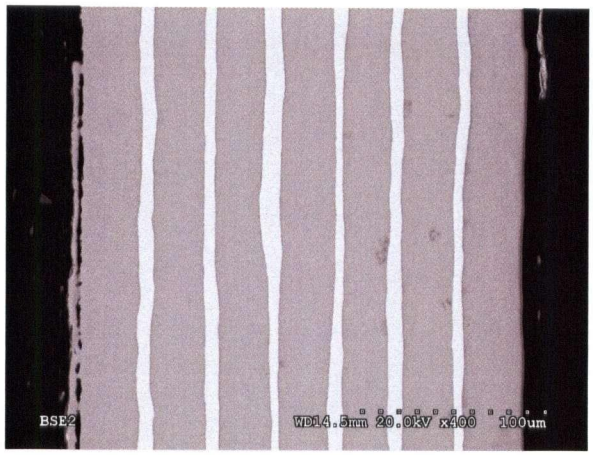


*(g)*


*(h)*

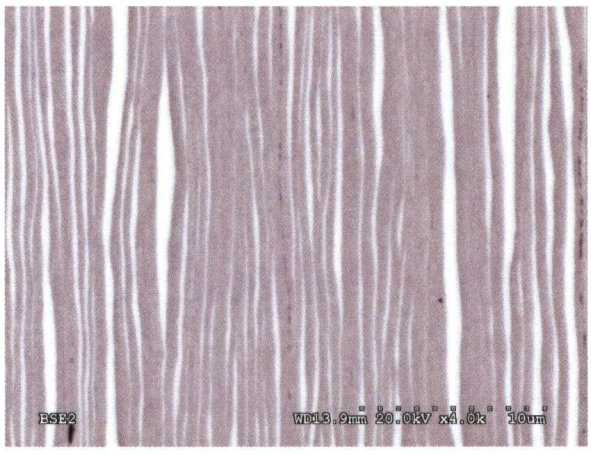


*(i)*

**Figure 5.3** *(continued) Secondary electron SEM micrographs of laminate showing the evolution of the microstructure for: (a) 40% Nb ε=2.76; (b) 40% Nb ε=5.70; (c) 40% Nb ε=6.99; (d) 25% Nb ε=2.76; (e) 25% Nb ε=5.87; (f) 40% Nb ε=7.22; (g) 17% Nb ε=2.66; (h) 17% Nb ε=5.53; (i) 17% Nb ε=7.00. Rolling direction is vertical and the normal to the sheet is horizontal in these images.*

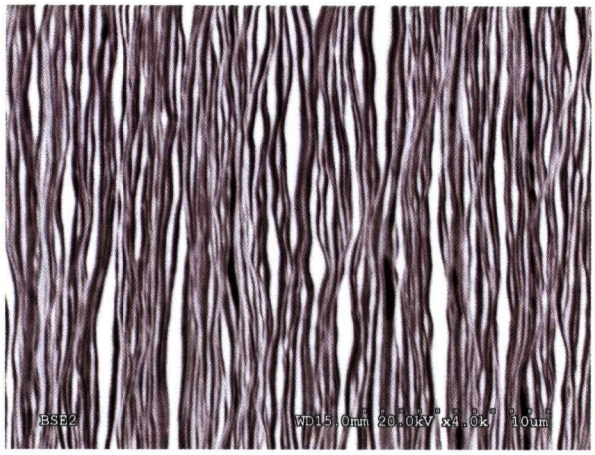


*(a)*

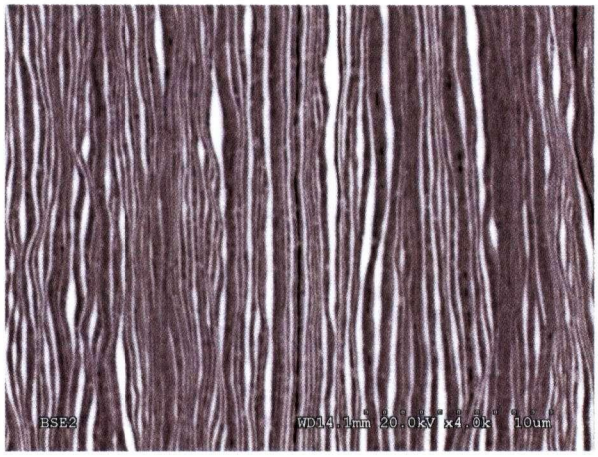


*(b)*


*(c)*

**Figure 5.4** *SEM micrographs of laminate where the rolling direction is normal to the page: (a) 40% niobium ε=6.99; (b) 20% niobium ε=7.22; (c) 17% niobium ε=7.00.*

At this level of strain the copper layers are composed of cells with dimensions of the layer spacing in the normal direction and at least several microns in the transverse direction (Figure 5.5a). In some cases, dislocations can be seen to be bowing out of the phase interface into the copper (e.g. Figure 5.5b).

In general the niobium layers are seen to be continuous. Detailed observation of the internal structure of the filaments, however, was limited due to the thickness of the layers and due to damage from the ion milling process.

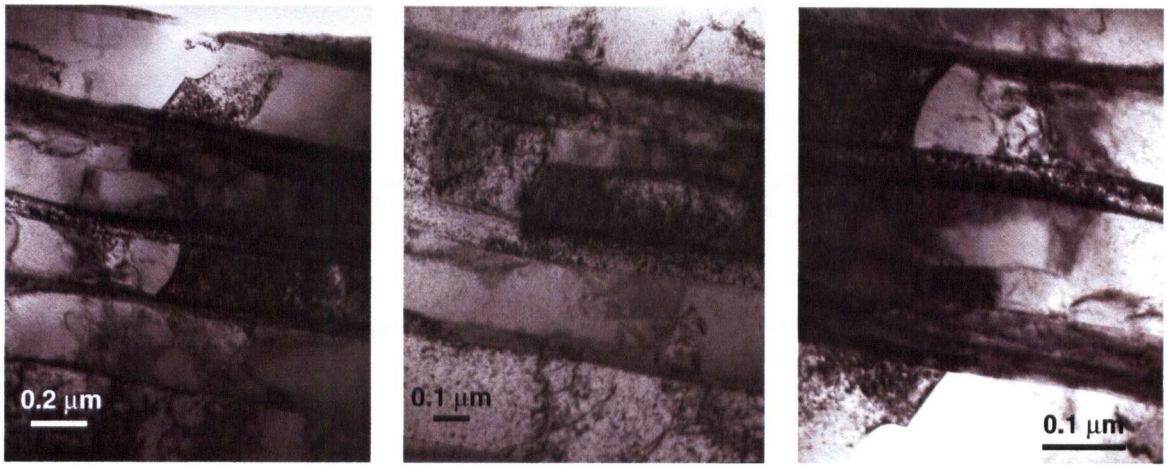


*(a)* *(b)* *(c)*

**Figure 5.5** *TEM micrographs showing three different regions in a 17% niobium sample after a stain of 7. Niobium appears as the dark bands in these micrographs.*

Though in general, the microstructures of the roll bonded materials were found to be relatively uniform, some regions were found to consist of poorly developed layers. Figure 5.6 shows an example of one of these regions in a sample with 25 percent niobium rolled to a strain of 7.0. These regions were exclusively found in samples with 25 and 40 percent niobium at the highest levels of strain studied at the location of previous roll bonded surfaces.

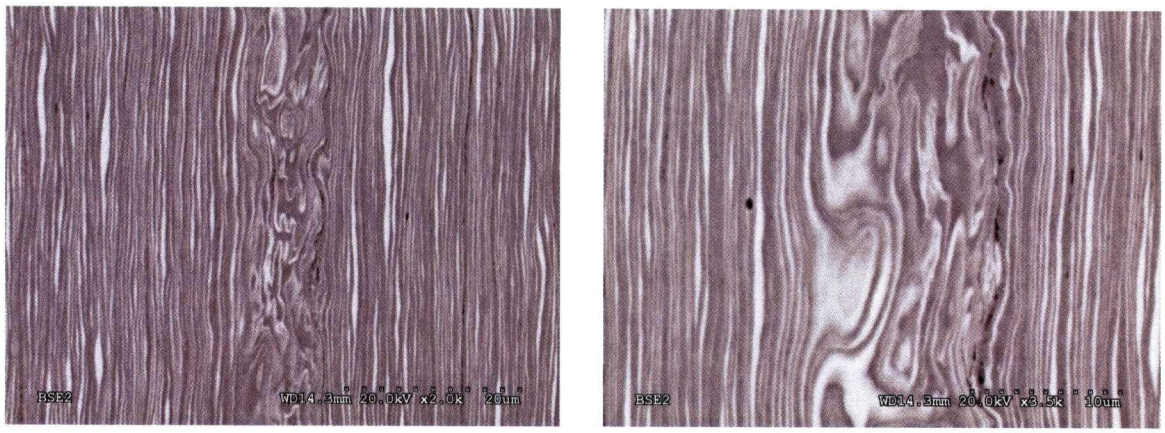


*(a)* *(b)*

**Figure 5.6** *Backscatter SEM images of the poorly developed layer structure*

From SEM micrographs of areas with uniform structure, similar to those shown in Figure 5.4, the layer thickness of the niobium filaments were measured as a function of rolling strain and niobium volume fraction. The measurements were made in the section viewed parallel to the rolling direction owing to the smaller variation in the width of the niobium layers. The average thickness of all of the measured layers are summarized in Figure 5.7 as a function of the imposed rolling strain (true strain = $\ln(t/t_o)$). Also shown on this plot are measurements made from TEM micrographs such as that shown in Figure 5.5. Though the measurements from TEM samples are of limited statistical significance, they do show good agreement with the observations from the SEM. The data obtained from SEM images of samples at high strains likely overestimate the true average thickness of the niobium given that it was difficult to resolve the finest sections of the niobium layers.

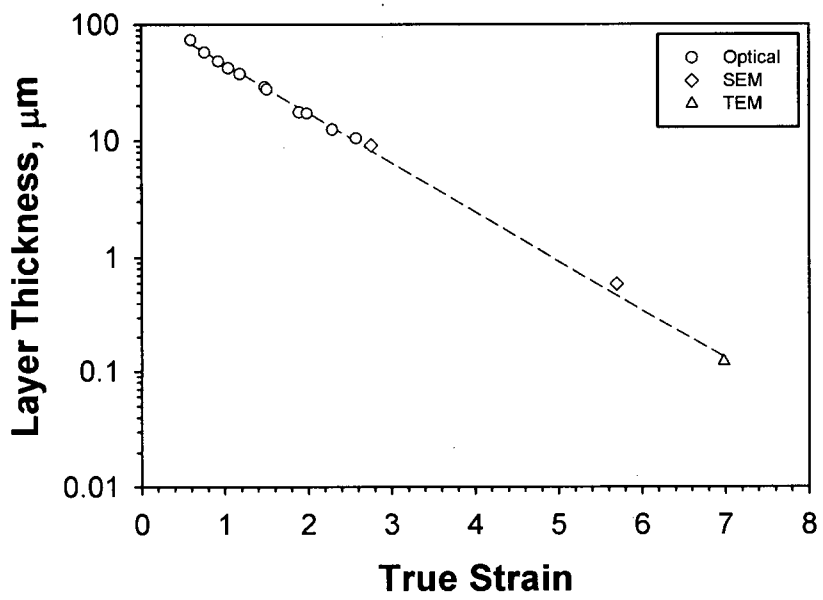


**Figure 5.7** *Layer thickness of layered composite as a function of imposed strain. The linear curve is described by 122.17exp(-0.978ε)*

To compare the tensile response for the various materials studied, it is important to ensure that the crystallographic texture of the material is not significantly different from one sample to the next. If there are differences in texture then the resulting mechanical properties should be corrected based on the value of the Taylor factors calculated from the textures. Figure 5.8 and Figure 5.9 show pole figures for niobium and copper from samples at two levels of strain. Both the copper and niobium layers exhibit preferred orientations consistent with those expected for bulk rolled materials. The important conclusion to draw from these observations is that there is little significant difference in the textures of the two levels of strains. Thus, for the remainder of this work, effects arising from textural differences between the rolled materials will be neglected.

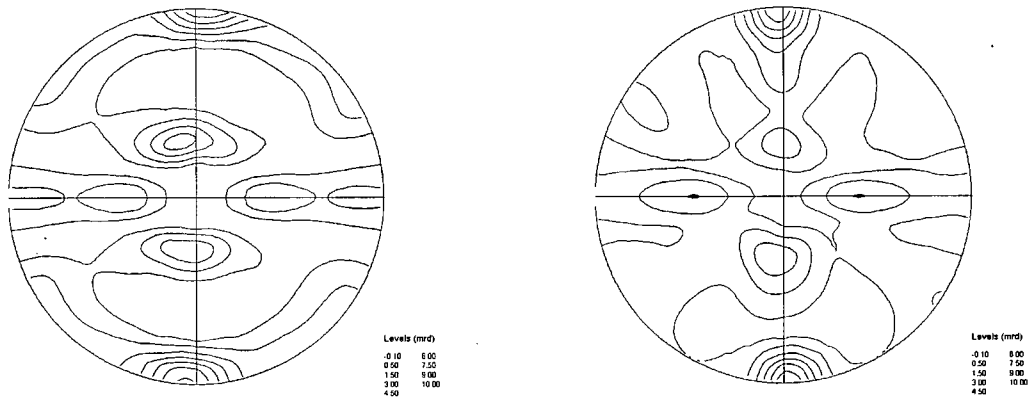

*(a)* *(b)*

**Figure 5.8** *{110} Niobium Pole figures: (a) 40% niobium ε=2.5; (b) 40% niobium ε=6.99.*

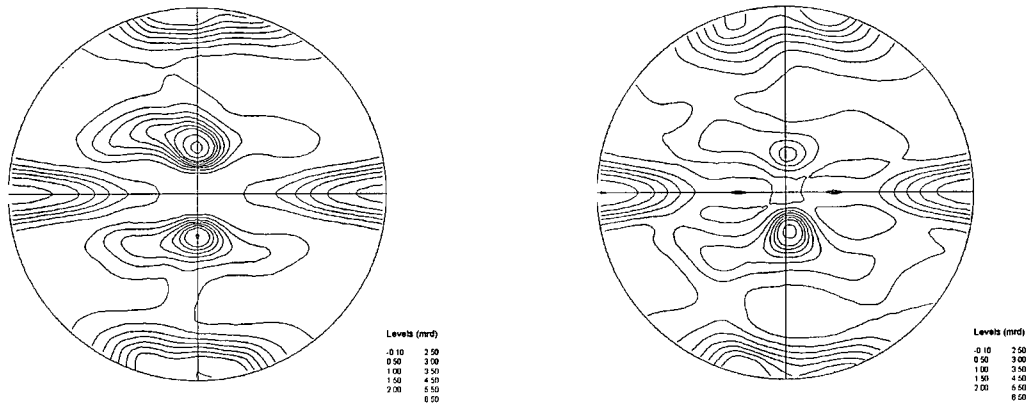

*(a)* *(b)*

**Figure 5.9** {111} copper *Pole figures: (a) 40% niobium ε=2.5; (b) 40% niobium ε=6.99.*

The tensile response for all of the conditions of niobium volume fraction and imposed rolling strain are summarized in Figure 5.10. Tensile tests were all conducted parallel to the rolling direction. Under all conditions, limited uniform elongation was observed, though all samples necked extensively before fracturing. Observation of most samples showed excellent bonding between the roll bonded layers with little or no evidence of debonding during necking. However, in some samples, it was found that debonding occurred during necking or even prior to necking. When it occurred prior to necking, it was accompanied by a visible drop in load. These samples were not considered for further analysis.

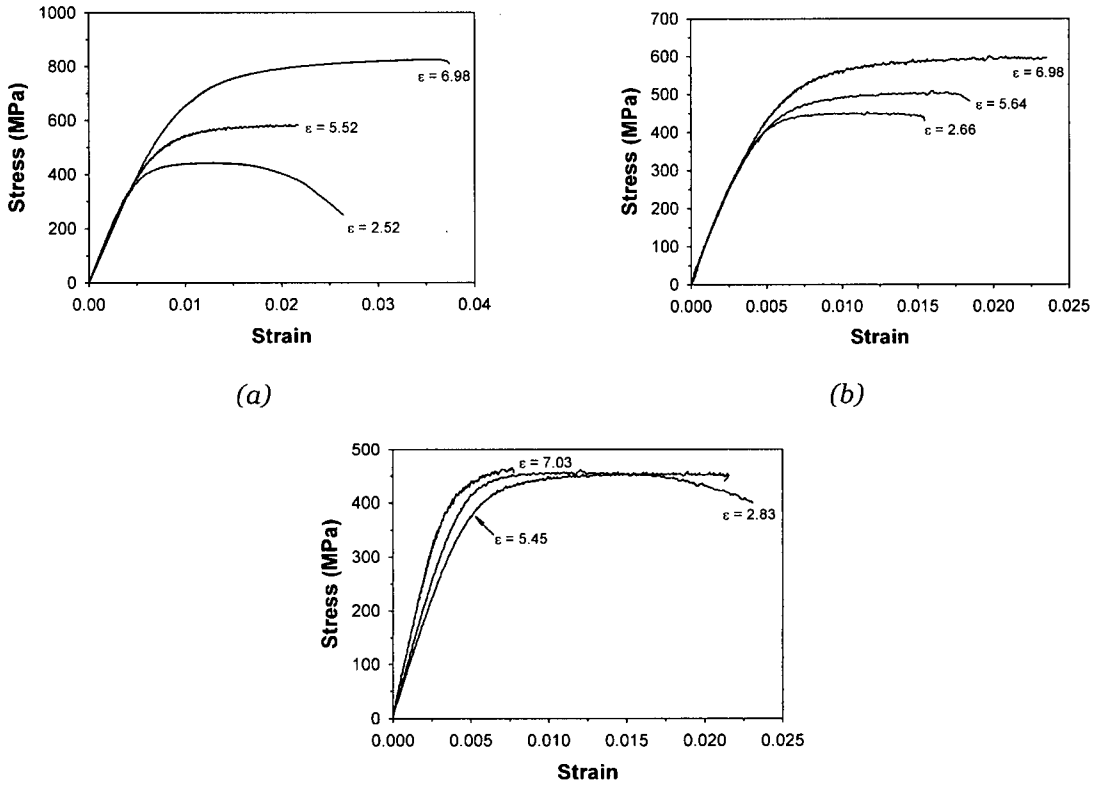


**Figure 5.10** *Monotonic tensile result: (a) 40% niobium; (b) 25% niobium; and (c) 17% niobium.*

Due to the small thickness of samples it was not possible to perform tension-compression Bauschinger tests on the laminates. Instead the hysteresis in the loading/unloading response has been observed. Figure 5.11 shows illustrative examples of the type of response observed in different samples. All samples showed some degree of hysteresis in their loading-unloading response. The results of the stress-strain response recorded in the load-unload experiments fell within the envelope of the monotonic tests as seen in Figure 5.11. However, in the case of the most heavily deformed materials with 40%Nb, much less uniform elongation was obtained in the load-unload experiments as compared to the monotonic tests.

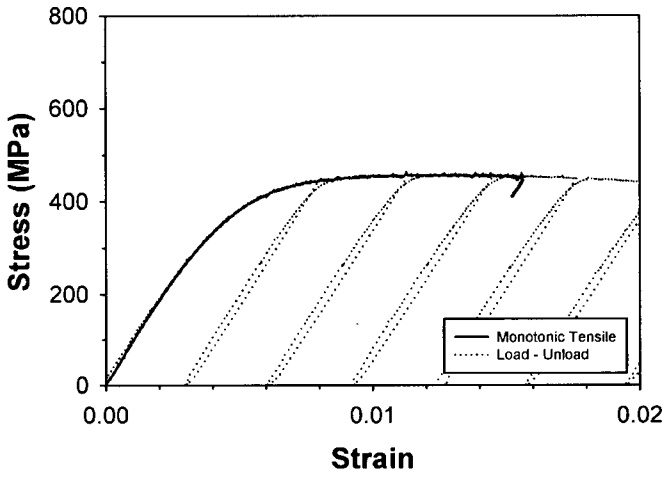


*(a)*

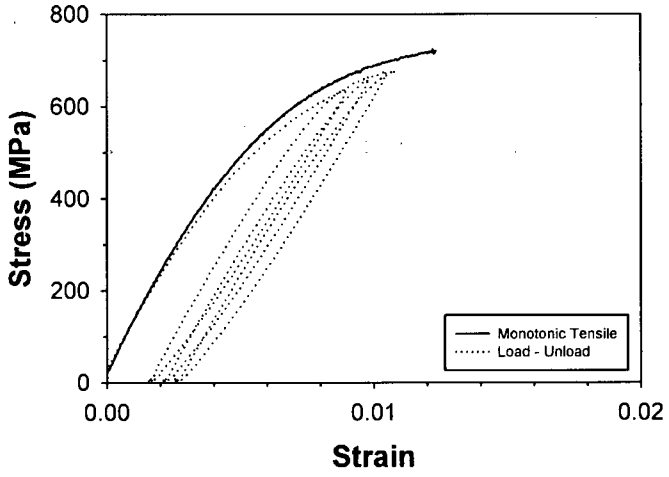


*(b)*

**Figure 5.11** *Examples of load-unload loops and monotonic tensile data for two of the laminate materials produced (a) 17%Nb, ε = 7.03 (b) 40%Nb, ε = 6.98. Solid black lines represent the monotonic tensile response.*

From the unloading portions of the loading-unloading curves the offset reverse yield stress was measured and used to compute $\Delta\sigma$ as discussed in Chapter 3. The results of these measurements are shown in Figure 5.12.

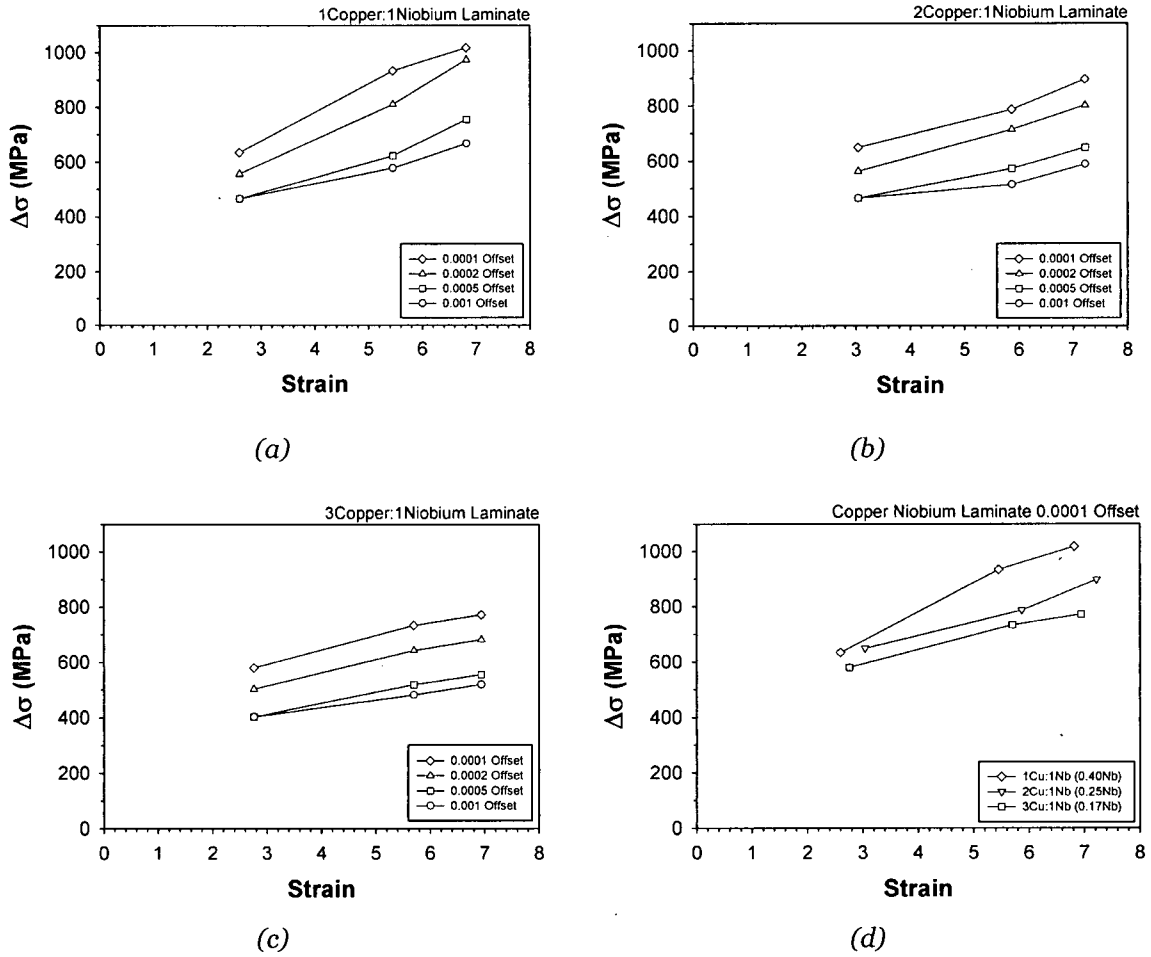


**Figure 5.12** *⊿σ vs. strain for: (a) 40 volume percent niobium; (b) 25 volume percent niobium; (c) 17 volume percent niobium; and (d) shows the effect of volume fraction.*

## 5.2 Wire Drawn Materials: In-Situ Materials

The structure of the as received samples viewed transverse to the wire drawing axis are shown in Figure 5.13. The structure is shown to be made of two regions at the mesoscopic scale; copper channels resulting from the bundling process and the original copper-niobium castings. The copper channels were found to comprise 25% of the microstructure (not including the exterior copper surrounding the sample which was removed prior to any mechanical testing).

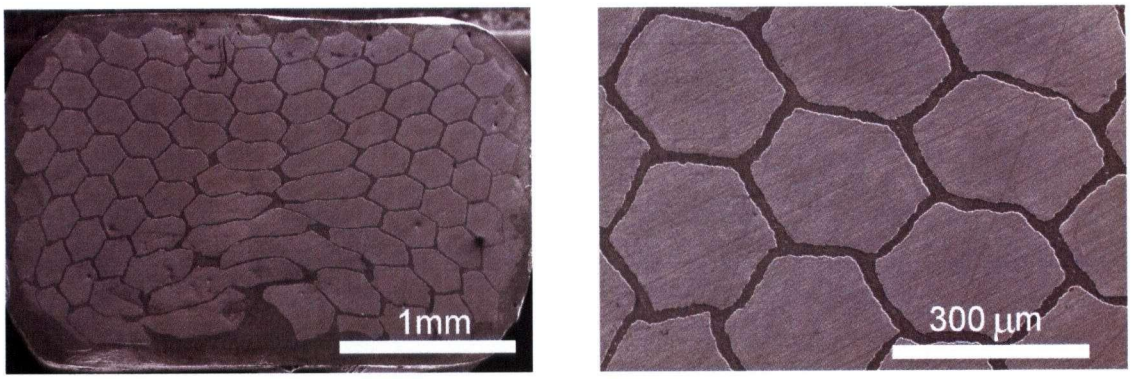


*(a)* *(b)*

**Figure 5.13** *Optical micrographs of as received in-situ drawn wire.*

Extracted niobium filaments are shown in Figure 5.14. The filaments tend to adhere to one another making definitive measurement of their size difficult. In general the smallest dimension of the fibres is less than 1 µm. On annealing spherodization of the niobium filaments was observed to commence at temperatures above 500°C.

Annealing at temperatures as low as 200°C for 3 hours allowed for complete recrystallization of the coarse copper channels. Figure 5.16 shows a micrograph of the recrystallized channels in a sample annealed at 300°C for 3 hours.

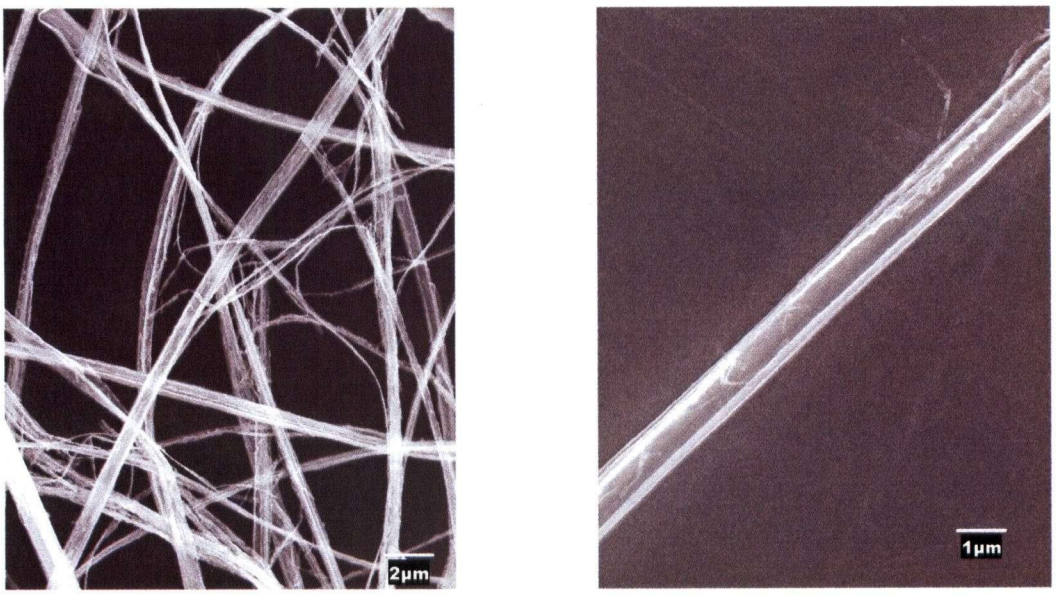


*(a)* *(b)*

**Figure 5.14** *SEM micrographs of as received in-situ drawn wire: (a) shows many fibres which tend to bundle with one another (b) shows a single fibre.*

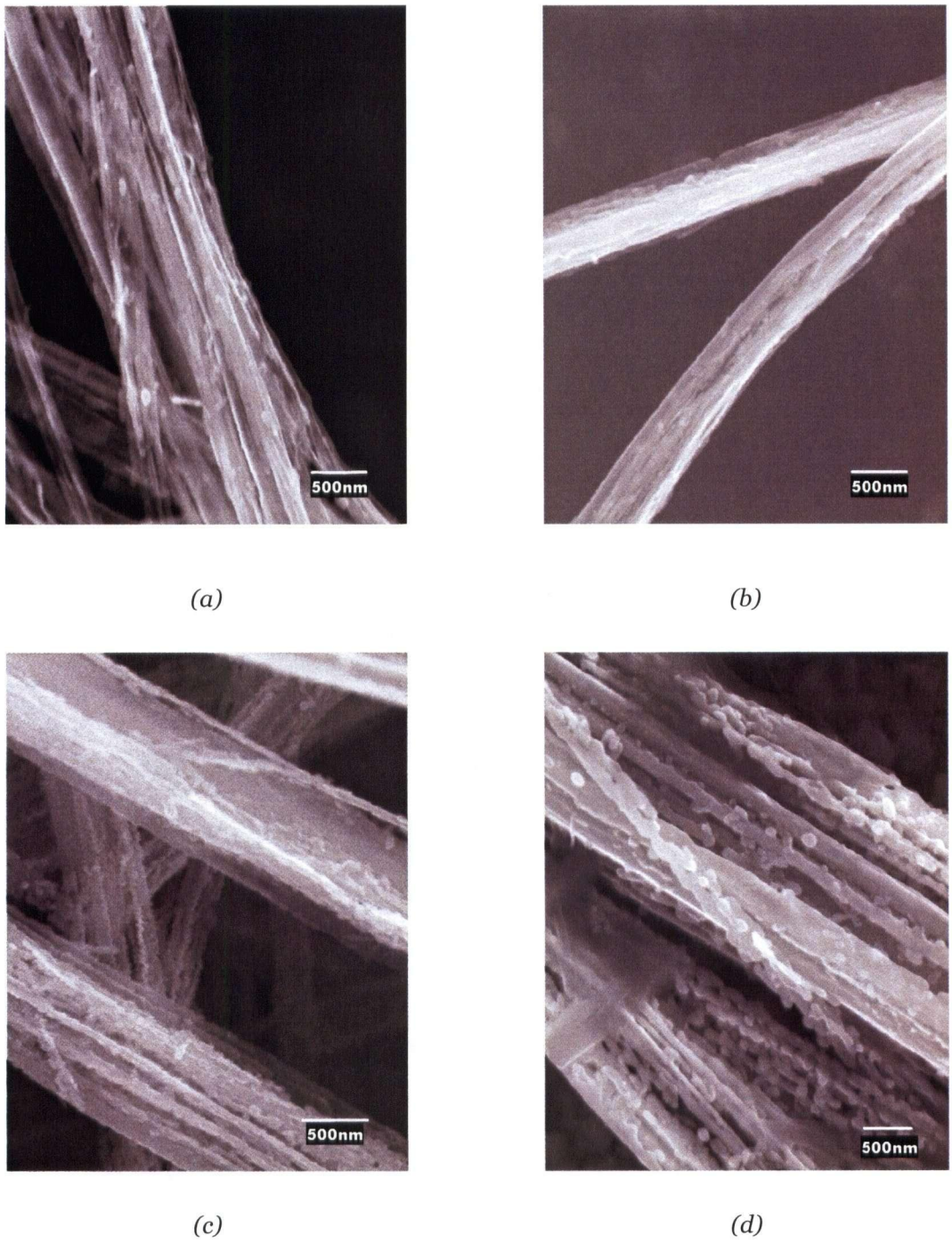


*(a)* *(b)*

*(c)* *(d)*

**Figure 5.15** *SEM micrographs of in-situ drawn wire annealed for 3 hours: (a) 300°C; (b) 400°C; (c) 500°C; and (d) 600°C.*

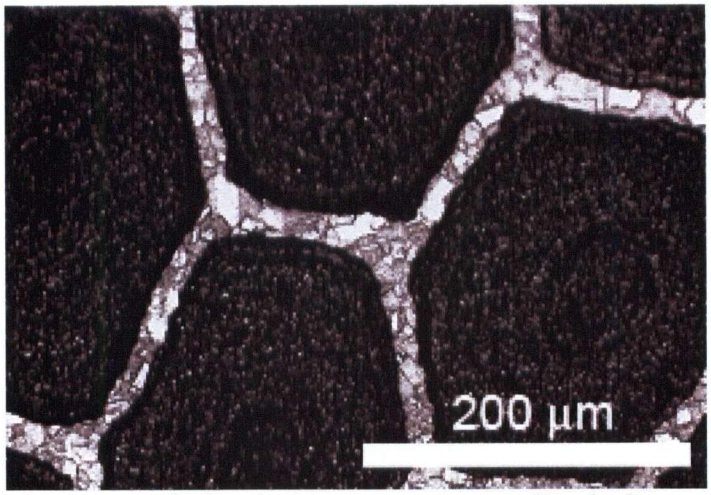


**Figure 5.16** *Optical micrograph showing copper as recrystallized after annealing at 200°C for 3 hours. The dark regions correspond to the previously cast copper-niobium.*

Figure 5.17 shows the tensile response of the as received wire as well as wire annealed for 3 hours at 200°C, 300°C, 400°C, and 500°C. A significant drop in the tensile strength of the material was not observed until a temperature of 500°C, though a change in the initial work hardening rate is observed. This correlates to the measured change in the hardness for the copper channels and copper-niobium cast regions. The cast copper-niobium regions, alternatively, don't show significant softening until temperatures above 500°C.

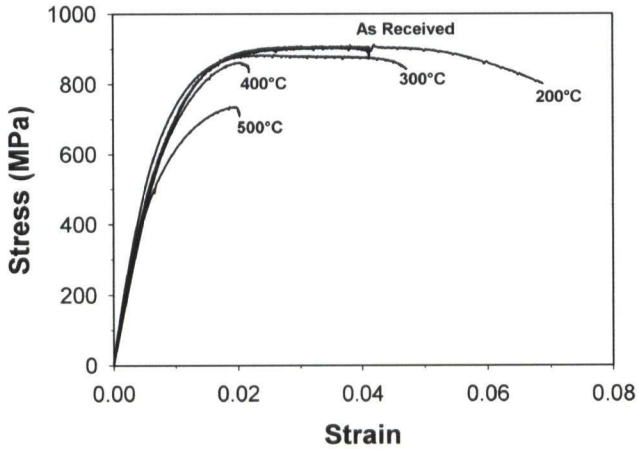


**Figure 5.17** *Monotonic tensile curves for in-situ drawn copper-niobium composite wires after annealing for 3hours at the indicated temperatures.*

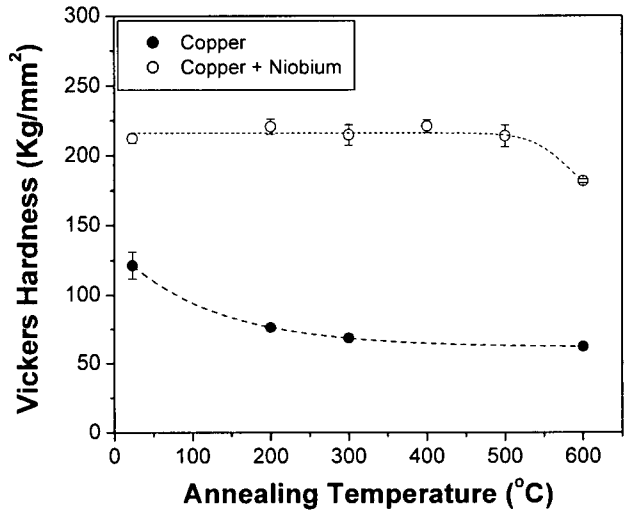


**Figure 5.18** *Microhardness of copper and copper-niobium region as a function of annealing temperature in the in-situ composite.*

As with the roll bonded material, it was not possible to perform full tension – compression tests due to the dimensions of the as received wire and so the hysteresis of the loading – unloading response was observed for the above conditions. Figure 5.19 shows an example of the resulting loading-unloading response for one condition. Figure 5.20 shows the variation in $\Delta\sigma$ (equation 2.27) for the various annealing temperatures. A slight increase is initially observed, which is followed by a strong drop for temperatures above 400°C.

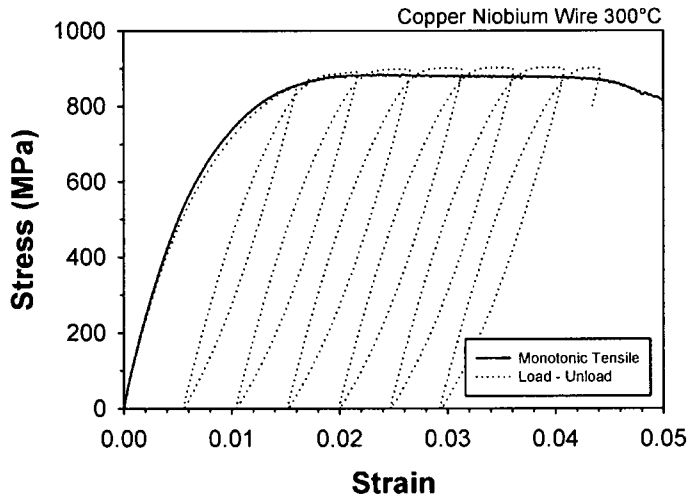


**Figure 5.19** Load-unload curve and *monotonic tensile curves for in-situ drawn copper-niobium composite wires after annealing for 3 hours at 300°C*

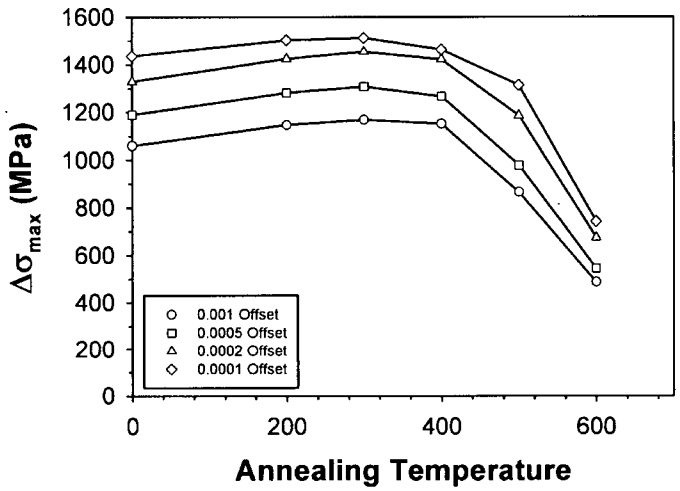


**Figure 5.20** *$\Delta\sigma$ max as a function of annealing temperature. The different curves correspond to the use of a different offset strain to determine the reverse flow stress.*

## 5.3 Wire Drawn Materials: Bundle Drawn Composite

The bundle drawn material exhibits a similar microstructure to that of the in-situ wire. However, in this case the structure is composed of three mesocopic regions; 1) coarse copper channels (Figure 5.21a) 2) fine copper channels (Figure 5.21b) and copper-niobium regions (Figure 5.21c). Extracted niobium fibres appear similar in the as received state to those extracted from the in-situ wire. On annealing, however, the niobium filaments in the bundled material were observed to resist spherodization to higher temperatures (Figure 5.23).

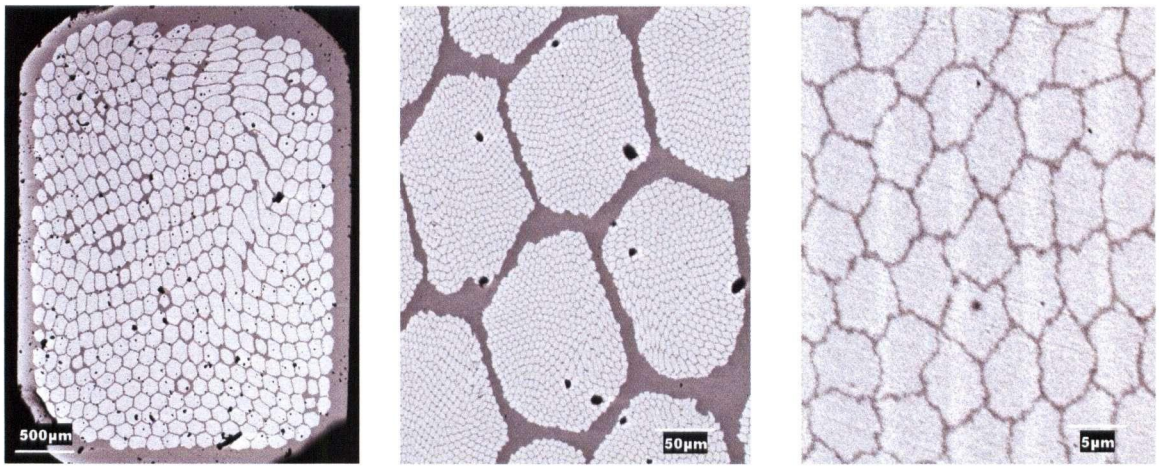


*(a)* *(b)* *(c)*

**Figure 5.21** *SEM micrographs of as received bundle drawn wire: (a) macroscopic image; (b) secondary bundles; and (c) the initial bundles.*

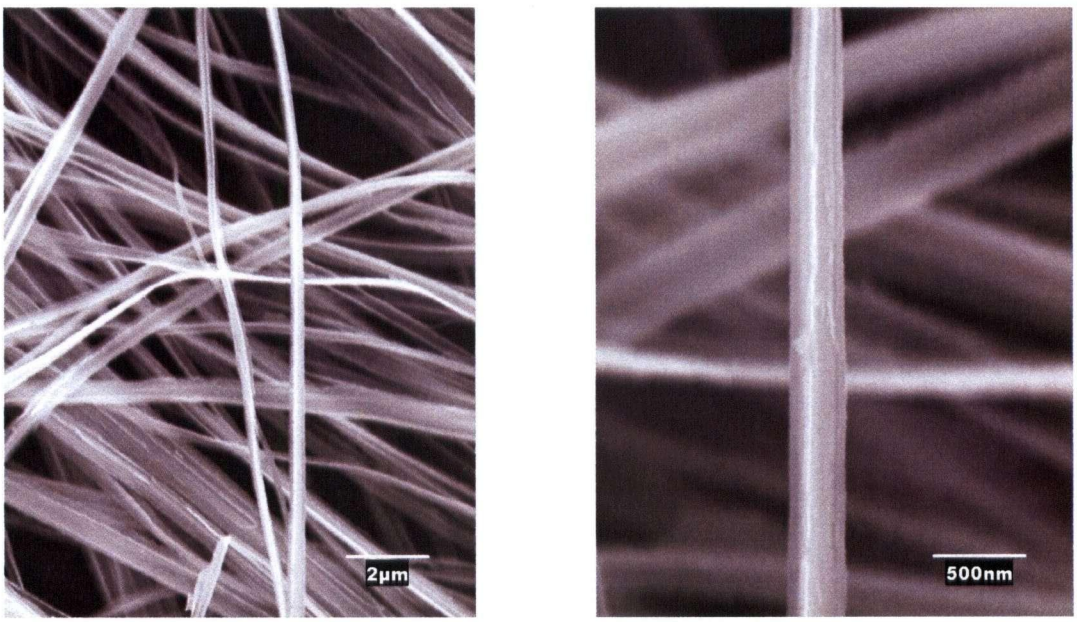


*(a)* *(b)*

**Figure 5.22** *SEM micrographs of the extracted niobium filaments of the as received bundle drawn wire: (a) shows many twisted fibres and (b) shows a single fibre.*

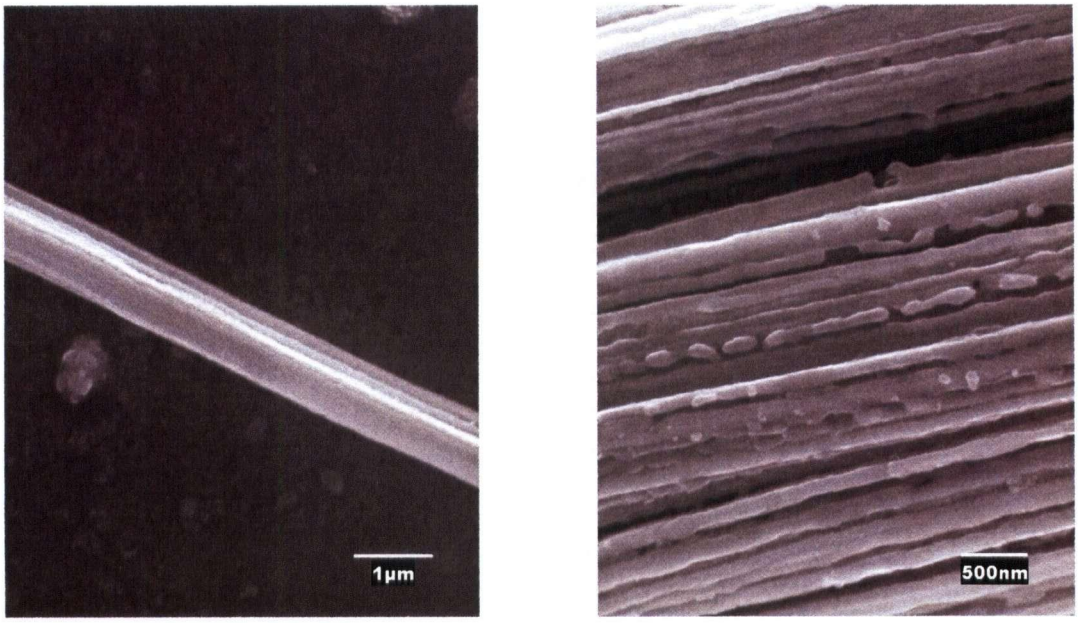


*(a)* *(b)*

**Figure 5.23** *SEM micrographs of annealed bundle drawn wire: (a) 500°C and (b) 600°C for 3 hours.*

Representative tensile curves for the various annealing conditions are shown in Figure 5.24. Softening was observed under all annealing conditions. With annealing, the uniform elongation was observed to drop significantly. Hardness measurements were made on the coarsest copper regions as well as measurements on the regions on the fine copper channels and the copper-niobium regions. Compared to the in-situ wire, the bundle drawn materials exhibit softening of the coarsest copper at higher temperatures.

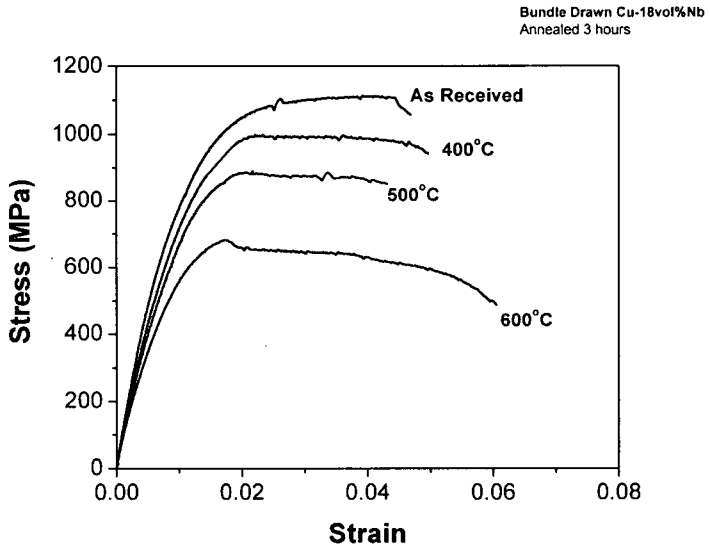


**Figure 5.24** *Tensile curves for the bundle drawn Cu-Nb wires annealed for three hours at the indicated temperatures.*

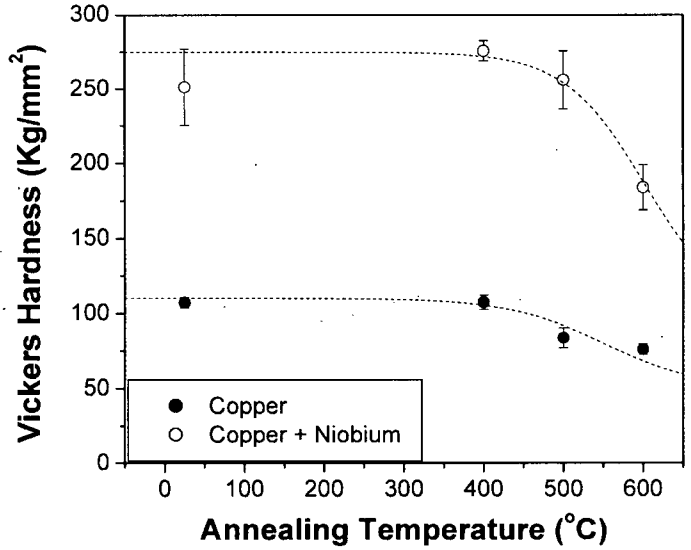


**Figure 5.25** *Hardness of different regions in the bundle drawn material. The black circles represent the hardness measured in the coarsest copper region while the white circles represent the average hardness measured in the remaining copper-niobium regions.*

Unlike the in-situ wires and the roll bonded material, the bundle drawn material was large enough in diameter to produce samples for tension-compression Bauschinger tests. Samples typically buckled in compression at reverse strains between 1% and 2%. Buckling was observed based on the observed difference in behavior between the two extensometers mounted on the sample. Figure 5.26 shows an example of the response of one extensometer plotted versus the other. The point of buckling is clearly indicated by the nonlinearity in the response.

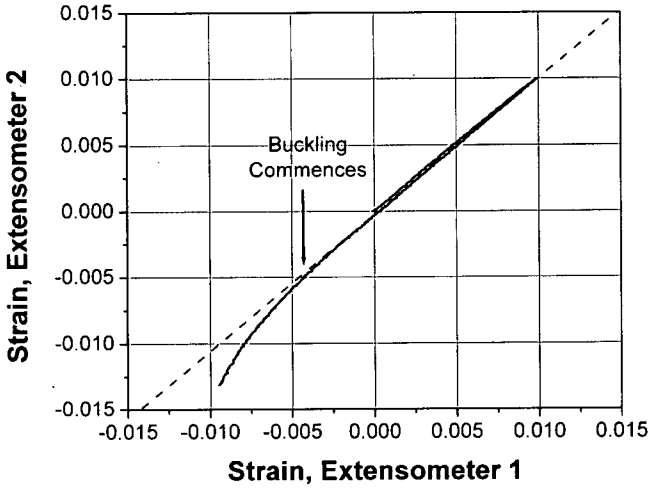


**Figure 5.26** *How the point of buckling in compression for tension/compression tests was determined.*

The results of the tension-compression tests are plotted in Figure 5.27 as the forward and reverse flow curves along with the reverse portion of the flow curve mirrored about the elastic unloading line. This construction facilitates the calculation of $\Delta\sigma$. Reversing of the direction of testing at each condition was performed after 1% and 2% forward plastic stain.

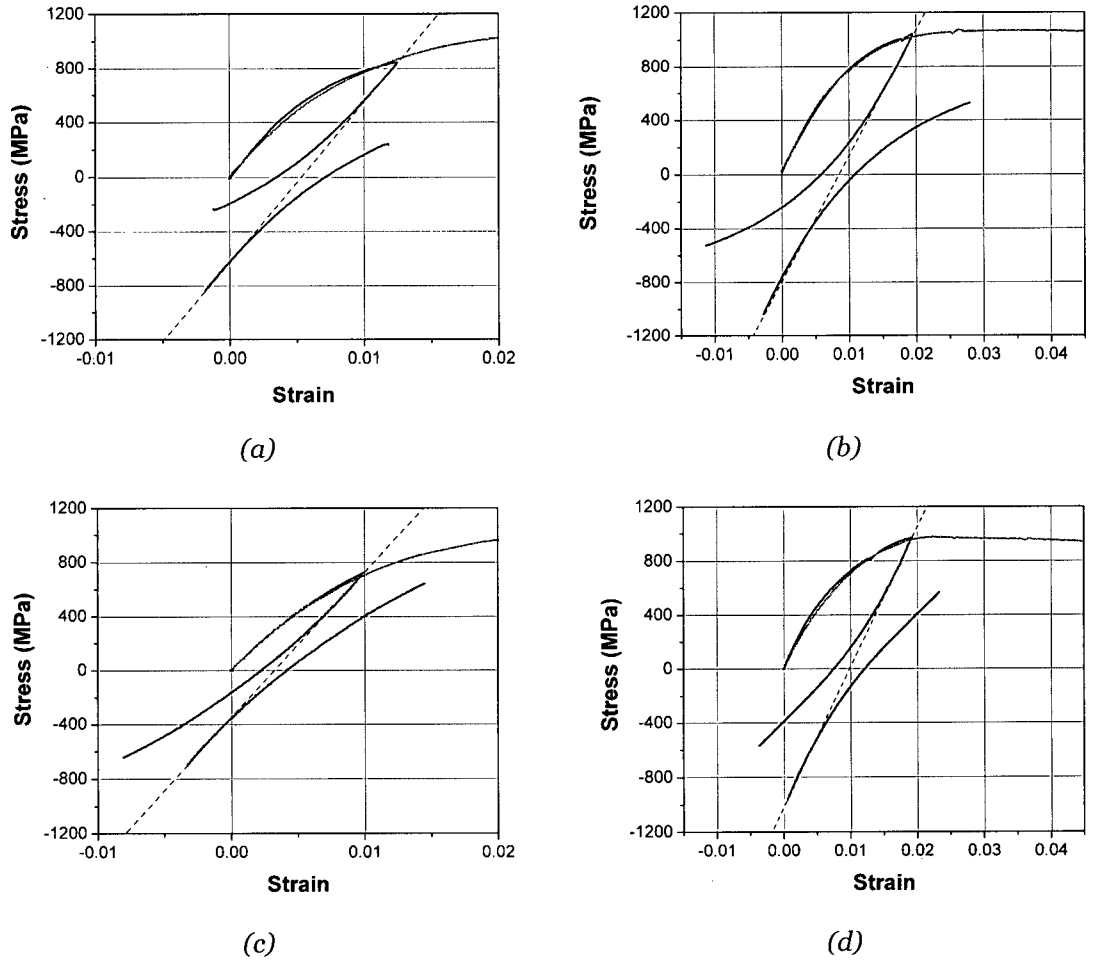


**Figure 5.27** *Left Hand Column: Stress-strain curves with inverted reverse flow curves after ~ 1% forward plastic strain (top row = as received, second row = 400°C, 3hrs, third row = 500°C, 3hrs, bottom = 600°C, 3hrs) Right Hand Column: As above but for 2% forward plastic strain. For 600°C, the forward flow curve has been extrapolated as the sample commenced necking just beyond 2% strain.*

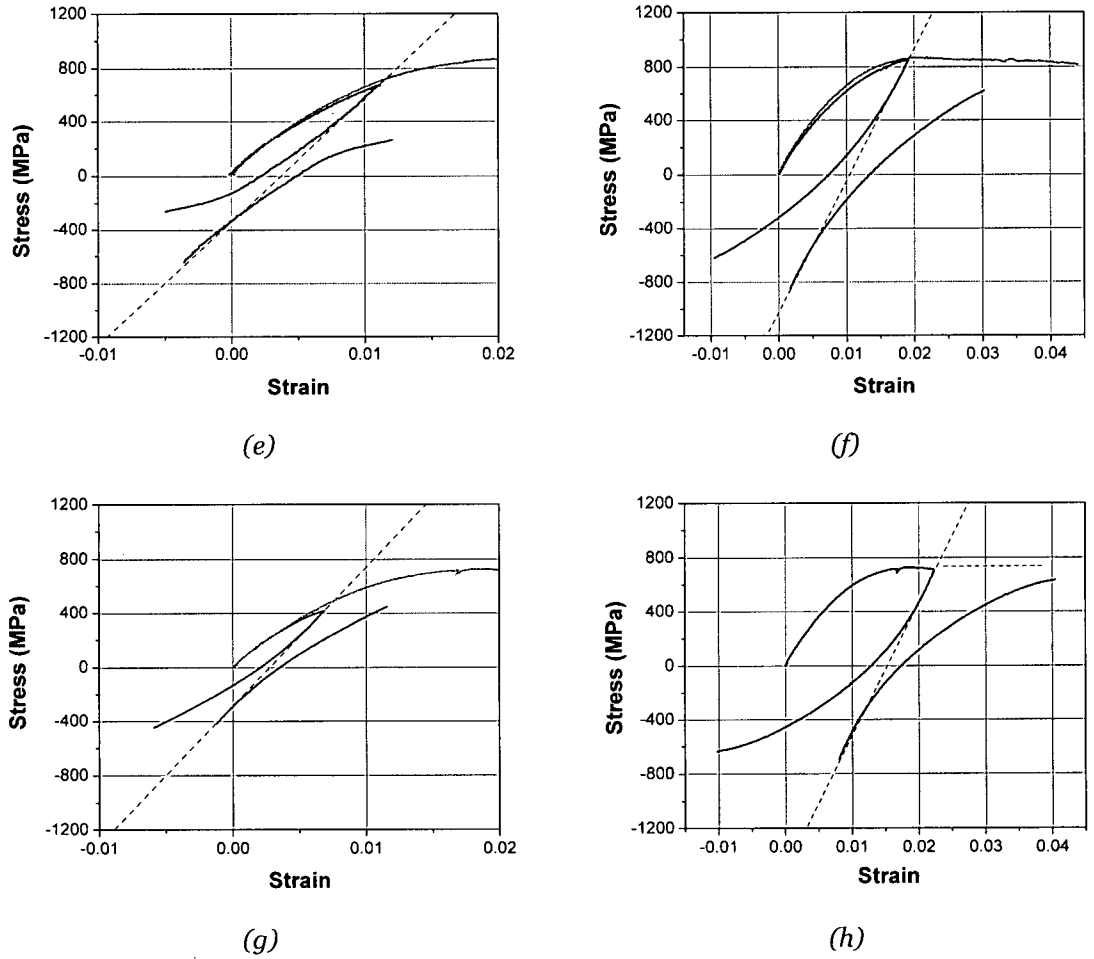


**Figure 5.27** *(continued) Left Hand Column: Stress-strain curves with inverted reverse flow curves after ~ 1% forward plastic strain (top row = as received, second row = 400°C, 3hrs, third row = 500°C, 3hrs, bottom = 600°C, 3hrs) Right Hand Column: As above but for 2% forward plastic strain. For 600°C, the forward flow curve has been extrapolated as the sample commenced necking just beyond 2% strain.*

# CHAPTER 6

# DISCUSSION

A range of tests have been used to resolve the mechanical response of two forms of codeformed copper-niobium wire and of roll bonded copper-niobium sheet. The goal of this discussion will be to interpret theses results for each material with the aim to identify the role of the microstructure and internal stresses on the overall mechanical response.

## 6.1 Wire Drawn Composites

This study examined the thermal stability of the strength of codeformed copper-niobium wires produced using two different methods. Annealing of these heavily codeformed two phase materials may have two consequences for the tensile properties. First, annealing may act to reduce or eliminate the internal stresses developed during co-deformation. This occurs as the material relaxes via plastic flow at elevated temperatures under the influence of the internal stresses. The effect of this is expected to be primarily observed in the initial loading of the samples after annealing. Once the material is loaded to the point where plasticity is achieved in both phases the full set of internal stresses will be re-developed. The second consequence of annealing may be to cause a reduction of the flow stress of one or both of the phases due to recovery and/or recrystallization. The effect of this will be observed both in the initial tensile loading as well as in the internal stresses observed during a Bauschinger test.

Both the *in-situ* and bundle drawn wires studied here contained a equal volume fraction of niobium, however, the different starting conditions and different levels of strain make it difficult for quantitative comparison between the two types of wire. Consequently the two types of wire will be treated and discussed separately. Although quantitative comparison is difficult, some qualitative comparisons will be made as these two materials could potentially serve the same practical use.

### 6.1.1 Macroscopic Tensile Behavior

During monotonic tensile tests both the *in-situ* and bundle drawn wires were found to show only a small amount of uniform elongation prior to necking. When necking occurred, it was found that the *in-situ* materials showed more elongation to fracture than did the bundle drawn materials. The key features in the tensile response of both materials are the high work hardening rates prior to reaching the ultimate tensile strength and the pronounced roundness of the initial plastic flow regime. By plotting the work hardening rate ($d\sigma/d\varepsilon$) versus strain and versus stress the nature of the tensile response can be examined. Figure 6.1 and Figure 6.2 show these plots for both types of wires. In these cases the work hardening rate has been plotted on a logarithmic scale so as to emphasize the elastic-plastic transition.

The rounded behavior of the stress strain curve of the drawn material has been attributed to progressive yielding of the composite by Han *et al.* [56]. Upon annealing this progressive yielding becomes even more strongly pronounced.

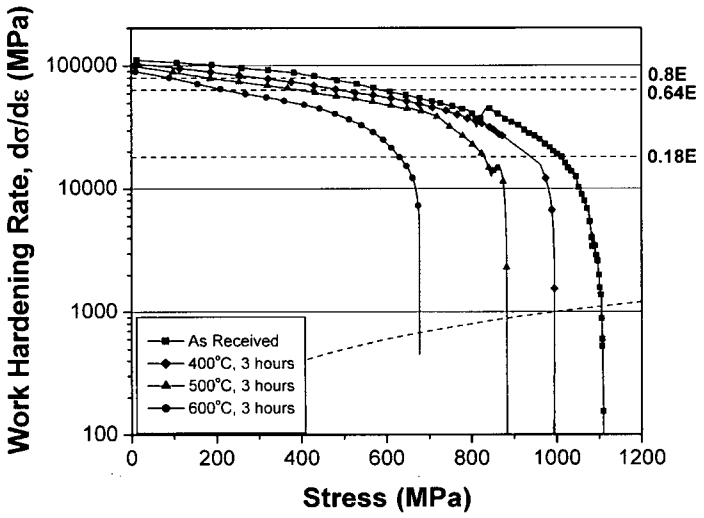


*(a)*

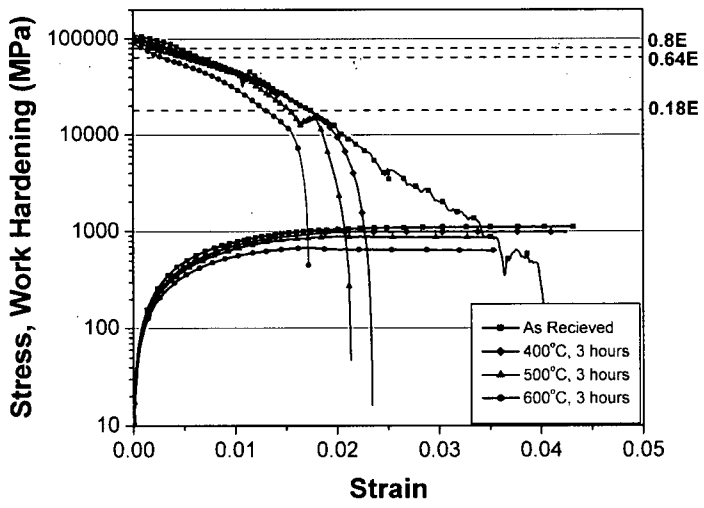


*(b)*

**Figure 6.1** *Work hardening curves for the bundle drawn wire as a function of: (a) stress and (b) strain.*

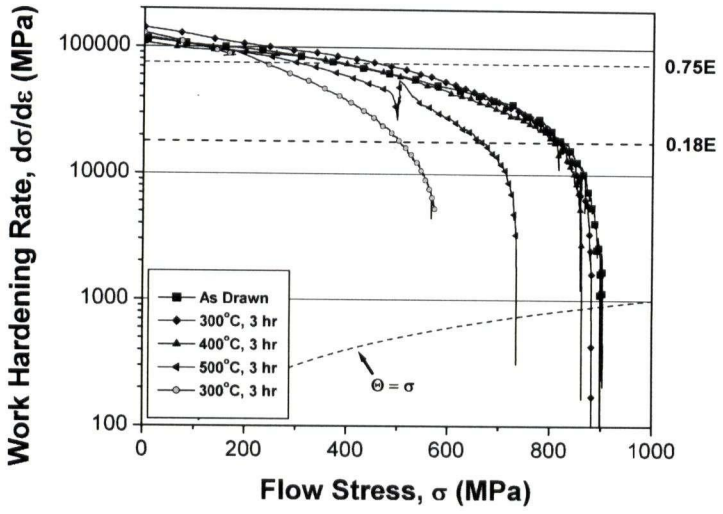


*(a)*

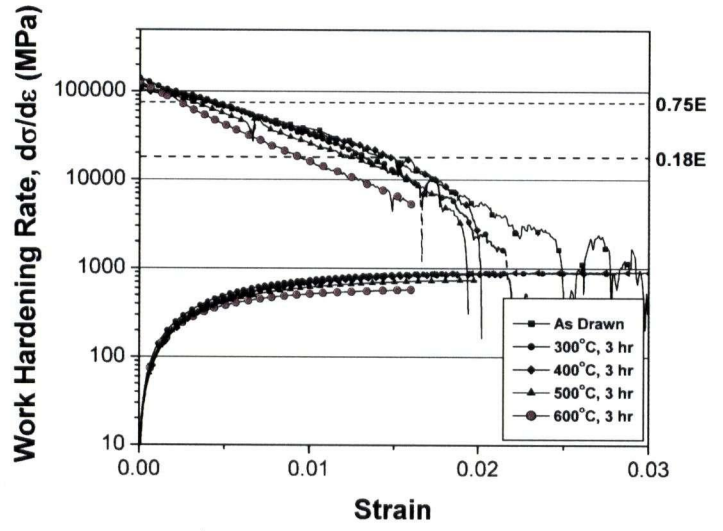


*(b)*

**Figure 6.2** *Work hardening curves for the in-situ wire as a function of: (a) stress and (b) strain.*

To properly understand the tensile response it is important to reflect on the nature of the microstructures and the expected elastic properties of the phases.

The elastic moduli for copper and niobium can be calculated based on the texture in the materials. Although texture measurements were not made on the wire examined in this study, Han *et al.* [56] measured pole densities for a similar drawn material that contained a lower volume fraction of niobium. If only the two principal orientations parallel to the tensile axis are considered, 80 percent of copper $\langle 100 \rangle$ poles are parallel to the drawing axis while the remaining 20 percent have their $\langle 111 \rangle$ poles parallel to the drawing axis.

A Voight (equal strain) estimate of the modulus for the copper, $E$, is given by,

$$E = f_{\langle 111 \rangle} E_{\langle 111 \rangle} + f_{\langle 100 \rangle} E_{\langle 100 \rangle} \qquad \textit{Equation 6.1}$$

where $f$ is the fraction of poles in a certain orientation. If $E_{\langle 111 \rangle}$ and $E_{\langle 100 \rangle}$ are taken as 192 GPa and 67 GPa [77] respectively the modulus of the copper is 92 GPa based on equation 5.1. For the niobium the $\langle 110 \rangle$ direction is the only predominant texture and its modulus is 92 GPa [77], the same as calculated for the copper. The values for elastic modulus of the two phases are also in agreement with the tensile results which show a measured modulus of between 90 and 105 GPa for the composite.

Based on the SEM macrographs presented in the previous chapter of the two wire drawn materials, their structures can be represented by the idealized microstructure shown in Figure 6.3. The structure is hierarchical based on the microstructural scale and phases present. This structure is the result of the processing route which involves repeated canning and bundling. For the case of the *in-situ* wire the ideal structure is more straightforward as there are only two distinct types of copper, $Cu^{o}$ and $Cu^{II}$ + Nb, as it was only bundled once.

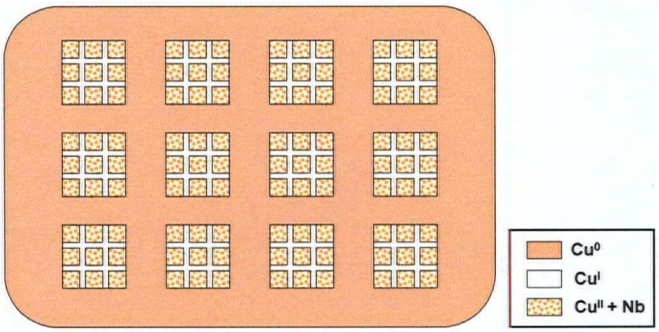


**Figure 6.3** *Ideal hierarchical structure of the bundle drawn wire*

These observations on the elastic properties and microstructures of the materials allow us to make some first order approximations to simplify the analysis of their behaviour. The first assumption made will be that the moduli of the phases can be considered equal for the two phases. This means that internal stresses that would arise due to elastic modulus mismatch can be neglected. To further simplify the analysis, only stress in the axial direction will be considered. This is based on the highly elongated nature of the phases parallel to the testing axis where an equal axial strain assumption is reasonable. The relevance of this assumption for these materials has been previously discussed in the literature and has been shown to be a reasonable first order approximation [78].

In the case of the as-drawn wire it might be expected that the slope of the loading curves in Figure 6.1 and Figure 6.2 should remain elastic up to a point where the sample begins to deform in a plastically homogeneously manner through the cross section of the sample. This situation would arise given that during drawing, plastic flow generates internal stresses in the individual components such that the overall stress in the system is balanced. Subsequently when the sample is loaded during a tensile test, all components would begin plastic flow at the same overall macroscopic sample stress. However, it is seen in the tensile response of the as-drawn material that there is no clearly defined elastic-plastic transition. This rounded yielding response has been

previous noted and discussed by Han *et al.* [56]. The source of the rounding of the as-received tensile response stems from the fact that some reverse plasticity occurs on unloading of the sample due to internal stresses. This is observed in the tensile tests conducted in this study. This effect is similarly expected to occur after the material has passed through the wire drawing die. Stobbs and Paetke have discussed this for pearlitic steel wire [79]. This small amount of reverse plastic flow modified the internal stresses reducing them in both phases thereby accentuating the elastic-plastic transition.

Upon annealing several processes may occur that can further affect the shape of the tensile response of these materials. The first change expected is a reduction of the internal stresses in the material. This will tend to make the elastic plastic transition more gradual as is observed in Figure 6.1 and Figure 6.2.

By allowing for a relaxation of the internal stresses without a lowering of the flow stress of the materials via recovery and/or recrystallization, the elastic plastic transition would be extended (more rounding of the initial portion of the tensile curve) but the flow stress of the material at the point where plasticity has spread throughout the sample would remain unchanged. Clearly this is not the case in Figure 6.1 or Figure 6.2. For the annealing treatments applied during this study the most important microstructural change is expected to occur on the coarsest copper, $Cu^{o}$. It is clearly seen that the $Cu^{o}$ is fully recrystallized after 3 hours at 400°C from optical microscopy (Figure 5.16), as well as from the hardness measurements made as a function of annealing (Figure 5.18). Although the coarse copper is strongly affected by the annealing it is not expected that recrystallization/recovery of the niobium will be significant given that 600°C is approximately one quarter of its melting point. However, at this temperature morphological instability of the niobium, in the form of spherodization, was observed. Spherodization will reduce the load transfer between the two phases and the assumption of equal axial strain in both phases would be poor. The net result of these effects should

be a lowering of the flow stress corresponding to plastic flow of all components of the microstructure and a further modification of the elastic plastic transition (e.g. a lowering of the onset of plastic flow in the tensile curve). The effect of the annealing treatments on the finest scale copper, $Cu^{II}$, was not clearly established from the work in this study. It is unclear in this case where the copper is very fine in scale how processes such as recovery and recrystallization take place. Previous studies have shown that recrystallization is much slower in these fine scale materials than it is in bulk materials [80-81]. In this study there is some evidence for this in the annealing behaviour of the copper-niobium wire materials (cf. Figure 5.18).

### 6.1.2 Internal Stresses: Tension - Compression

The internal stresses in the as received and annealed samples have been assessed macroscopically in the wire materials through unloading and tension-compression experiments. In these experiments the materials are pulled in tension to 1% or 2% strain, and then the direction of loading is reversed. As discussed above, the effect of annealing can be to reduce the internal stresses present in the material and/or to cause softening of the phases present. In these experiments it is the effect of the latter that is primarily assessed. Though annealing may reduce the internal stresses developed from drawing, a new set of internal stresses will be re-developed as the material is tested in tension. At the point where both phases have yielded plastically, these internal stresses should be fully developed.

Due to the geometry of the various materials examined during this study it was only possible to perform complete tensile-compression Bauschinger tests on the bundle drawn composite wire. To characterize the internal stresses the parameter $\Delta\sigma$ is computed by comparing the forward and reverse flow curves, as shown in Figure 6.4.

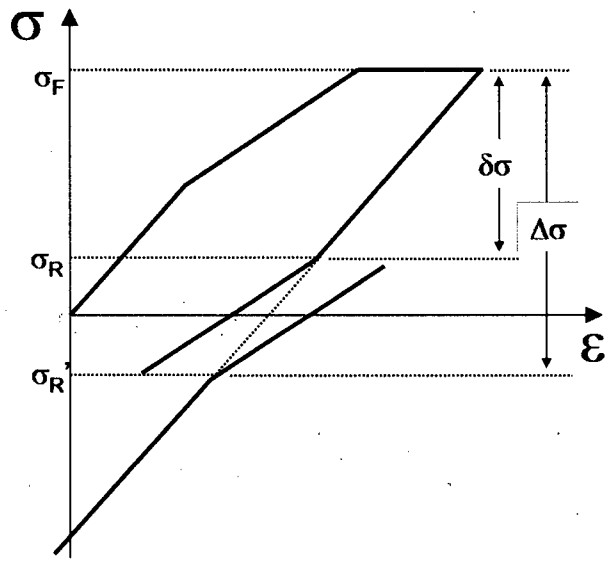


**Figure 6.4** *Schematic for calculating of Δσ from the forward and reverse loading curves*

To better describe the reverse yielding behavior relative to the forward behavior, Δσ is plotted as a function of the reverse plastic strain as measured during the load-unload tests (Figure 5.27). Figure 6.5 describes the relationship for the case of 1% and 2% initial forward plastic strain. In the case of 1% prestrain in tension, the measured Δσ is complicated by the fact that many of the samples tested required more than 1% prestrain to exit from the initial elastic-plastic transition in tension (Figure 6.1). By 2% prestrain in tension, all samples appeared to have reached the point of full plasticity as evidenced by the low work hardening rates (Figure 6.2). Because of this observation, the discussion will focus on the data shown in Figure 6.5b.

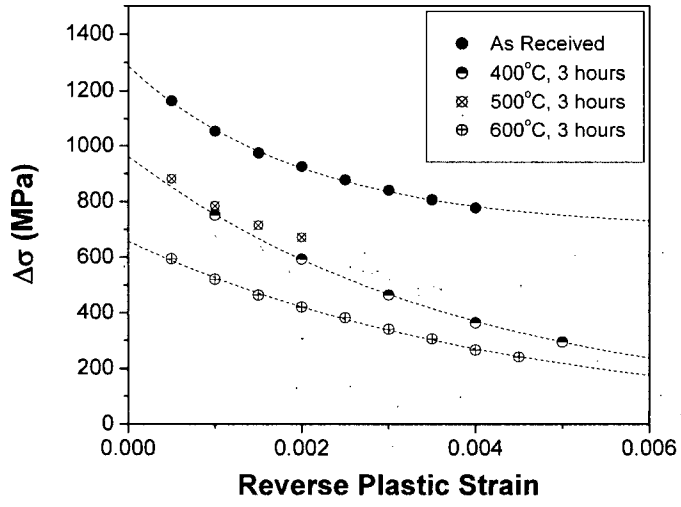


*(a)*

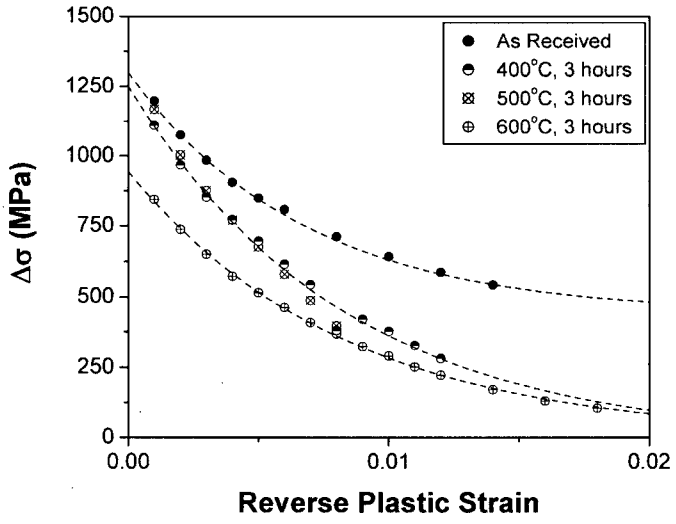


*(b)*

**Figure 6.5** *Delta sigma as a function of reverse plastic strain: (a) for 1% forward strain and (b) for 2% forward strain.*

The curves in Figure 6.5 can be separated into three regimes:

1. At low reverse strains initial yielding occurs in one portion of the microstructure, i.e. in the Cu° which is the coarsest scale copper (the last 'can' in the bundling process).
2. Next there is a transient region during which progressive yielding occurs.
3. The last section of the curve describes the approach of the forward and the reverse stress-strain curves to parallelism. The forward and the reverse curves will only become parallel when the sample becomes fully plastic in the reverse direction.

Each of these portions of the reverse loading response will be dealt with in turn below.

During reverse loading, the first portion of the composite to yield in compression will be the softest region of the composite. This portion of the material will have the lowest flow stress and will have accumulated the largest compressive internal stresses from the forward component of the deformation. In this case the coarse copper, Cu°, will be the first region of the microstructure to yield.

Based on the assumption of equal axial strains in the Massing model (cf. section 2.4.2), as the material is unloaded from its forward flow stress, all components of the microstructure are unloaded by an equal amount elastically until the yield stress *in compression* of the first component of the microstructure is reached. If one follows the unloading of the Cu° region in this case, at the point where unloading is commenced, the Cu° is at its tensile flow stress. Upon elastic unloading, its stress is first reduced to zero in tension then rises in compression until it reaches a compressive stress equal in magnitude to its flow stress in tension. Thus, under these conditions, the macroscopically observed drop in stress from the forward flow stress to the stress at which reverse flow is observed, i.e. $\delta\sigma = (\sigma_F - \sigma_R)$, should correspond to twice the magnitude of the flow stress of the Cu° region (Figure 6.4).

To verify this, the observed drop in stress from the forward flow stress to the onset of reverse yielding were halved and compared to the hardness (converted to an approximate yield stress) as shown in Figure 6.6. The values for yield strength using both methods show good agreement, suggesting that the initial yield of the Cu° is responsible for the initial yielding of the composite on unloading. One can also relate this to the initial values of $\Delta\sigma$ shown in Figure 6.5.

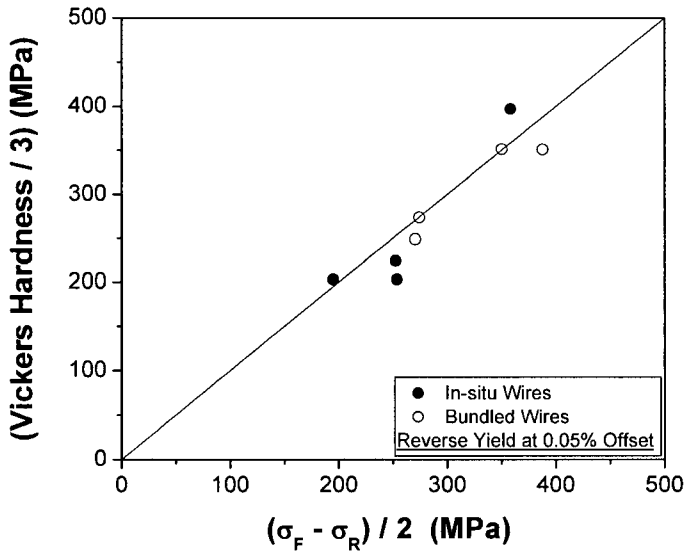


**Figure 6.6** *Comparison of the value of $\delta\sigma/2$ measured from the reverse yielding response of both in-situ and bundle drawn wires to the hardness of the copper used in the final bundelling process. The good agreement reinforces that the initial reverse yielding in the sample is a result of yielding of this coarse copper region*

In this case $\Delta\sigma$ has been defined as before,

$$\Delta\sigma = \sigma_F + \sigma_R \qquad \textit{Equation 6.2}$$

where the value of $\Delta\sigma$ taken at the onset of reverse flow. This can be re-written in terms of the flow stress of the Cu°, $\sigma_y^{Cu,0}$.

$$\Delta\sigma = 2(\sigma_F - |\sigma_y^{Cu,o}|) \qquad \textit{Equation 6.3}$$

Thus, in Figure 6.5 and Figure 6.6 the initial value of $\Delta\sigma$ must depend on both the magnitude of the forward flow stress of the composite and the flow stress of Cu°. In the case of samples annealed at 400 and 500°C it is observed that the initial value of $\Delta\sigma$ drops only slightly. This can be attributed to the fact that the decrease of $\sigma_y^{Cu,o}$ on annealing is similar in magnitude to the drop of $\sigma_F$ that occurs on annealing, suggesting that softening is not confined, initially, just to the Cu° region. This is confirmed by the hardness measurements shown in Figure 5.25 which show a lowering of the flow stress in both the coarsest copper region as well as the fine scale copper-niobium regions.

For the sample annealed at 600°C, the initial value of $\Delta\sigma$ is observed to drop relative to the lower temperature annealed samples. Again, with reference to Figure 5.25, one can see that the hardness in the Cu° has essentially reached a plateau by this temperature, while softening continues in the copper/niobium regions. In this case it is expected that the continued drop in the forward flow stress is likely due to softening of the copper/niobium regions. This will be assisted by the onset of spherodization observed at this temperature.

As unloading is continued past the onset of reverse yielding the curves in Figure 6.5 are defined by a transient response corresponding to the progressive yielding of the material. The shape of the $\Delta\sigma$ versus reverse strain curves reflects the gradual transition of material from elastic to plastic deformation in the reverse direction and thus is a measure of the distribution of strengths for the different microstructural elements of the material. In this case it is expected that the copper phase can not be described by a single flow stress owing to the different microstructural scales and levels of cold work that have been accumulated due to the bundling technique. Moreover, as discussed above, there is evidence that suggests that on annealing the behaviour of these

different regions consisting of copper with different length scales may be quite different, i.e. that as the scale of the region becomes finer the kinetics of softening are reduced.

As reverse yielding takes place one would expect that the slope of the reverse flow curve will progressively approach 18% of the elastic modulus corresponding to the condition where the niobium is the only remaining unyielded portion of the microstructure. In the case of the as received material, it is observed that this condition is reached relatively rapidly on the reverse loading, corresponding to the fact that the copper yields progressively prior to yielding of the stronger niobium.

Examining the initial rate of drop of $\Delta\sigma$ for samples annealed at different temperatures, one observes the highest rate for samples annealed at 400 and 500°C. This is a reflection of the fact that, while some regions of the copper (e.g. Cu°) may have softened at these temperatures, other portions (those with the finest scale) retain high strength and thus require large reverse strains to achieve their flow stress. At 600°C, significant microstructural evolution has begun in the finest scale copper-niobium regions including spherodization. Thus, at this point softening commences in this area therefore reducing the rate of drop of $\Delta\sigma$.

The final part of the curves, the approach to parallelism corresponding to constant $\Delta\sigma$, occurs as plasticity spreads throughout the sample in the reverse direction. It was not possible to achieve large enough compressive strains to achieve parallelism between the reverse and forward flow curves, though all of the curves appear to be closely approaching this condition.

Two types of behaviour can be observed in these samples. In the case of all of the annealed samples, the value of $\Delta\sigma$ approaches zero over the range of strains achieved. This means that the reverse flow curve eventually becomes equivalent to that produced in the forward direction. In order for this situation to occur, the internal stresses built during the initial 2% forward tensile strain must be destroyed and replaced by an equal

but opposite set of internal stresses that will add to the compressive flow of the material (Figure 6.7). It is, thus, not surprising that this condition has been reached at a reverse strain approximately twice the forward strain required to achieve plasticity in both phases [70]. In these cases the entire Bauschinger effect is contained in the transient softening behaviour and there is no permanent softening.

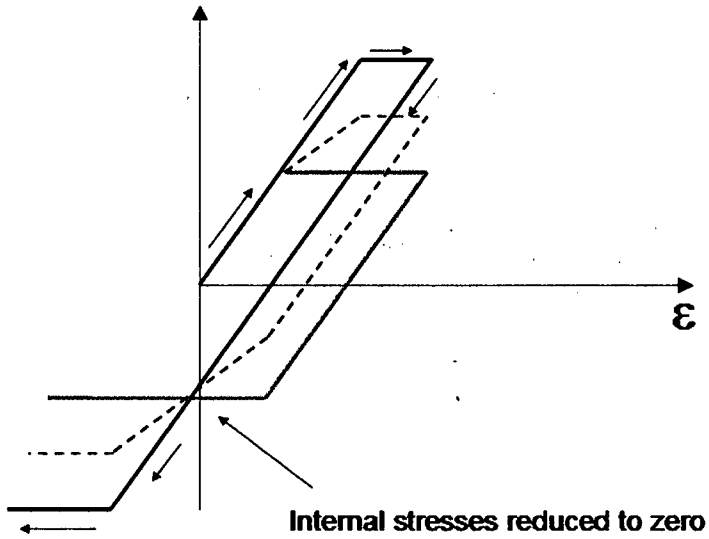


**Figure 6.7** *Schematic illustration of a simple two-element Massing model comprised of equal fractions of strong (black) and soft (grey) phases having the same elastic modulus (composite response given by the dotted line). The plot illustrates how the internal stresses are reversed on reversal of the loading direction, complete reversal occurring at a strain in compression twice that performed in tension.*

In the case of the as received material the rate of drop of $\Delta\sigma$ diminishes quickly as the sample is loaded in compression but then slows as the forward and reverse flow curves appear to reach parallelism faster than the forward and reverse flow stresses approach one another. Examining the forward and reverse flow curves in this case, one sees that the reverse flow curve does continue to approach the forward flow stress (i.e. parallelism has not been reached), however it does so at a relatively slow rate compared to the other annealed samples. Examining the shape of the reverse flow curve (re-plotted in Figure 6.8), one notes that the slope of the hardening curve at the largest reverse strains is well described by,

$$\frac{d\sigma_{rev}}{d\varepsilon} \approx 0.18E \qquad \textit{Equation 6.4}$$

where $E$ is the elastic modulus of the composite (approximately the modulus of niobium). One explanation for this observation would be that at this point all of the copper has yielded in compression but that the niobium (being the strongest element, under the largest tensile internal stress at the onset of unloading) remains elastic. It is expected in this case, if the reverse straining were continued, $\Delta\sigma$ would continue to drop at a rate dictated by the elastic loading of the niobium until its yield stress was reached in compression.

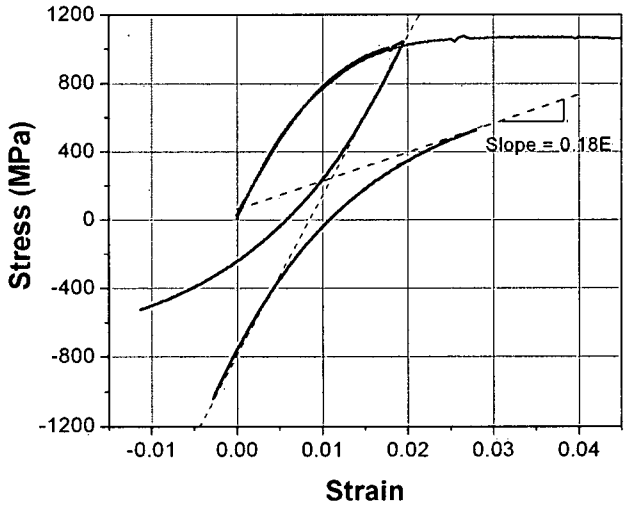


**Figure 6.8** *Bauschinger curve for the as-received bundle drawn material reproduced from Figure 4.29 showing that the slope near the end of the reverse loading cycle is approximately that expected for the case where the copper has completely yielded and the niobium remains elastically loaded.*

In summary, it would appear that annealing affects the microstructure, strength and internal stresses in the bundle drawn wires in a number of complex ways. It is observed in these cases that most of the Bauschinger effect can be attributed to transient softening. No true permanent softening was observed. The strong transient softening reflects the hierarchical microstructure of the material and the inhomogeneous manner by which the different elements of the microstructure respond to annealing.

### 6.1.3 Internal Stresses: Load-Unload

In the case of the *in-situ* drawn wire it was not possible to perform tests in combined tension and compression due to the fine diameter of the wires. However, from the observations in the bundle drawn wires of reverse yielding during the tensile portion of the reverse loading, it was decided to perform unloading experiments to gain some insight into the initial portion of the transient softening response. The same annealing treatments were performed on the *in-situ* wires as were performed on the bundle drawn wires.

The results of the unloading experiments for samples annealed at different temperatures were presented in Figure 5.19. These results correspond to the low reverse strain portion of Figure 6.5 (i.e. the initial values of $\Delta\sigma$). In Figure 5.20 the value of $\Delta\sigma$ is observed first to slightly increase with annealing then to rapidly drop for temperatures above 500°C.

As in the case of the bundle drawn wire, this response can be explained with reference to the softening behaviour of the different microstructural elements of the material. In the case of the bundle drawn wire, the microstructure is divided into two components, the fine scale copper-niobium region produced from the cast wires and the coarse copper region used in the final bundling of these copper-niobium wires together. Figure 5.18 shows the variation in the hardness of these two regions with annealing temperature. It is observed that the coarse copper regions are completely softened (recrystallized) by a temperature of 300°C. The copper-niobium regions, on the other hand, strongly resist softening up until temperatures of approximately 500°C. Above this temperature, softening commences in parallel with spherodization of the niobium filaments.

Referring to Equation 6.3 and the data in Figure 5.18, the initial drop in $\Delta\sigma$ can be explained by the rapid drop in the flow stress of the coarse copper region combined

with the constant hardness in the copper-niobium region. With reference to Equation 6.3, $\left|\sigma_y^{Cu,0}\right|$ decreases but $\sigma_F$ is expected to remain approximately constant, given that $\sigma_F$ is dominated by the strength of the copper-niobium regions. For temperatures above 500°C the rapid drop in $\Delta\sigma$ is due to the fact that the coarse copper region is already fully softened ( $\left|\sigma_y^{Cu,0}\right|$ doesn't change with temperature) and $\sigma_F$ begins to drop as the copper-niobium regions begin to soften. In this manner, the source and magnitude of the initial transient portion of the Bauschinger effect appear quite similar for both the *in-situ* and bundle drawn wires.

### 6.1.4 Summary: Stability of the Strength of Copper-Niobium Wires on Annealing

Given the qualitative similarity in the nature of the Bauschinger effect for the two types of wires, it is interesting to compare the overall thermal stability of their strength. Referring to Figure 6.1 and Figure 6.2, it is observed that the strength of the *in-situ* drawn materials remains relatively stable up to temperatures of 500°C for the annealing time considered here. The bundle drawn material, on the other hand, exhibits significant softening at temperatures as low as 400°C. This is reflected in the differences of the evolution of hardness with annealing temperature in the fine-scale copper-niobium regions for these samples (Figures 4.19 and 4.25). The *in-situ* produced copper-niobium regions appear to be much more resistant to softening compared to the bundle drawn copper-niobium regions. Though the source of this difference has not been studied further in this work, it appears to be consistent with the concept that refined microstructures tend to more strongly resist softening compared to coarser regions as discussed above. In the case of the bundle drawn materials, the copper-niobium regions contain copper with scales ranging from ~ 2 μm to < 0.1 μm whereas in the case of the

*in-situ* drawn material the scale of all of the copper in the copper-niobium regions is expected to be < 0.1 μm in scale.

## 6.2 Layered Composites

Fine scaled copper-niobium layered composite was produced using the accumulated roll bonding technique. The goal of these studies was two fold. First, this method has been selected in an attempt to examine the feasibility of producing high strength copper-niobium via roll bonding and to help examine some of the limitation observed previously for materials produced in this way. Secondly, unlike the wire drawing operations which, as seen above, produce very heterogeneous microstructures due to the canning processes, and/or are limited in the volume fractions and scales of niobium that can be produced, the roll bonding technique has been selected for the study of strength and internal stresses because of the potential for greatly improved sample homogeneity and less limitation on the scale and volume fractions of the components.

### 6.2.1 Fabrication and Microstructural Characterization

Production of the laminate material became more difficult as the total imposed strain and volume fraction of niobium increased. Thus, it was found that the material produced containing the largest volume fraction of niobium was the most difficult to roll bond up to a total strain of approximately 7. The principle difficulty with producing the materials was with achieving sufficiently strong bonding of the layers. Examination of samples in the SEM (Figure 6.1) revealed incomplete bonding always existed along the last portions of the sample to be bonded for the 40%Nb samples strained to ~ 7. For samples with lower volume fractions of niobium the problem was less acute. As mentioned in the results section, this led to significant statistical spread in the strength and tensile response of these samples.

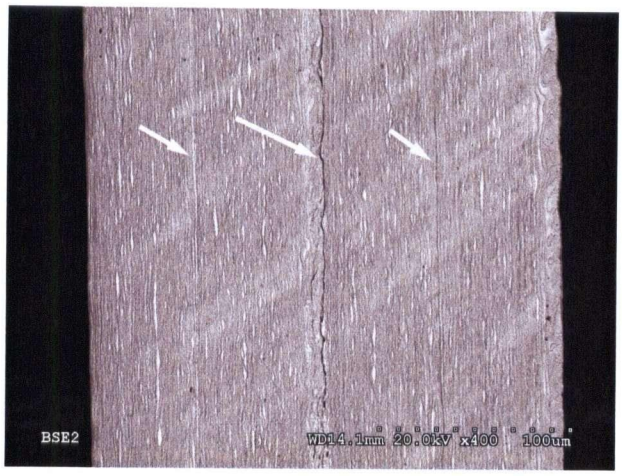


**Figure 6.9** *Incomplete bonding of layers in 40% Nb sample after imposed strain of approximately 7 (arrows indicate poor bonding).*

During the final rolling step of all the samples, the rolls were positioned such that there was no space between them. This was done to achieve the maximum level of imposed strain. However, due to the increasing strength of the samples with high strains and high niobium volume fractions, it was not always possible to achieve equivalent strains in this last rolling step. As the volume fraction of niobium and the imposed strain increased the flow stress of the samples increased. Figure 6.10 shows how the minimum achieved sample thickness relates to the overall flow stress of the material. As the flow stress of the material increases the minimum achievable sample thickness also increases. As a result of this, the strain that can be imposed during the final rolling step is reduced, in turn, reducing the likelihood of producing a strong bond between layers.

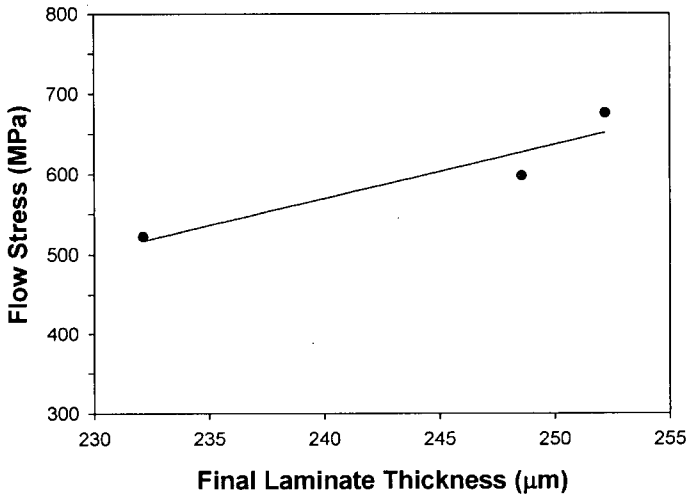


**Figure 6.10** *Final laminate thickness as a function of flow stress.*

The bond quality for samples with high volume fractions of niobium at large strains was further affected by the annealing response of these samples. It was found through a series of initial experiments that intermediate annealing of the samples during the rolling sequence led to softening of samples and an improved bonding response of the material. However, Figure 5.2 shows that the effect of this annealing treatment on samples containing large volume fractions of niobium rolled to high strains is weak. Thus, it was not possible to appreciably soften the materials with the highest volume fractions of niobium with the finest microstructures, thus further increasing the difficulty of achieving strong bonds.

The reason for this lack of softening is not entirely clear from this study. Certainly, it is expected that during annealing at 200°C, little softening of the niobium is expected. Thus, in general, one would expect less softening of the higher volume fraction niobium samples than lower volume fraction niobium samples. However, this does not explain the observation that the material, for the same volume fraction of niobium, softens less after it has been heavily deformed. One possible explanation may reside with the effect of very fine scale microstructures on hindering the processes of recovery and recrystallization [80-81].

In general, the microstructures produced via roll bonding consisted of well developed, mostly continuous layers. Figure 5.3 shows typical images of the laminate materials for all three volume fractions of niobium at three levels of strain. When viewing the laminate from the transverse direction, the layer development appears uniform with increasing strain. Although there is a large variation in the layer thickness, the change in average niobium layer thickness is well described by the macroscopic imposed strain, i.e. the strain in the individual layers is well approximated by the macroscopic strain. When the laminate is viewed from the rolling direction, Figure 5.4, the uniformity of the layer thickness is much lower compared to that of the layer thickness when viewed from the transverse direction. These results suggest that during rolling deformation occurs uniformly in the rolling direction but heterogeneously in the transverse direction.

During the SEM investigation it was also found that at a small percentage of layer interfaces, the areas where bonding took place, there was a high degree of non-uniform deformation had occurred. This non-uniform deformation resulted in the 'wavy' areas shown in Figure 5.6. Although a material consisting of a microstructure such as this would behave very differently than one containing uniform layers it is assumed that this type of structure makes up a small fraction of the total material and its effects on the laminates mechanical response are negligible. This type of microstructure could be a result of the folded sample sliding during rolling or an artifact of the folding process.

TEM investigation into the microstructure provided several important pieces of information. First, on the scale of the layer thickness the layers of both copper and niobium are uniform in thickness and continuous. Dislocation cells, developed during the deformation and typical of heavily deformed metals, were apparent in the copper but not in the niobium layers. In general, the dislocation density observed in the niobium layers was low though a proper statistical measurement could not be made owing to the difficulty of sample preparation for these materials.

Because this work compares materials processed to various levels of strain it is important to understand how the elastic properties vary with strain. X-ray diffraction was used to determine the pole densities of both the copper and niobium at various levels of strain (Figure 5.8 and Figure 5.15). It was found that both the copper and niobium exhibit preferred orientations even at the lowest level of strain examined in this work. At the highest levels of strain the textures were very pronounced, a feature that has been previously observed in codeformed copper-niobium materials [23, 82].

### 6.2.2 Mechanical Properties

As discussed in Chapter 2, several models have been developed to describe the strengthening of copper-niobium codeformed materials. In order to assess the ability of these models to predict the mechanisms of deformation and strengthening, one would like to be able to compare the models against materials with a wide range of microstructural scales and volume fractions of phases. Such a range of materials has been produced using the roll bonding process and these results are discussed in relation to the models described in the literature.

The simplest possible model for the behaviour of these materials would be based on the rule of mixture between the strengths of pure, bulk copper and pure, bulk niobium. Comparing the data for the flow stress of the copper-niobium laminate materials to the predicted value given by the rule of mixtures using Spitzig's [1] data for bulk drawn pure copper and niobium (Figure 2.3), shows that at the levels of strain achieved using the accumulated roll bonding technique, the resulting material posses strengths similar to what the rule of mixtures would predict, this is shown in Figure 6.11. The strength data in Figure 2.3 is in terms of drawing strain, thus the rolling strain was converted to the Von Mises equivalent strain by multiplying the rolling strain by $2/\sqrt{3}$.

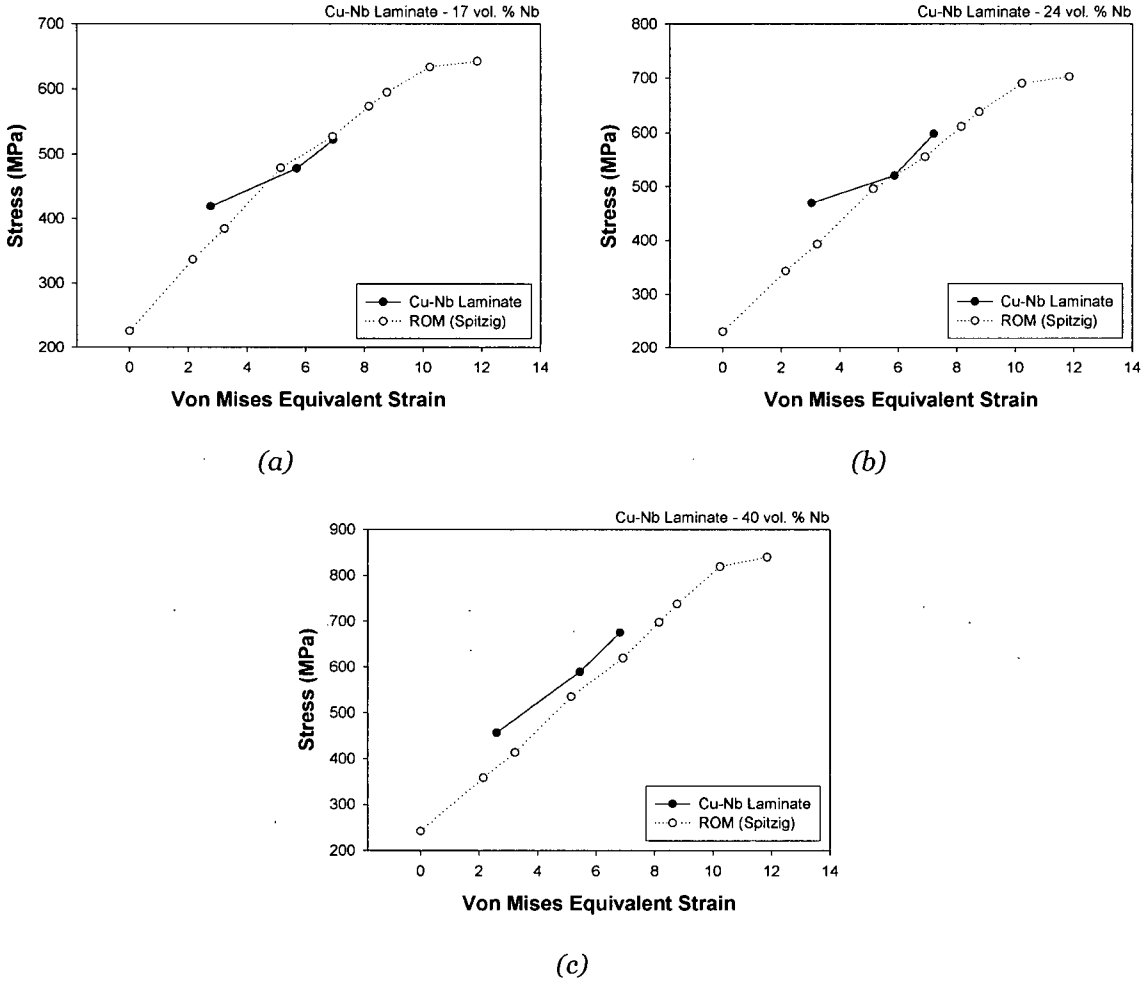


**Figure 6.11** *Experimental flow stress for the roll bonded laminate: (a) 17 % Nb; (b) 24 % Nb; and (c) 40 % Nb.*

Figure 2.3 shows copper-niobium drawn wire can exhibit an anomalous increase in strength at high drawing strains when compared to what the rule of mixtures predicts; however, this is not seen in the layered material examined in this work. This could imply that there is little effect of the refinement of scale on the strength of the materials studied. This is surprising given the microstructural observations discussed above, i.e. the low dislocation density observed in the finest scale niobium layers at high strains. Moreover, these observations tend to preclude the explanation of the results via a geometrically necessary dislocation argument.

An alternative to these explanations could be based on a barrier strengthening model similar to that proposed by Spitzig and co-workers [24]. Figure 6.12 shows a relationship between the flow stress of the composite and the copper layer thickness, where $\sigma = \sigma_0 + k/\sqrt{t_{Cu}}$. This expression is equivalent to that used previously by Spitzig *et al.* to describe the strength of wire drawn copper-niobium and shows a good correspondence with the experimental data from this study. In this case, $\sigma_0$, should be the flow stress of pure unstrained copper, as the presence of niobium is neglected in the fore mentioned equation. $\sigma_0$ has a value of approximately 385 MPa, which is higher than a typical value of the flow stress of copper at zero strain, but is not unreasonable for copper which has been deformed to 20 or 30% strain in tension.

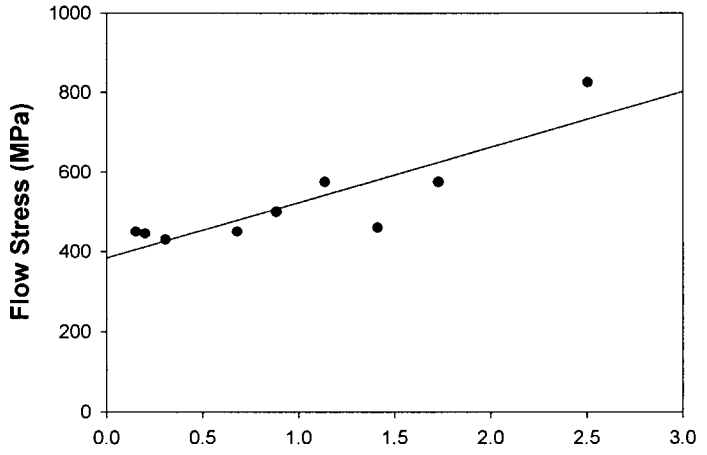


**Figure 6.12** *Relationship of flow stress to copper layer thickness*

The principle objection to the use of this type of model is that it neglects the contribution to the flow stress arising from plastic deformation within the niobium phase. At the volume fractions of niobium considered in this study, it is hard to rationalize such an argument. More elaborate schemes such as a combined rule of mixtures with a barrier like response for both phases [32, 83] can also adequately describe the observed strength, however, the physical basis for such a model becomes unclear.

### 6.2.3 Internal Stress

The discussion of the previous section illustrates the need for more information about the response of the individual phases during deformation in order to be able to explain the overall mechanical response. In this study, the measurement of internal stresses is one method that has the potential for giving insight into the flow stress of the individual phases.

As in the discussion of the behaviour of the copper-niobium wires, the internal stresses in the laminate material has been assessed from their response on unloading from their forward flow stress. Owing to the geometry, most importantly the small thickness, of the laminates it was not possible to perform tests in compression. In assessing the internal stresses, the point at which reverse yielding is observed on unloading has been used in relation to the forward flow stress. This has been used to calculate the parameter $\Delta\sigma$ as described above.

If the strengthening was, for instance, explainable simply based on a rule of mixtures of the response of bulk copper and bulk niobium then it should also be possible to predict the internal stresses present within such a material. The predicted variation of $\Delta\sigma$, with the level of imposed rolling strain can be calculated as the difference between the forward flow stress and the stress at which reverse yielding commences. This can be found from Spitzig's data using the flow stress predicted by the rule of mixtures and the flow stress of bulk drawn copper ( $\Delta\sigma = \sigma_{ROM} - \sigma_{Cu}$ ).

The calculated values of $\Delta\sigma$ from Spitzig's data are plotted against the values found experimentally for the laminate material in Figure 6.13.

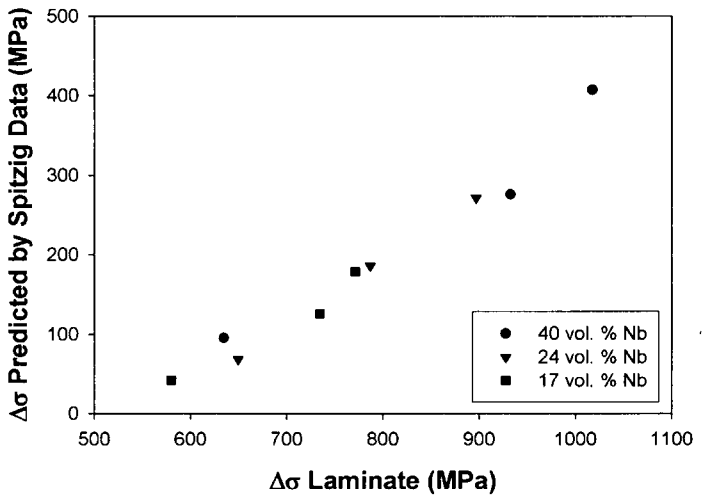


**Figure 6.13** *Delta-sigma from the Spitzig data vs Delta-sigma experimental data.*

The rule of mixtures estimates $\Delta\sigma$ based on the bulk behaviour of copper and niobium, and predicts a much lower value of $\Delta\sigma$ compared to that observed from the reverse yielding response of the samples studied here. Spitzig's data suggests a sample would be required to go into the compression before reverse yielding would begin, which is not observed in this study.

The main problem with this analysis is that it assumes uniform behaviour and internal stresses within the two phases. As discussed in relation to the wire material studied here, the reverse yielding response observed in the case of the laminates suggests strong transient reverse yielding. One of the reasons for attempting to perform experiments on the laminate material rather than wire drawn material was due to the relative homogeneity of the microstructure in the laminate versus the wires. Unlike the hierarchical structure in the wires arising from the bundling process, all of the layers in the laminates have experienced similar levels of deformation.

Despite this, it is clear that the assumption inherent in the use of the simple the Masing model described in Section 2.5.2, i.e. yielding occurs homogenously through the

phases, is not true for the laminates. Figure 6.14 shows the ratio of the unloading slope and the elastic modulus of the composite (measured from the initial unloading slope) as a function of the unloading stress. Initially on unloading, the material deforms in an elastic fashion. As yielding commences the regions with the highest compressive internal stress begin to yield. Assuming that the hardening rate of the yielded material is small relative to the elastic modulus, then the unloading slope should simply be given by the elastic modulus multiplied by the volume fraction of elastically deforming material. In Figure 5.11b the unloading response is shown for a material containing 40%Nb after an imposed rolling strain of ~7. If all of the copper yielded simultaneously on reverse loading, then the slope would drop from the elastic modulus to 40% of the elastic modulus. It is clear from Figure 6.14 that the slope is decreasing continuously, meaning the copper yields in compression progressively. Furthermore, over the unloading response observed, there is a certain portion of copper that remains elastic, meaning when the sample is completely unloaded approximately 65% of the material remains elastic.

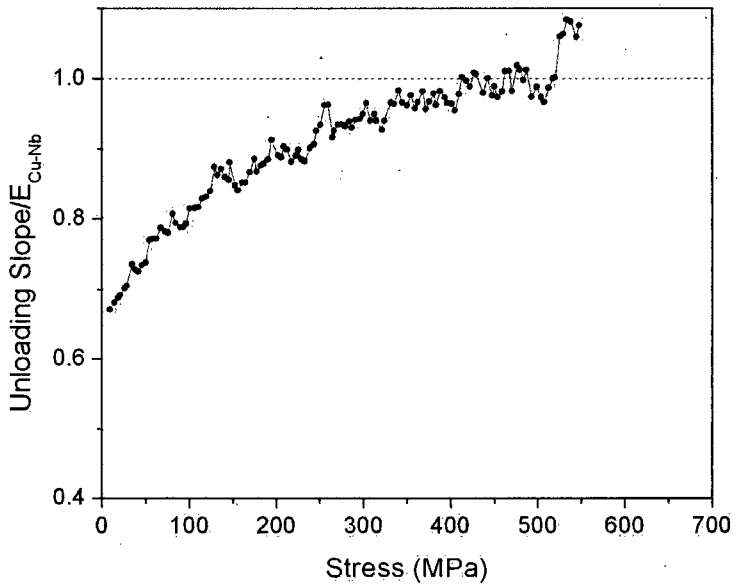


**Figure 6.14** *Progressive yielding of copper-24%niobium (ε~7) composite upon unloading.*

This progressive yielding of the copper phase can also be shown by back calculating the yield stress of the copper phase using the experimental load unload data. Again using the simplified Masing model, the yield stress of the copper phase can be found as one half of the difference between the forward flow stress and reverse yield stress ($1/2(\sigma_F - \sigma_R)$). At the levels of strain examined in this work the yield stress of pure copper would be expected to be on the order of 400 MPa. However, the calculated values are less than half of this value, again suggesting the progressive yielding of the copper phase.

The largest consequence of this assumption is that upon unloading all of the copper phase is assumed to yield at the same stress; however, this is clearly not the case. The fact that progressive yielding is noticed indicates that internal stresses within the copper phase are not equally distributed. In certain areas of the material, internal stresses are large and in other areas they may be small. It is the areas with large internal stresses that will begin to yield first followed by areas where the internal stresses are less. Due to the geometry of the samples it was not possible to place the sample under any compressive loading and thus it was impossible to determine if the transient softening during unloading was also accompanied by any permanent softening of the material.

If the strength of the composite were due to a barrier model whereby dislocations are inhomogeneous distributed within the copper (and niobium layers), with a higher density at the phase interface, there will be large variations in the levels of stress throughout the soft copper phase. Dislocations that are held up at the phase interface will, on unloading, tend to relax backward into the interior of the layers owing to the build up of internal stresses at the phase interface [84]. This will be observed as reverse plastic flow occurring at small amounts of unloading. This type of behaviour is observed in other forms of composites (i.e. MMC's [72] and other codeformed two phase materials

[78]) where the microstructures are uniform relative to the wire drawn materials discussed above.

### 6.2.4 Summary of Laminate Discussion

Producing copper-niobium layered composites using accumulated roll bonding techniques allowed for control of the volume fraction of niobium and the final microstructure. Although no anomalous increase in strength above that predicted based on a simple rule of mixtures was noticed at the levels of strain examined during this work, the strength of the laminate material could be analyzed with reference to the internal stresses causing yielding on reverse loading. The most important observation in this regard was the large but non-homogeneously distributed internal stresses. These resulted in a transient softening of the composite during reverse loading similar to that observed in the wire materials, despite the more homogeneous nature of the microstructures. An attempt was made to compare the internal stresses that would arise from a simple rule of mixtures estimate based on the Masing model, however, this model will not predict the source of the transient softening. The non-homogeneous stress distribution may be associated with stresses generated by dislocation pile-up at the phase interfaces, however further work is necessary in order to clarify this.

# CHAPTER 7

# CONCLUSIONS

The mechanical properties of three types of copper-niobium composite were studied during this work: *in-situ* drawn wire, bundle drawn wire and roll bonded laminate. First, the wire drawn composites were examined to determine their mechanical properties, level of internal stress and microstructural stability on annealing. Finally, production of the laminate composite allowed for the study of microstructural evolution, mechanical properties and development of internal stresses as a function of both the volume fraction of niobium and the level of imposed strain.

## 7.1 Wire Drawn Copper-Niobium Composites

Examination of the two types of wire drawn copper-niobium composite resulted in the following important points:

1) Both the *in-situ* and bundle drawn wire possessed "as received" flow strengths above that predicted by the rule of mixtures, high work hardening rates prior to reaching the ultimate flow strength and a pronounced roundness of the tensile curve during the onset of plastic flow. The roundness of the stress-strain curves is a result of the composite's progressive yielding.
2) Internal stresses have been shown to represent an important mechanism for the strengthening these fine scaled composites. The level of internal stress was found to

be strongly related to the microstructure of the composites and non-homogeneously distributed through the material, causing transient yielding.

3) Due to differences in the microstructure of the *in-situ* and bundle drawn materials the stability of the strength on annealing also found to vary. The bundle drawn materials showed significant softening when annealed at a temperature of 400°C while the strength of the in-situ material remained stable up to a temperature of 500°C. It is though that this is a result of the finer copper-niobium regions formed during *in-situ* production being more resilient to softening. Further work would be required to determine if this is indeed the case.

## 7.2 Laminate Copper-Niobium Composite

The following conclusions can be made concerning the roll bonded copper-niobium composite:

1) Laminate copper-niobium composite was successfully produced using an accumulated roll bonding technique. Material containing 17, 24 and 40 percent niobium by volume was produced containing a total imposed rolling strain on the order of 7. Difficulty arose only during the final bonding step due the increase in the hardness of the material, which limited the amount of strain that could be imposed.

2) The anomalous gains in strength commonly associated with fine scales two-phase materials was not seen in the laminate material. At the levels of strain examined throughout this work the strength of the laminate composite showed good correlation with that predicted by a rule of mixtures. The strength of the laminate was also found to correlate well to a barrier strengthening model, based on the copper layer thickness; moreover due the lack of sufficiently high dislocation densities a geometrically necessary dislocation density argument may not be adequate to predict the observed strengths.

3) Large internal stresses were found in the laminate material, however they were found to be non-homogeneously distributed. As a result, significant transient softening was noticed during the unloading of the material during load-unload tests. The source of the non-homogeneous stress distribution could be a result of dislocation pile-ups at the phase interfaces; however further work would be required to show this.

## 7.3 Comments for Future Work

Understanding the strengthening of the copper-niobium system, where there are no intermetallic phases produced and sharp boundaries are produced, will not only help in the understanding of mechanisms occurring in codeformed composite materials, but may also lead to a better understanding of fine scale single phase materials as well.

Further work should include but may not be limited to: quantitatively identifying the levels of internal stresses in two-phase codeformed materials using other methods, such as neutron diffraction; more thorough examination of the softening behavior of the fine scale regions of these materials; and a further comprehensive modeling of the strength possibly combining the affects of internal stresses, the presence of closely spaced barriers and the rule of mixtures.

Caution must be taken in the interpretation of internal stress data found using methods such as x-ray or neutron diffraction. The transient softening phenomena found during this work results from the distribution of internal stresses being largely non-homogeneous. Results could represent a large range of internal stresses or limited to a specific region of the microstructure, such as the phase interface, depending on the technique used.

# REFERENCES


[1] W. A. Spitzig, P. D. Krotz. *Scripta Metall.*, 21 (1987) 1143

[2] K. Han, J. D. Embury, J. R. Sims, et al. *Mat. Sci. Eng.* A267 (1999) 99

[3] J. Bevk, J. Harbison, J. L. Bell. *J. Appl. Phys.*, 49 (1978) 6031

[4] J. D. Embury, C. W. Sinclair. *Mater. Sci. Eng.* A319 (2001) 37

[5] J. D. Embury, R. Fisher. *Acta Metall.*,14 (1966) 147.

[6] W. A. Spitzig, P. D. Krotz. *Acta Metall.*, 36 (1988) 1709.

[7] A. Jankowski. *NanoStruc. Mat..* 6 (1995) 179

[8] N. Mara, A. Sergueeva, A. Misra. *Scripta Mater.* 50 (2004) 803

[9] A. Misra, X. Zhang, D. Hammon, R.G. Hoagland *Acta Mater.* 50 (2005) 221

[10] A. Misra, R. G. Hoagland, H. Kung. *Philos. Mag.* 84 (2004) 1021

[11] W. A. Spitzig, C. L. Trybus. *Mat. Sci. Eng.* A145 (1991) 179

[12] J. Bevk, J. Harbisn. *J. Appl. Phys.* 49 (1978 6031

[13] S. Hong, M. Hill. *Scripta Mater.* 42 (2000) 737

[14] C. Biselli, D. Morris. *Acta Mater.* 44 (1996) 493

[15] J. D. Embury, K. Han. *Current Opinion in Solid State & Materials Science.* 3 (1998) 304

[16] T. Kitai, M. Higuchi. K. Osamura. *Cryogenics.* 37 91997) 389

[17] T. Takeuchi, K. Tagawa. T. Kiyoshi. *IEEE Trans. App. Supercond.* 9 (1999) 2682

[18] S. C. Jha, R. G. Delagi, J. A. Forster, P. D. Krotz. *Met. Tans. A.* 24A (1993) 15

[19] W. A. Spitzig, A. Pelton, F. C. Labbs. *Acta Metall.* 35 10 (1987) 2427

[20] W. Callister *Materials Science and Engineering an Introductio*n, 3rd Ed. Wiley, New York, NY, USA, p532.

[21] ASM International. *ASM Handbook Volume 3, Alloy Phase Diagrams*, Online 2003

[22] M. Bauccio. *Metals Reference Book*, 3rd Ed. ASM International, Park, Ohio, USA, (1993)

[23] D. Raabe, F. Heringhaus, U. Hangen. *Z. Metallkd.* 86 (1995) 405

[24] W. A. Spitzig, P. D. Krotz. *Scripta Metall.* 21 (1987) 1143

[25] W. A. Spitzig. *Acta Metall. Mater.* 39 6 (1991) 1085

[26] E. Hall., *Proc. Phys. Soc. Lond.* B64 (1951) 747

[27] N. Petch, *J. Iron Steel Inst.* 174 (1953) 25

[28] P. D. Funkenbusch, T. H. Courtney. *Acta Metall.* 33 5 (1985) 913

[29] P. D. Funkenbusch, J. K. Lee, T. H. Courtney. *Met. Trans.* 18A (1987) 1249

[30] J. D. Embury, R. Fisher. *Acta Metall.* 14 (1966) 147

[31] K. Yasuna, M. Terauchi, A. Otsuki. *Mat. Sci. Eng.* A285 (2000) 412

[32] P. D. Funkenbush, T. H. Courtney. *Scripta Metall.* 16 (1981) 1349

[33] R. Everett, *Scripta Metall.* 22 (1988) 1227

[34] M. F. Ashby. Strengthening Methods in Crystals. Jon Whiley & Sons Inc. 1971

[35] M. F. Ashby. *Phil. Mag.* 21 (1970) 399

[36] Y .Estrin, H. Mecking. *Acta. Metall.* 32 (1984) 57

[37] H. Lilholt. *Mechanical Properties of Metallic Composites.* Marcel Dekker, Inc (1994) 389

[38 ] U. Kocks. *J. Eneng. Mater. Technol.* 98 (1976) 76

[39] A. D. Rollett. *Strain Hardening at Large Strains in Alumunium Alloys.* 1988

[40] J. Bevk, J. Harbison, J. Bell. *J. Appl. Phys.* 49 (1978) 6031

[41] W. A. Spitzig, *Acta Metall. Mater.* 39 (1991) 1085

[42] P. D. Funkenbush, T. H. Courtney. *Scripta Metall. Mater.* 24 (1990) 1175

[43] P. D. Funkenbush, T. H. Courtney. *Scripta Metall. Mater.* 23 (1989) 1719

[44] W. A. Spitzig, J. Verhoeven, C. Trybus. *Scripta Metall. Mater.* 24 (1990) 1171

[45] W. A. Spitzig, J. Verhoeven, C. Trybus. *Scripta Metall. Mater.* 24 (1990) 1181

[46] P. D. Funkenbush, T. H. Courtney. *Scripta Metall. Mater.* 24 (1990) 1183

[47] J. Sevillano *J. Phys. III.* 1 (1991) 967

[48] G. Frommeyer, G. Wassermann. *Acta Metall.* 23 (1975) 1353

[49] L. Thilly, M. Veron, O. Ludwig. *Phil. Mag.* A82 (2002) 925

[50] S. Brenner. *J. App. Phys.* 27 (1956) 1484

[51] S. Brenner. *J. App. Phys.* 28 (1957) 1023

[52] J. Greer, W. Oliver, W. Nix. *Acta Mater.* 53 (2005) 1821

[53] J. Greer, W. Nix. *Appl. Phys.* A80 (2005) 1625

[54] W. Webb, W. Forgeng. *Acta Metall.* 6 (1958) 462

[55] C. W. Sinclair, J. D. Embury, G. Weatherly. K. Conlon. *Phil. Mag.* 85 (2005) 3137

[56] K. Han, A. Lawson, J. Wood. *Phil. Mag.* 84 (2004) 2579

[57] M. Fitzpatrick, M. Huchings, P. Withers. *Acta Mater.* vol 45 (1997) 4867

[58] W. Hosford, R. Caddell. Metal Forming, (1993)

[59] J. Wood. Ph.D Thesis, McMaster University, Canada (1994)

[60] R. Asaro. Acta Metall. 23 (1975) 271

[61] J. Eshelby. *Proc. Roy. Soc. Lond.* A241 (1957) 376

[62] T. Cline, P. Withers. *An Introduction to Metal Matrix Composites.* New York: Cambridge University Press (1993)

[63] L. Brown, D. Clarke. *Acta Metall.* 23 (1975) 821

[64] R. Sowerby, D. Uko, *Mat. Sci. Eng.* 41 (1979) 43

[65] A. Abel, *Materials Forum.* 10 (1987) 11

[66] N. Chawla, B. Jester, D. Vonk. *Mat Sci. Eng.* A346 (2003) 266

[67] D. Wilson. *Acta Metall.* 13 (1956) 807

[68] W. Stobbs, S. Paetke. *Acta Metall.* 33 (1985) 777

[69] S. Tao, J. D. Embury. *Met. Trans.* 24A (1993) 713

[70] P. B. Prangnell, T. J. Downes, P. J. Withers. T. Lorentzen. *Mat. Sci. Eng.* A197 (1995) 215

[71] G. Moan, J. D. Embury. *Act Metall.* 27 (1979) 903

[72] S. F. Corbin, D. S. Wilkinson, J. D. Embury. *Mat. Sci. Eng.* A207 (1996) 1

[73] R. Klassen, K. Conlon, J. Wood. *Scripta Mater.* 48 (2003) 385

[74] D. Wilson, Y. Konnan. *Acta Metall.* 12 (1964) 617

[75] T. Suzuki, Y. Tomota, M. Isaka. *ISIJ International.* 44 (2004) 1426

[76] J. Atienza, M. Martinez-Perez, J. Ruiz-Hervias. *Scripta Mater.* 52 (2005) 305

[77] J. Hirth, J. Lothe. *Theory of Dislocations.* McGraw Hill, New York, 2nd Edition, (1982)

[78] C. W. Sinclair, G. Saada, J. D. Embury. *Phil. Mag.* (in print)

[79] W. Stobbs, S. Paetke. *Acta Metall.* 33 (1985) 777

[80] D. Hardwick, C. Rhodes, L. Fritzemeier. *Met. Trans.* 24A (1993) 27

[81] H. R. Sandim, M. J. Sandim, H. Bernardi, J. F. Lins, D. Raabe. *Scripta Mater.* 51 (2004) 1099

[82] D. Raabe, J. Ball, G. Gottstein, Scripta *Metall. Mater.* 27 (1992) 211

[83] U. Hangen, D. Raabe. *Acta Metall. Mater.* 43 (1995) 4075

[84] G. Saada. *Phil. Mag.* 85 (2005) 3003